Cofactor assembly in the Cu-dependent nitrite reductase, AniA, from pathogenic Neisseria

WILLIAM JOHN EARL

Cofactor assembly in the Cu-dependent nitrite reductase, AniA, from pathogenic *Neisseria*

William John Earl

March 2025

A thesis presented for the degree of
Master of Science by Research

Supervisor: Dr Karrera Djoko
Department of Biosciences
Durham University

Abstract

Neisseria gonorrhoeae infects the human genitourinary tract. In its O_2-limited host niche, *N. gonorrhoeae* relies on nitrite as the terminal electron acceptor in anaerobic respiration. In this process, nitrite is reduced to nitric oxide by the copper (Cu)-dependent nitrite reductase, AniA.

AniA is essential for biofilm formation and therefore, *N. gonorrhoeae* infection. AniA exists on either side of the outer membrane and is a target for vaccines and novel antimicrobials. Cu insertion into the AniA active site, and thus enzyme activity, requires a periplasmic Cu-binding accessory protein AccA. AccA is thought to be specific to AniA, however AccA is part of a larger family of periplasmic Cu binding proteins. Therefore, another protein may be able to replace AccA. To test this, AccA was replaced with PCu_AC from *Thermus thermophilus*, creating an $\Delta accA/pCu_AC^+$ mutant strain. Microaerobic cultures of this mutant did not grow or consume nitrite, however, both could be rescued upon the addition of Cu salt. This suggests that in the presence of PCu_AC but without AccA, AniA does not acquire Cu and is inactive unless Cu is supplied. This suggests PCu_AC cannot insert Cu into AniA and AccA is required for this process in cells. This was tested using purified proteins, Cu transfer to *apo*-AniA via Cu(I)-PCu_AC was found to be 15X slower than from Cu(I)Cu(II)-AccA. Therefore, showing PCu_AC cannot insert Cu into AniA at a rate to support bacterial growth.

This study indicates that the interaction between AccA and AniA is specific and favourable for the transfer of Cu. This specificity suggests the feasibility of targeting the AccA-AniA interactions for novel antimicrobials against multi-drug-resistant *N. gonorrhoeae*.

Contents

List of figures

List of tables

Page

List of abbreviations

AccA	AniA Copper chaperone A
BCA	Bicinchoninic acid
BCS	Bathocuproinedisulfonic acid
C.V.	Column volumes
Cys	Cysteine
Fz	ferrozine
GCBL	Gonococcal base medium liquid
His	Histidine
ICP-MS	Inductively-coupled plasma mass spectrometry
IPTG	Isopropyl β-D-1- thiogalactopyranoside
K_D	dissociation constant
K_{ex}	exchange constant
LB	Lysogeny broth
LIC	Ligation independent cloning
Met	Methionine
NirK	Copper-dependent nitrite reductase
NO	nitric oxide
NO_2^-	nitrite
PBS	Phosphate-buffered saline
PCR	Polymerase Chain Reaction
PCu_AC	Periplasmic Cu_A Chaperone
PES	Polyethersulfone
ROS	Reactive oxygen species
specR	Spectinomycin resistance cassette
T1Cu	Type 1 Cu binding site
T2Cu	Type 2 Cu binding site
Tt-PCu_AC	PCu_AC, from *T. thermophilus*

Declaration

I declare that the contents of this work are original, and the work conducted is my own work, except where specific reference is made in the text to the work of others. This work has not been submitted in whole or in part for any other degree or qualification, except as specified.

Statement of copyright

Acknowledgements

Firstly, I would like to thank my supervisor Dr Karrera Djoko, whose invaluable guidance and support has not only been essential for this project's progression but has allowed me to improve massively as a scientist. I would also like to thank Dr Samantha Firth, whose previous work laid the foundations for this project, and for providing pertinent insights throughout. I would like to thank the members of Lab 10 for both practical and moral support, especially Dr Jack Bolton who helped greatly with my microbiology skills.

I would like to thank the members of the Morris Lab who helped with protein purification, notably Rosella Pickney. Finally, I would like to thank the members of the Chivers and Sharples labs for their guidance in lab meetings.

Chapter 1 – Introduction

1.1 Metals in biology

Metals are essential for life, with a third of proteins and nearly half of enzymes requiring a metal ion for function (1). Metalloproteins contribute to all areas of cellular metabolism and the metal cofactors can have different roles. Metals can impart structure upon proteins, such as the role of zinc in zinc finger motifs. Metals can also act as Lewis acids to coordinate and activate a substrate through binding to a lone pair of electrons, such as in zinc hydrolases (2). Alternatively, metals can act as reducing or oxidising agents in catalysing redox reactions, such as copper (Cu) in cytochrome *cbb*$_3$ oxidase (3–5). Metals can bind to the protein scaffold directly, via the amino acid side chains, with those containing N, O and S being common ligands, including His, Glu, Asp, Met, Cys, and to a lesser extent Trp and Tyr (6). Metals also bind to proteins indirectly via organic ligands, such tetrapyrroles in vitamin-B12 or haem, and sulfides in iron-sulfur clusters (5).

Proteins and their metal binding sites are inherently flexible, and the binding affinity of proteins to metals follows the Irving-Williams series (7). Therefore, if a metal higher in the Irving-Williams series is present in surplus, then metal-binding sites that favour metals lower in the series can be mis-metalated by the metal with higher binding affinity (8). Metal homeostatic mechanisms, such as metal sensors, metal transporters, metallochaperones and storage proteins, are required to maintain the correct metal availability in cells(9). These systems ensure that metalloproteins receive their correct metal cofactors and protect other proteins from becoming mis-metalated (5,8). If the homeostatic mechanisms fail or the capacity is exceeded, the cellular availability of metals increases, this can have a detrimental effect on the cell. Excess metals can catalyse the production of reactive oxygen species (ROS) from Fenton-like reactions, or can cause toxicity through the mis-metalation of proteins (*Fig.* 1.1) (1,5).

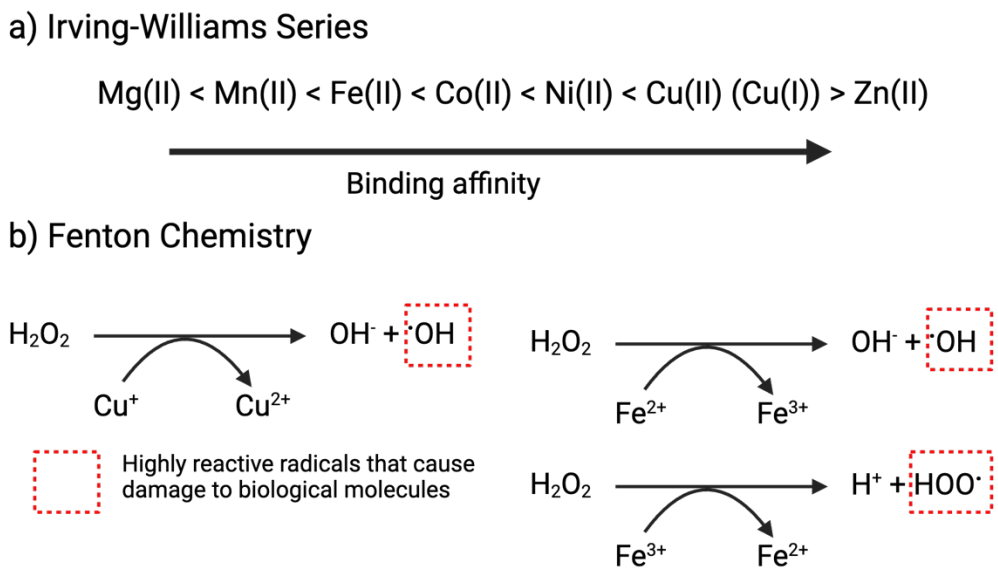

Figure 1.1*. The toxic effects copper a**) Irving-Williams series of transition metal protein binding affinities with Cu(II) binding the tightest. Cu(I) is not a transition metal however it is known for competitive binding to proteins (8). **b)* Fenton chemistry by redox-active iron and copper to produce ROS.

1.2 Copper in biology

The evolution of photosynthesis resulted in the formation of an O_2-rich atmosphere. This resulted in the oxidising of sulfides to sulfates, which led to the release and increase in bioavailability of previously sequestered Cu(II), therefore kickstarting the evolution of cuproproteins (10). It is thought that cuproproteins first evolved to deplete the levels of free dioxygen within cells. One of the earliest cuproenzymes, phenol oxidases, reduce dioxygen and couple this reduction to the oxidation of a phenol and the production of water (11). Cuproproteins now have key roles in electron transfer due to their redox activity, including in aerobic and anaerobic respiration, and superoxide dismutation in bacteria (12–14). However, the redox activity of Cu can also be detrimental to life, as it can catalyse Fenton-like reactions to produce ROS (*Fig.* 1.1b). In addition, Cu is prone to mis-metalating other metal binding sites, as it has the highest binding affinity to proteins in the Irving-Williams series (*Fig.* 1.1a). For example, in *Escherichia* coli, Cu mis-metallates the iron-sulfur clusters in dehydratases which prevents growth (10,15).

1.2.1 Copper homeostasis in cells

Due to the position of Cu in the Irving-Williams series and its tendency to mis-metalate proteins, copper levels are tightly controlled by homeostatic mechanisms which keep "free" copper levels to almost zero (15). Cu is buffered by numerous Cu chelators including transcriptionally-induced metallochaperones and small molecules, such as glutathione, which contribute to buffering Cu when transcriptionally-induced homeostatic mechanisms are impaired (16). Under normal conditions this high affinity Cu buffer is maintained at a high enough concentration that under normal conditions, at equilibrium, metalation of the buffer is thermodynamically favoured so Cu is not transferred to unwanted metal sites (*Fig.* 1.2) (16).

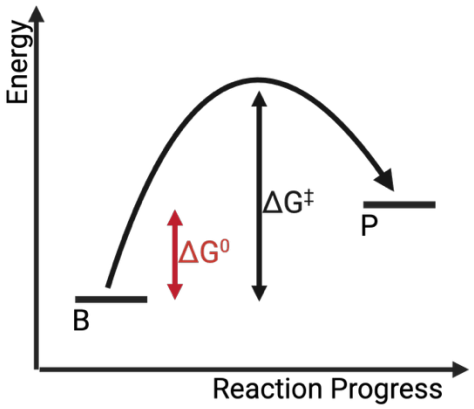

Figure 1.2. Energy diagram of the metalation of a non-specific metalloprotein from a high affinity Cu buffer. P – metalloprotein B – Buffer. Red = unfavourable.

The transcriptional regulation of Cu homeostatic proteins is predominantly controlled by Cu sensors. Bacterial metal sensors bind metals in accordance with the Irving-Williams series, however the correct allosteric change in the protein only occurs upon binding of the correct metal. This results in the DNA binding affinity being altered; inducing or repressing transcription (15,17). In response to increased Cu levels, Cu-sensing metallosensors regulate multiple genes relating to Cu homeostasis. This includes the upregulation of Cu exporters, such as, the P_1-type ATPase, CopA, by cueR (18), and the Cu efflux system CusCBA by CusR (19). Other Cu resistance proteins are also upregulated. For example, the multi-Cu oxidase CueO and the metallochaperone CopZ by CopY (3), CueP (20) and CopG (19), which sequester Cu and traffic it to export systems.

In bacteria, cuproproteins and their folding are compartmentalised to the periplasm to avoid mis-metalation of proteins that bind weaker binding metals. For example in the cyanobacterium *Synechocystis* PCC 6803, manganese cupin A (MncA) and Cu cupin A (CucA) have the same structure and metal binding site (21). Therefore, MncA folds and is metalated in the cytoplasm, before being exported to the periplasm by the Tat pathway whereas CucA is exported by the Sec pathway where it is metalated and folds in the periplasm (21).

1.2.2 Cuproproteins

Cu sites within proteins can bind either Cu(I) or Cu(II) which favour different coordination geometries. Cu(I) centres favour a tetrahedral conformation as Cu(I) has a full d orbital (d^{10}) meaning the Crystal Field Stabilisation Energy is 0 for both octahedral and tetrahedral geometries (22). This results in no electronic preference for either coordination and therefore steric preferences are dominant, and a tetrahedral geometry is preferred due to its lower coordination number. As Cu(I) is a soft acid, it favours soft bases such as sulfurs and conjugated nitrogens. Therefore, Cu(I) often forms complexes with His, Cys, and Met (22). On the other hand, Cu(II) centres, favour a square planar geometry because of the orbital degeneracy of its d^9 electron configuration. This results in a tetragonal distortion of the d_{x2-y2} and d_{z2} orbitals to remove the degeneracy and increase the stability of the complex. This is known as the Jahn-Teller effect and results in a shortening of the equatorial metal-ligand bonds, and an elongation of the axial metal-ligand bonds to the point where they are lost resulting in a square planar geometry(22).

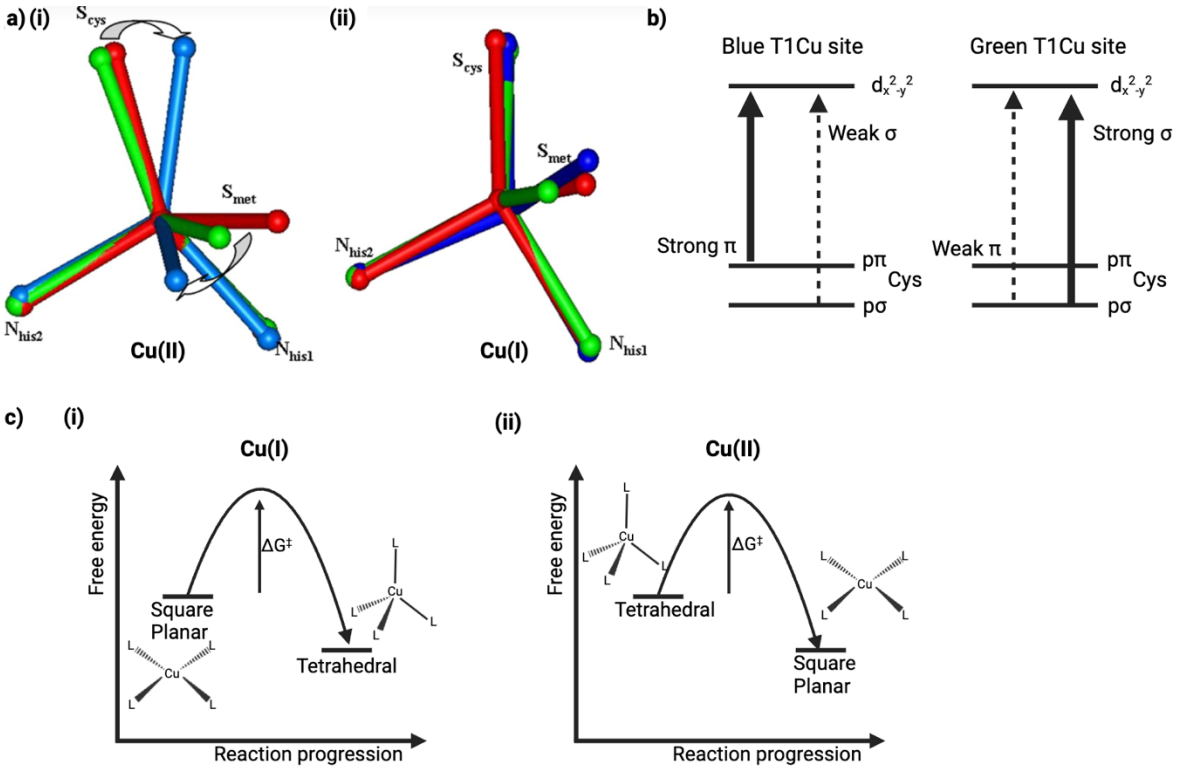

Figure 1.3. **The type I Cu site a**) Oxidised (**i**) and reduced (**ii**) T1Cu sites showing the structures of red, green, and blue sites as well as the angle changes from green to blue. b) Schematic of the Cys-S – Cu charge transfer in blue and green T1Cu sites which result in their characteristic absorbance spectra. c) Relative energy of square planar and tetrahedral complexes for both oxidation states of Cu, as well as the kinetic barrier imposed by the protein between the two states. Parts (**a**) and (**b**) were taken and adapted from "Thermodynamic equilibrium between blue and green Cu sites and the role of the protein in controlling function", respectively (23).

The chemistry underlying Cu binding results in distinct classifications of Cu-binding sites, notable for this study are the Type I (T1Cu) and Type II (T2Cu) Cu sites (24). The T2Cu site predominantly binds Cu with 3 or 4 ligands, with at least one being His, and are classified based upon very little to no absorption in the UV/Vis range due to the lack of a thiol in the binding site. The T2Cu centre is redox-active, and the prevalence of 3 ligand binding sites allows for the vacant coordination position to be occupied by an exogenous ligand meaning the site is often catalytically-active and binds to the substrate (25).

The presence of T1Cu sites classifies a protein as a blue Cu protein due to the strong blue colour exhibited by strong absorbance at 600 nm, and often a weaker absorbance at 460 nm. In these sites, Cu is bound by 2 His, 1 Cys and 1 other ligand (often Met) (26). The Cu ion present is redox-active; allowing switching between Cu(I) and Cu(II). Consequently, the energetically favoured geometry for the site switches between tetrahedral and square planar upon reduction or oxidation of Cu (23). However, switching between two geometries is not kinetically possible, due to the structural constraints of the protein; providing a large kinetic energy barrier (*Fig.* 1.3c). Therefore, the ligands in the site allow for the geometry of the Cu site to sit between square planar and tetrahedral in a distorted tetragonal geometry. This allows for the greatest energetic favourability for Cu(I) and Cu(II), and the minimal energy for reorganisation between

the two Cu oxidation states, whilst accounting for any steric effects imposed by the protein (27). The blue character of T1Cu sites depends on the positions and bond lengths of the Cu-Cys and Cu-Met bonds. A more blue T1Cu site has greater distortion towards tetrahedral, resulting in longer Cu-S_{met} bond and shorter Cu-S_{cys} bond. This leads to weak thiolate σ to Cu charge transfer (high energy) and a strong π to Cu charge transfer (low energy), which results in greater absorbance at ~600 nm and a blue appearance. The green T1Cu results from a more tetrahedral shape and a strong thiolate σ to Cu and a weak π to Cu charge transfer, resulting in greater absorbance at lower wavelengths (~460 nm) and the protein appearing more 'green' (*Fig.* 1.3b). Sites are often partially flexible and intermediates between the two sites are common, resulting in absorbance at both wavelengths to varying degrees. This allows for the tuning of the reduction potential of the Cu site (*Fig.* 1.3a) (23).

1.2.3 Copper Metallochaperones

A consequence of Cu being buffered within cells is that the rate of Cu acquisition directly from the buffer by cuproenzymes is often too slow to meet biological needs. Instead, many cuproenzymes rely on Cu metallochaperones to acquire Cu ions (*Fig.* 1.4 b(iii)). Cu metallochaperones can also protect against Cu stress as Cu trafficking and direct metalation of cuproproteins prevents Cu from becoming solvated and also avoids mis-metalation by ensuring specificity (5). The transfer of Cu from the metallochaperone occurs through a process of associative ligand exchange. The two proteins form a complex with both bound to the metal, then the metal binding ligands of the target protein displace the ligands of the metallochaperone (*Fig*. 1.4 a) (28). The transfer of the metal from the metallochaperone to the target results in a conformational change in both proteins and thus the dissociation of the complex (28). Metalation occurs down a thermodynamic gradient from the metallochaperone with a lower binding affinity and higher free energy, to the target protein with a higher binding affinity and lower free energy in a favourable interaction (*Fig.* 1.4 bi) (29). Buffers, such as glutathione, and other small molecules bind Cu weaker than metallochaperones. Therefore, the difference in free energy is greater and therefore more thermodynamically favourable (*Fig.* 1.4 b(ii)) (29). However, due to no favourable interactions between buffer molecules and the target protein, the kinetic barrier to metalation is far greater, thus making the rate of metalation too slow for biological process to occur. Metallochaperones provide a smaller kinetic barrier to metalation whilst still offering a thermodynamically favourable route (30).

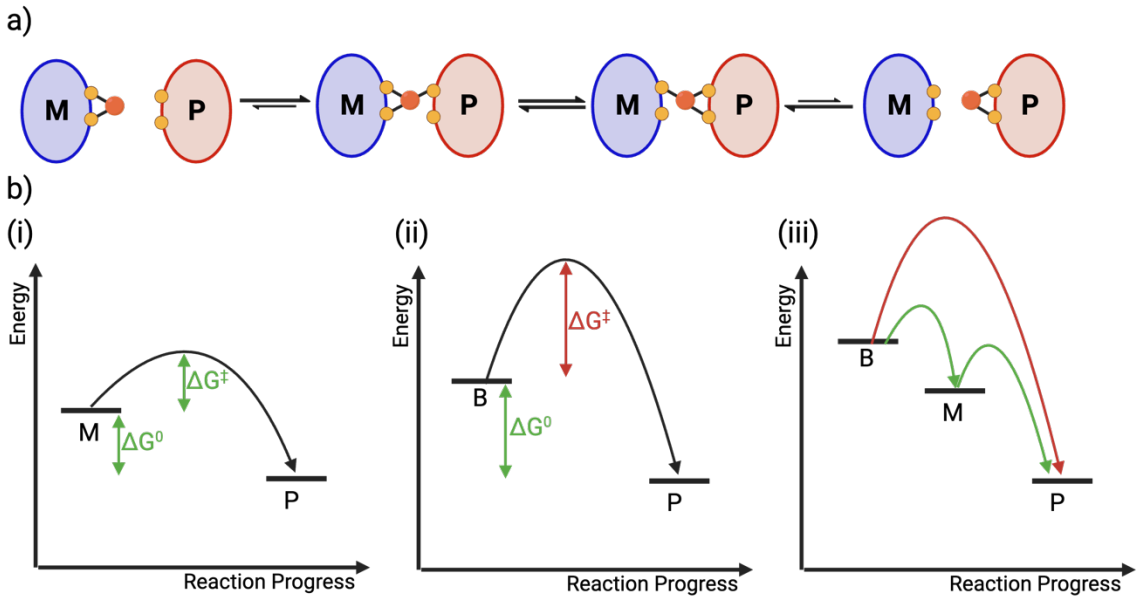

Figure 1.4. **Metallochaperone to target protein Cu transfer**. **a**) ligand transfer between a metallochaperone and the target protein in metalation. **b**) Energy diagrams for metalation of proteins by Cu by metallochaperones (**i**), from small buffer molecules (**ii**) and overall metalation process in cells. M - metallochaperone P - target protein B – Buffer. Green = metalation occurs at a sufficient rate, red = metalation is slow.

In addition to metalation having to be thermodynamically favourable, the metallochaperone and target protein must have favourable protein-protein interactions based on structure and complementary amino acid residues. For example, metalation of the Ccc2 ATPase (the target cuproprotein) from *Saccharomyces cerevisiae* by Atx1 (the Cu metallochaperone) resulted in favourable hydrophobic and hydrophilic intermolecular interactions between pairs of amino acid residues, holding the 2 proteins together (28). Similarly, the formation of transient metallochaperone-target protein complexes between Atox1 and Wilson Disease protein 4 was enthalpically and entropically favourable, making the complex more thermodynamically stable than the individual proteins; promoting metalation (31). On top of this, specific interactions are required between amino acid residues. For example, CopZ, but not the structurally similar MNKr2, could metalate CopY, due to the proteins having distinct surface charges, Substituting Q38, R39, D45 and N46 in the protein interface with lysine to introduce a positively charged face subsequently resulted in MNKr2 being able to metalate CopY (32). This suggests that the correct surface charge distribution is likely essential for Cu transfer due to intermolecular salt bridges increasing the stability of the complex.

Studies have shown that Cu is essential for the metallochaperone-target protein complex to occur (28). *Apo*-metallochaperone and *apo*-target protein interactions are less favourable than interactions where Cu is present (28,31,33). The metallochaperone, Hah1, bound to Cu(I) or Cd(II), showed different interactions with target cuproprotein, MNK1, at the interface of the metal binding loops. There were also differing ligands in the metal complexes formed: Hah1-Cu(I) formed more favourable interactions and metalated MNK1,whereas Hah1-Cd(II) did not (33). These results suggest that Cu is required to form metallochaperone-protein complexes,

preventing mismetalation as well as the formation of complexes without Cu, which would block the site from metalation by *holo*-metallochaperones.

1.3 Copper in *Neisseria gonorrhoeae* and metalation of AniA

Neisseria gonorrhoeae is a obligate human pathogen that infects the genitourinary tract (34). Cu is required for essential enzymes in *N. gonorrhoeae*, including the nitrite reductase, AniA, and cytochrome cbb_3 oxidase (35). *N. gonorrhoeae* lacks a complete Cu homeostasis pathway: lacking *cueR* and *cueO*, as well as many other known Cu resistance genes (36). The genome of *N. gonorrhoeae* does encode the Cu efflux protein, CopA, however unlike in other species, it is transcriptionally regulated by NmlR, which responds to nitrosative stress, as opposed to Cu (36).

Upon infection, *N. gonorrhoeae* inhabits an O_2-limited host niche. Under these conditions, the Cu-dependent nitrite reductase, AniA, utilises nitrite as the terminal electron acceptor in anaerobic respiration, where it reduces nitrite (NO_2^-) to nitric oxide (NO) in the denitrification pathway (37). AniA is upregulated by the FNR transcription factor in response to low oxygen conditions, and has been shown to be essential for biofilm formation and therefore infection (*Fig.* 1.5) (38,39). Antibodies against AniA have also been found in the serum of infected patients, suggesting it is located on either side of the outer membrane (40). This has led to interest in AniA being a potential target for vaccines, as well as the development of small peptide inhibitors (41,42).

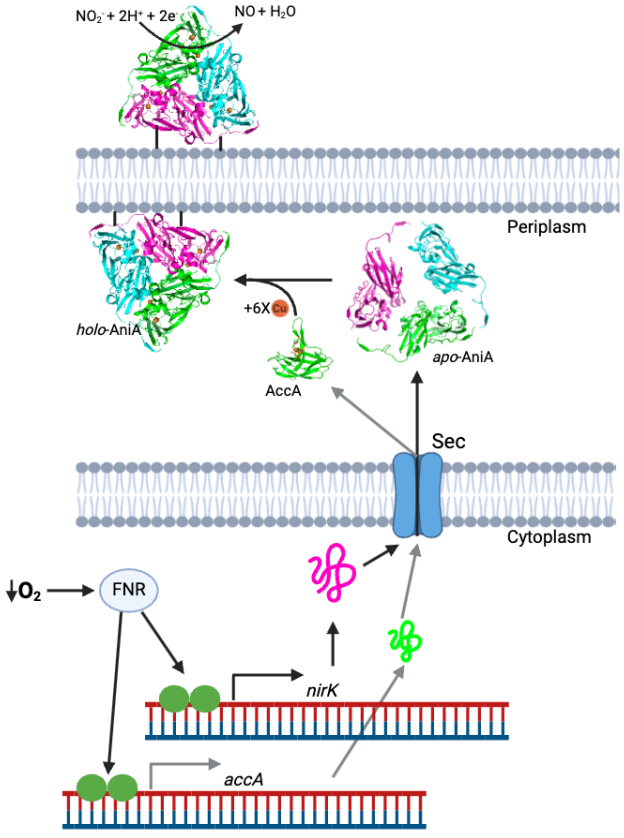

Figure 1.5. **Regulation, Cu insertion, and function of AniA**

AniA is a member of a larger family of Cu-dependent nitrite reductases encoded for by the gene *nirK*. Although most NirKs are found in the periplasmic space, AniA contains a lipid soluble domain, which allows its association to the outer membrane (43). AniA is a homotrimer, with each monomer consisting of two structurally similar cupredoxin domains, with the N-terminal domain containing the T1Cu site. AniA also contains 3 T2Cu sites with ligands across each monomer-monomer interface (*Fig.* 1.6 a,b) (37). The T2Cu centre acts as the active site of AniA and directly binds nitrite (NO_2^-) through its vacant coordination position (*Fig*. 1.6 b). NO_2^- can be reduced via a Cys-His bridge directly linking the T1Cu site to the T2Cu site, which allows for electron transfer from one Cu ion to the next and then to the substrate (*Fig.* 1.6 b) (41). Each monomer of AniA also has an extended C-terminal which allows for inter-subunit β-strand complementation between two monomers. This extension is seen in most NirKs that have been structurally characterised, and deletion has been shown to reduce the trimer stability and enzyme activity of NirKs (41,44–47).

There are three classes of NirKs, class I, II, and III, with classes I and II being trimers containing 2 domains per monomer, and class III being a hexamer containing 3 domains per monomer with an extra T1Cu or haem group. AniA is considered part of the class II family of NirKs which are almost exclusively found in extremophiles and pathogens (37). Classes I and II can be classified based on the electronic properties of the T1Cu site which causes them to appear different colours, with class I NirKs absorbing light at ~600 nm and consequently appearing more blue, and Class II NirKs showing greater absorbance at ~450 nm compared to at ~600 nm, therefore appearing more green. Class II NirKs are more structurally diverse, and like AniA, are often membrane-bound (43). The key structural difference between class I and II are two shortened loops, namely the linker loop and the tower loop in Class IIs (*Fig*. 1.6 a). This structural difference explains why AniA is a Class II NirK, despite higher absorbance at 600 nm (*Fig*. 1.6 c). The shortening of the linker loop, which sits between the two cupredoxin domains, may allow for closer association with the membrane and the shortening of the tower loop is thought to allow for the interaction with its electron donor (37).

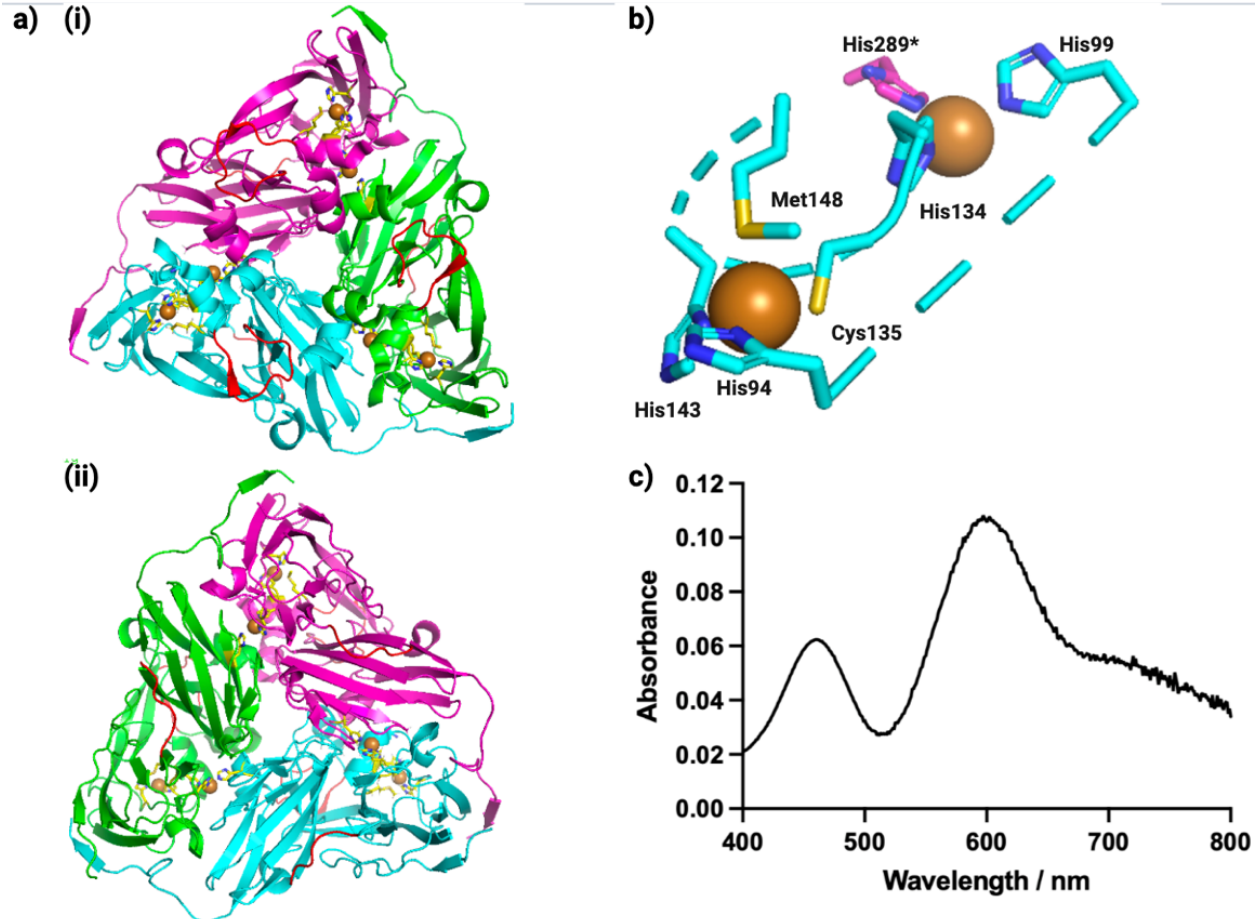

Figure 1.6. Structural and biochemical characterisation of AniA. a) Crystal structure of AniA 'Front' (**i**) and 'back' (**ii**) with the Cu sites highlighted in yellow and the tower (i) (K217-P227) and linker (ii) loops (G199-K205) in red (41). **b**) The T1Cu (H94, C135, H143, M148) and T2Cu (H99,H134,H289*) sites of AniA. **c**) Absorbance spectrum of the T1Cu site of fully Cu-loaded AniA, absorbance peaks at 460 nm and 600 nm.

1.4 AccA and periplasmic copper metallochaperones

In *N. gonorrhoeae,* AniA is thought to be metalated by the periplasmic Cu metallochaperone, AccA (14). AccA has found to be essential for AniA activity *in vivo*, and therefore microaerobic growth. *In vitro*, it has been shown that AccA delivers Cu to both the Type I and Type II Cu sites within AniA (30). Like AniA, AccA is regulated by the FNR transcription factor in response to low oxygen levels and shows no regulation in response to changes in Cu levels (30). AccA consists of a cupredoxin-like fold with an extended finger like domain. The primary Cu binding site lies between these two domains and consists of a His-X_{10}-Met-X_{22}-His-X-Met (*Fig*. 1.7) (48). AccA also has a His and Met rich C-terminal extension that preferentially binds Cu(II), which is thought to be unstructured both with and without Cu (G. Luscombe, MRes thesis, 2024) This gives AccA a Cu binding stoichiometry of 2:1. AccA also has 4 metal binding ligands surrounding the primary Cu binding site, which increases the site's binding affinity for Cu. This has been termed the Cu-track (*Fig* 1.7b) (30).

a)

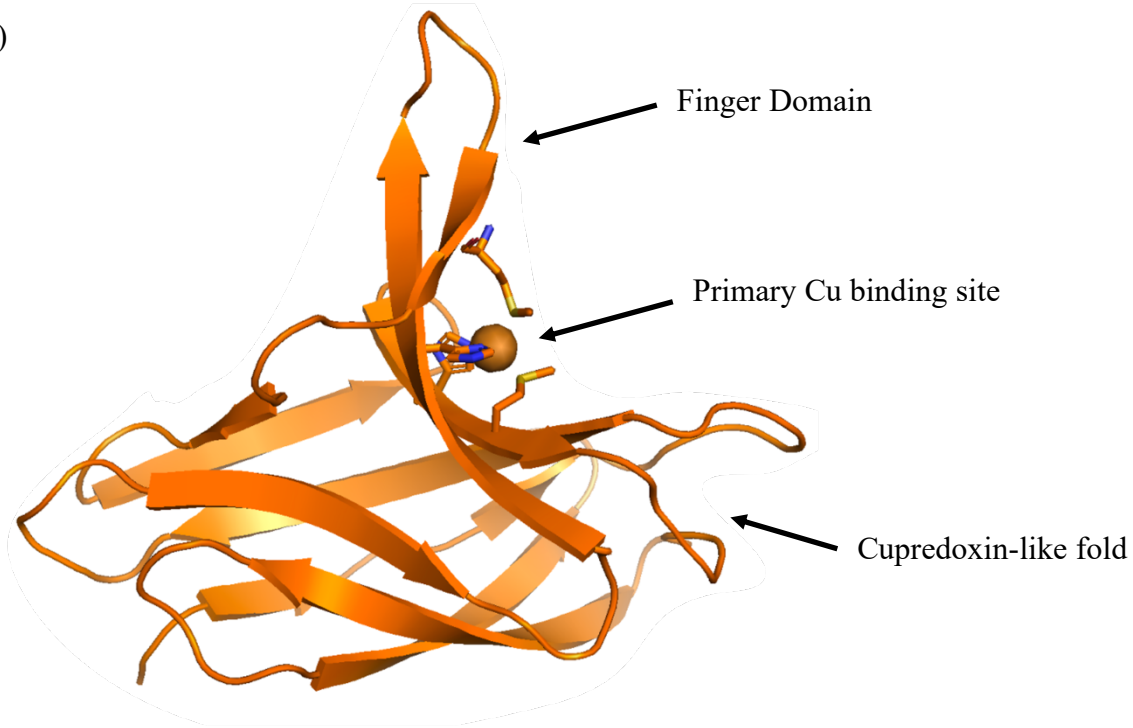

b)

```
         10         20         30         40         50
MKKLLAAVMM AGLAGAVSAA GVHVEDGWAR TTVEGMKMGG AFMKIPNDEA
         60         70         80         90        100
KQDFLLVGSS PVADRVEVHT HINDNGVMRM REVKGGVPLE AKSVTELKPG
        110        120        130        140        150
SYHVMFMGLK KQLKEGDKIP VTLKFKNAKA QTVQLEVKTA PMSAMNHGHH

HGEAHQH
```

***Figure 1.7*. The copper metallochaperone, AccA a**) Draft Crystal structure of AccA from *N. gonorrhoeae* without the C-terminal tail (48). **b**) the amino acid sequence of AccA with the key regions of the protein labelled: the signal peptide (purple), the Cu track (green), the primary Cu binding site (red), and the Met and His-rich C-terminal tail (blue).

AccA is essential for microaerobic growth in *N. gonorrhoeae* and can metalate AniA under Cu-starved conditions. However, upon supplementation with Cu AccA is no longer required for microaerobic growth or AniA activity. AccA has no effect on aerobic growth of *N. gonorrhoeae* with a Δ*accA* strain showing the same growth phenotype as the wild type. This suggests that AccA is a specific metallochaperone for AniA (30). In *N. gonorrhoeae*, any mutations to reduce the binding affinity of AccA results in no growth, suggesting relatively high binding affinity of AccA to Cu(I) ($K_D = 2.0 \times 10^{-17}$ M) is essential for the acquisition of Cu within *N. gonorrhoeae.* The exact mechanism for the metalation of AniA by AccA is not fully known, with AccA mutants without the primary Cu binding site, Cu track, and C-terminal tail still being able to metalate AniA *in vitro*. This suggests that all of the regions identified may play a role, but none are essential. In some PCu_AC-family metallochaperones, where a C-terminal tail is present, the C-terminal tail has been shown to be the site of Cu transfer to its Cu target site, this does not appear to be the case for AccA (49).

AccA is member of the PCu_AC-family of Cu metallochaperones proteins, which stands for periplasmic Cu_A chaperone after one of the first characterised PCu_AC proteins which metalates the Cu_A site in cytochrome *c* oxidase in *T. thermophilus* (12). All of the metallochaperones consist of a cupredoxin-like fold with the finger domain extension, many share the His-X_{10}-Met-X_{22}-His-X-Met, but this is not universally conserved (Discussed in chapter 5). The C- terminal tail is also not conserved. As well as the Cu_A site in cytochrome *c* oxidase site both the T1Cu and T2Cu sites in AniA, PCu_AC proteins have other targets, including Sco like proteins (50) and multiple sites in the pMMO complex (51). Often in the metalation of membrane-tethered Sco like proteins, this occurs upstream to Cu_A and Cu_B Cu centre assembly. Here, PCu_AC is not always essential for the final assembly to occur, possibly suggesting that the metallochaperones may only be required under Cu starved conditions (52).

In addition to the PCu_AC family of metallochaperones, many other families of Cu metallochaperones exist in the periplasm across bacterial species. Many of these periplasmic Cu chaperones are responsible for Cu efflux and protection against oxidative stress. These include CusF and CopG, both thought to load Cu(I) into the CusCBA efflux pathway, with CopG either replacing or loading CusF (53). CopG is thought to have dual role as a Cu oxidase, protecting against Cu stress by oxidising the more toxic Cu(I) to Cu(II) (53), as well as aiding in Cu efflux as a Cu metallochaperone. CueP is a periplasmic Cu chaperone found in *Salmonella enterica* sv. *Typhimurium.* CueP metalates the Zn-Superoxide dismutase to Cu,Zn-superoxide dismutase, preventing build-up of reactive oxygen and nitrogen species as well as sequestering Cu. This proteins are often induced by Cu sensors in response to Cu intoxication (20)(53).

1.5 project aims

Across bacterial species, the presence of both *aniA* and *accA* is not conserved. Some species in *Achromobacter*, *Alcaligenes* and *Nitrosomas* contain the *aniA* gene, but not the *accA* gene. Furthermore, across *Neisseria* species, *accA* is conserved, but *N. shayeganii* and *N. wadsworthi* do not contain *ani*A, which is the case for the majority of the *Betaproteobacteria* species (30). This suggests that the interactions between AccA and AniA may not be universally specific. AccA-like proteins may potentially form favourable interactions with and metalate other target proteins in other bacterial species. AniA may be able to be metalated by other mechanisms and in other species either by forming favourable interactions with other metallochaperones or not requiring a metallochaperone at all (30). The face of AniA that allows for protein-protein interactions for Cu insertion may be flexible to allow for the acquisition of Cu from multiple sources. A NirK from *Sinorhizobium meliloti* has been shown to have a flexible surface for protein-protein interactions with the electron donor, two pseudo Azurins (*Sm*PAZ1 and *Sm*PAZ2) both donate electrons to NirK at the same site but form different protein-protein interactions with NirK (54). This suggests that the surface of AniA may also be innately flexible and therefore, be able to bind other metallochaperones in replace of AccA.

In this project we aim to test this hypothesis by seeing if the favourable interactions between AccA and AniA to allow for Cu insertion can be replicated with another metallochaperone

that is not present in the *N. gonorrhoeae* proteome. To do this we have chosen two metallochaperones: a structural homologue in PCu_AC from *Thermus thermophilus* and a structurally distinct metallochaperone in CueP from *Salmonella enterica* sv. *Typhimurium.* We aim to test first whether we can replace AccA in *N. gonorrhoeae*, then determine the mechanism to why or why not the metallochaperones cannot metalate AniA, using purified proteins. If we determine that the two non-native metallochaperones cannot replace AccA this would suggest that AccA is likely a specific metallochaperone for AniA. Therefore, the interactions between the two proteins could be targeted in the development of novel antimicrobials against the infection of *N. gonorrhoeae.*

PCu_AC, Thermus thermophilus

PCu_AC from *T. thermophilus* (hereafter PCu_AC) is one of the most structurally similar Cu metallochaperones to AccA (*Fig.* 1.8). PCu_AC binds Cu(I) in a 1:1 stoichiometry. PCu_AC inserts two Cu ions into the Cu_A site of the ba_3 cytochrome c oxidase with the aid of the disulphide reductase, Sco1, which is often found in the same operon (12). It is hypothesised that Sco1 reduces the disulfide bond in the Cu_A site, allowing two cysteines to aid in the formation of the metal complex via metalation by PCu_AC (12). PCu_AC binds Cu at the primary site via the His-X_{10}-Met-X_{21}-His-X-Met Cu binding motif (*Fig*. 1.8). PCu_AC lacks the secondary Cu binding site at the C-terminal tail. Therefore, 1 PCu_AC proteins will metalate one Cu site. In comparison, one AccA protein could, theoretically, metalate 2 Cu sites (30). Therefore, double the amount of PCu_AC would be required to metalate AniA compared with AccA. PCu_AC also does not contain any Cu-track surrounding the primary Cu binding site. This could be a contributing reason the lower binding affinity seen for PCu_AC to Cu(I) (K_D = 2.2 x 10^{-15} M)(12). This binding affinity is lower than AccA variants that cannot deliver Cu in *N. gonorrhoeae*, but can *in vitro* (30). If this binding affinity is correct, it is likely that PCu_AC will not be able to acquire Cu in *N. gonorrhoeae.*

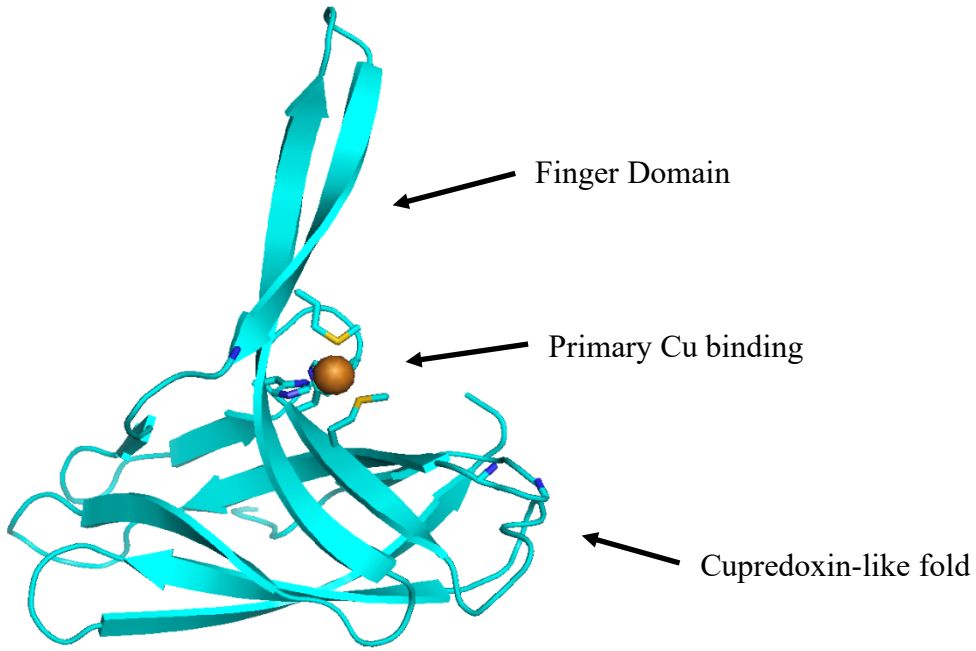

Fig. 1.8*. Structure of PCu$_A$C from *T. thermophilus. The amino acids in the primary Cu site are shown as well as the key regions of the protein (PDB ID: 2K70)

CueP, Salmonella enterica sv. Typhimurium

CueP is a Cu resistance protein from *Salmonella enterica* sv. *Typhimurium* that metalates Zn-superoxide dismutase to produce the active Cu,Zn-superoxide. CueP contributes to *S. enterica* virulence especially in limited oxygen conditions and is expressed in response to increased Cu (13). *Apo*-CueP is a homo dimer which upon binding of Cu is predicted to form a dimer of dimers with two Cu(I) ions at the dimer-dimer interface (55,56). The Cu binding sites are predicted to be identical, occurring between the separate monomers of each dimer. These Cu sites consist of His94 and Cys104 from each monomer to form a tetrahedral complex (*Fig.1.9*) (56). The binding affinities of the two sites is assumed to be identical with femtomolar affinity (K_D = 1 x 10^{-15} M) and it can be metalated by Cu(I) reduced by the disulfide reductases ScsB and ScsC (57). CueP shares no structural similarity with AccA, but each protein-Cu complex can bind 2 equivalents of Cu, therefore the same number of CueP proteins would be required to metalate AniA. CueP also has a binding affinity closer to the range seen for AccA and the ΔCu-track AccA variant, therefore it should be able to acquire Cu from the periplasm of *N. gonorrhoeae* (30).

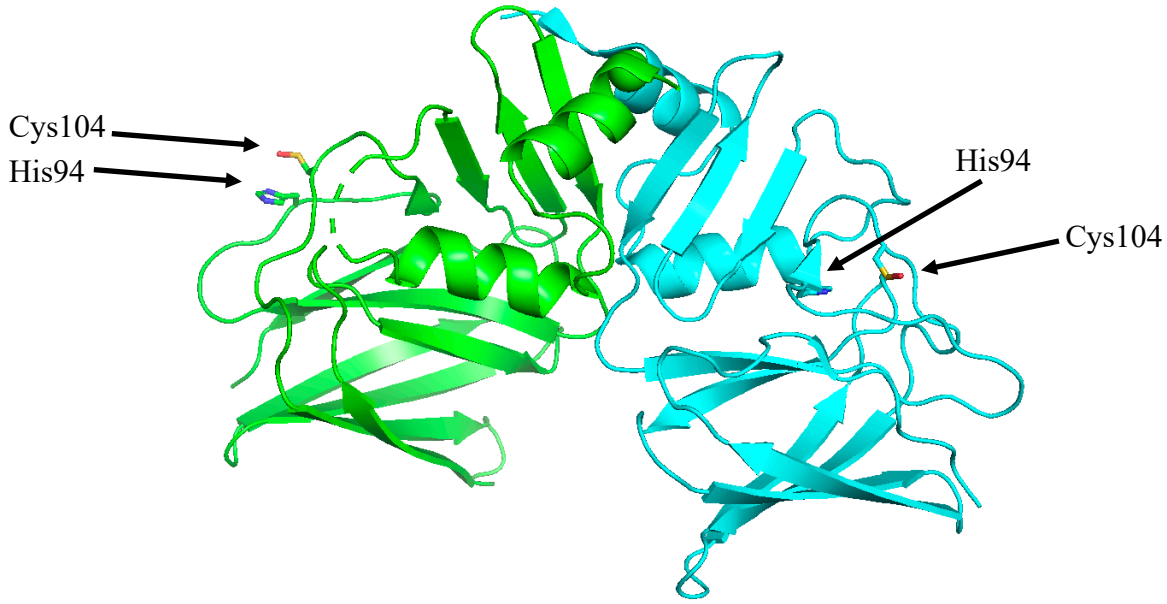

***Figure 1.9*. Crystal structure of the *apo*-CueP dimer** with the Cu-binding ligands of each monomer labelled (PDB ID: 4GQZ). The structure of the dimer of dimers is unknown.

Chapter 2: Materials and methods

2.1 Bacterial strains and growth methods

Table 2.1. **Reagents for microbial growth**. All chemicals were supplied by Melford.

Reagent	Concentration
Media	
GCBL • 300 g special peptone (Gibco bacto proteose peptone no. 3) • 100 g NaCl • 80 g K_2HPO_4 • 20 g KH_2PO_4	20 g/L
Lysogeny broth (LB)	20 g/L
LB agar	20 g/L LB 12 g/L agar
Soft GC agar	24g Oxoid GC agar base 12 g GCBL 20 X powder
Neisseria gonorrhoea **culture supplements**	
Kellogg's I • 40 g glucose • 1 g glutamine • 2 mg cocarboxylase	100 X
Kellogg's II • 10 mM $FeSO_4$	1000 X
Sodium bicarbonate 500 mM	100 X
Sodium nitrite 2 M	500 X
Antibiotics	
Ampicillin	100 μg/mL
Spectinomycin	100 μg/mL
Kanamycin	100 μg/mL
Chloramphenicol	30 μg/mL
Overexpression	
Isopropyl β-D-1-thiogalactopyranoside (IPTG) 0.1 M	1000 X

2.1.1 *Neisseria gonorrhoeae*

The strain used in this study was *Neisseria gonorrhoeae* strain 1291 (Lab collection). *N. gonorrhoeae* was propagated on soft GC agar (2:1 Oxoid agar powder to GCBL powder) supplemented with Kellogg's I and II, as described by Dillard (58). Bacteria were incubated

for 18-20 hours at 37 ˚C in an air-tight container (Oxoid AnaeroJar 2.5 L) with 5-9% atmospheric CO_2 (generated by CO_2 gas generator sachets, Oxoid).

N. gonorrhoeae microaerobic cultures (30 mL broth in 50 mL screw-capped tubes) were prepared with a starting OD_{600} value of 0.1 in gonococcal base medium liquid (GCBL) as described by Dillard (58). Kellogg's I and II supplements, and 5 (v/v) % sodium bicarbonate were added to the medium immediately before use, along with sodium nitrite to a final concentration of 2 mM. The medium was pre-warmed to 37 ˚C before inoculation. The liquid cultures were incubated for 8 hours at 37 ˚C without shaking. Sodium nitrite was additionally added to a final concentration of 2 mM at t = 5 and 7 hours. OD_{600} values were taken at t = 0, 4, 5, 6, 7, and 8 hours. After 8 hours, the liquid cultures were centrifuged (4800 RCF for 5 min at 4 ˚C in a Hettich Rotina 380 R) and the pellets were resuspended in 1 or 0.5 ml GCBL containing 20 (v/v)% glycerol for cultures with a final OD_{600} value of greater or less than 0.3, respectively. The suspensions were stored at -80 ˚C for subsequent biochemical assays.

N. gonorrhoeae aerobic cultures (15 mL broth in 50 mL screw capped tubes) were prepared in parallel to the microaerobic growths to a starting OD_{600} value of 0.1 in GCBL(58). Liquid cultures were incubated at 37 ˚C with continuous shaking in the orbital mode at 200 rpm. Sodium nitrite was supplemented to a final concentration of 2 mM at time = 0 hours. OD_{600} values were measured every hour of growth.

2.1.2 *Escherichia coli*

Escherichia coli DH5α was used for sub-cloning of all *N. gonorrhoeae* genetic constructs and the propagation of plasmids for the overexpression of both AniA and PCu_AC proteins. For overexpression of AniA, *E. coli* BL21(DE3) Rosetta 2 pLySs was used, and for PCu_AC, *E. coli* BL21(DE3) Codon(+) was used. *E. coli* strains were propagated from glycerol stocks on LB agar containing the appropriate antibiotics (*Table* 2.1) and incubating overnight at 37 ˚C.

2.2 Cloning and generation of constructs

The sequence of the PCu_AC protein was obtained from the genome of *Thermus thermophilus*, the sequence of CueP was obtained from *Salmonella enterica* sv. Typhrium and the sequence for CopG was obtained from *E. coli.* These constructs were designed by S. Firth and synthesised commercially by IDT as gBlockR gene fragments. The sequences for all constructs were confirmed using Sanger sequencing at Durham Biosciences Genomics Facility.

2.2.1 Generation of Golden Gate Assembly constructs in *N. gonorrhoeae*

All the *N. gonorrhoeae* mutant strains described in this project were generated by homologous recombination of constructs into the wild-type strain of *N. gonorrhoeae* 1291, which is naturally competent in its piliated form. Golden Gate assembly (New England Biolabs) was used to generate the genetic constructs. The sections of DNA being assembled were: 1000 bp of the 5'-upstream flanking sequence of the *accA* gene, the non-native metallochaperone gene fused to the gene encoding the *accA* N-terminal leader sequence, a

specR cassette encoding spectinomycin resistance (amplified from pCTS32 plasmid), and 1000 bp of the 3'-downstream flanking sequence of the *accA* gene.

The *specR* gene was directly downstream of the *accA* gene without its own promoter and it was upstream of the *accA* stop codon. The *specR gene* was followed by the *Neisseria* DNA uptake sequence GCCGTCTGAA, which allows for the uptake of the construct into the gonococci (58). The 5'-upstream and 3'-dpwnstream flanking regions of *accA* subsequently allow for the correct recombination into the genome.

Firstly, all sections of DNA, except the metallochaperone gene, were amplified by PCR using the Q5 DNA polymerase (New England Biolabs) and primers that contained *BsaI* cleavage sites and the appropriate overhangs (*Table* 2.2). PCR products were subcloned into the *SmaI* site of plasmid pTRB479 (Blower Lab, Durham University), which lacks *BsaI* cleavage sites, before assembly using the NEB® Golden Gate Assembly Kit (*BsaI*-HF®v2) following the manufacturer's protocol. The desired final assembly was in the order: 5'-upstream > *metallochaperone* > *specR* > 3'-downstream (*Fig*. 2.1). This assembly approach was ultimately unsuccessful (data not shown).

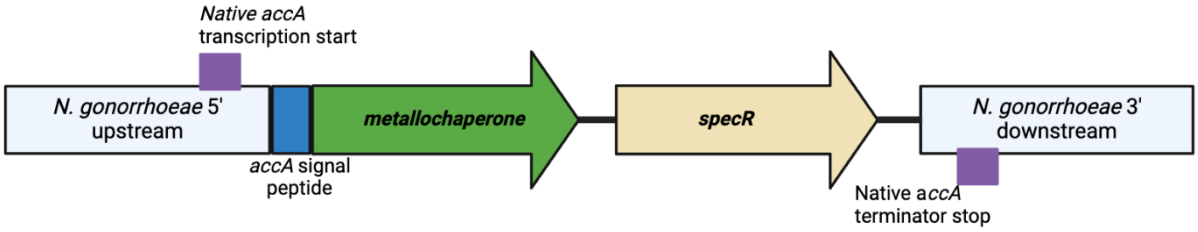

Figure 2.1. **Desired genetic construct for insertion into *N. gonorrhoeae,*** where *metallochaperone = pCu$_A$C, cueP,* or *copG.*

In the second approach the *accA→specR* vector was amplified by PCR, removing the *accA* gene (*Table* 2.2). This vector contains all aspects of the construct required for the transformation into the correct position in the genome of *N. gonorrhoeae*. The metallochaperone genes were also amplified by a separate PCR reaction (*Table* 2.2). All PCR products were then assembled using the NEB® Golden Gate Assembly Kit (*BsaI*-HF®v2) following the manufacturers protocol (*Fig.* 2.1). The assembled plasmids were checked by PCR, to verify insertion of the metallochaperone genes. The results showed the correct product lengths for *pCu$_A$C* and *copG* constructs, and a mixture of two products for *cueP*. The correct product for *cueP* was obtained by selection after transformation into *N. gonorrhoeae* 1291 (Chapter 3.2).

Transformation of all *pCu$_A$C*, *cueP*, and *copG* -containing plasmids into *E. coli DH5α* was attempted, however this was unsuccessful. Instead, the plasmids were amplified by PCR (*Table* 2.2). The PCR product was sent for Sanger sequencing at Durham Biosciences Genomics Facility. These sequencing results showed that the *pCu$_A$C* and *cueP* constructs, but not *copG*, were assembled correctly. Therefore, the *copG* construct was not used in any further investigation.

To transform into *N. gonorrhoeae,* the *pCu$_A$C* and *cueP*-containing constructs were linearised by PCR using primers 5'upstream-F and 3' downstream-R (*Table* 2.2). Transformation followed the procedure followed by Dillard (58). Briefly, 8 piliated (appear opaque) colonies of *N. gonorrhoeae* were selected and streaked through 10 µl of 1 µg of linearised DNA on GC agar plates. The plates were incubated at 37 ˚C for 7 hours and colonies were re-streaked onto fresh GC agar plates containing spectinomycin. These new plates were incubated at 37 ˚C for 18 hours. From each transformation, 8 colonies were selected at random, propagated on fresh GC agar plates containing spectinomycin, and verified by colony PCR and Sanger sequencing. For the *cueP* transformants, all GC agar plates were supplemented with 10 µM Cu (Chapter 3).

2.2.2 Generation of PCu$_A$C overexpression constructs in *E. coli*

Overexpression constructs for *Tt*-PCu$_A$C were generated by S. Firth using the *pCu$_A$C* gene previously codon optimised for *E. coli.* The gene was amplified by PCR for Ligation Independent Cloning (LIC) using primers PCu$_A$C O/E -F and -R to generate 5' and 3' LIC overhangs (*Table* 2.2). The gene was inserted into the *StuI* site of pSATL vector, which created an N-terminal His$_6$-SUMO tag for protein purification. To achieve this insertion, the vector and *pCu$_A$C* gene were incubated with dTTP or dATP, respectively, and T4 DNA polymerase (New England Biolabs) to create complementary overhangs.

Table 2.2. **Primers used in this study** with the *Bsa1* cleavage sites underlined.

Construct name	Primer Name	Sequence (5'→3')	Template	Use
Metallochaperone constructs for *N. gonorrhoeae*				
accA → specR construct for amplification of *specR → 5'-upstream* (S. Firth, PhD thesis, 2023)	5' upstream-F	CAGTTGGGTCTCCGGAGGACAAACGCATCTTGATTATCG	pUC19::*accA→specR*	Amplification and linearisation of construct for insertion and amplification of *5'-upstream* insert
	5' upstream-R	CAGTTGGGTCTCCATCTTCCTGCTCCTTTAATATCAG		Amplification of the *specR→5'upstream* vector
	Metallochaperone -F	CAGTTGGGTCTCCAGATGAAAAAATTATTGGCAGCCG		Amplification of the metallochaperone insert for insertion into the *specR → 5' upstream* vector
	specR -R	CAGTTGGGTCTCCGAAAGGTGTTTCCACCATTTTT		Amplification of the *specR* insert
	3' downstream-F	CAGTTGGGTCTCGTTTCTGCTGGAAATATTTGAAATGC		Amplification of *3'-downstream* insert
	3' downstream-R	CAGTTGGGTCTCGATGGCGTGAAACTCAAATCGTTCA		Amplification and linearisation of construct for transformation and amplification of *3'-downstream* insert
Metallochaperone → specR vector for GG assemply of the 4 constructs	*5' upstream-metallochaperone* -F	GGCTACGGTCTCAGAGCAGGAAGATGAAAAAATTATTGGC		Amplification of the *metallochaperone* insert for GG assembly of the 4 inserts
	5' upstream-metallochaperone -R	GGCTACGGTCTCAGCTCCTTTAATATCAGACGGG		Amplification of the *5' upstream* insert for GG assembly of the 4 inserts
	Metallochaperone-specR -F	GGCTACGGTCTCCTAATAGGTACTAATGAAAATAGTGAGGAGG		Amplification of the *specR* for GG assembly of the 4 inserts
pCu$_A$C → specR	*pCu$_A$C* -R	GGCTACGGTCTCTAGTACCTATTTCAGCGTGCTTCAACCGG	GenScript synthesised DNA – *pCuAC T. thermophilus*	Amplification of the *pCuAC* insert for insertion into the *specR → 5'upstream* vector
	pCu$_A$C-specR -F	GGCTACGGTCTCTTACTAATGAAAATAGTGAGGAGG		Amplification of the *specR → 5'upstream* vector
	pCu$_A$C -R	GGCTACGGTCTCAATTATCAGCGTGCTTCAACC		Amplification of the *pCuAC* for GG assembly of the 4 inserts
cueP → specR	*cueP* -R	GGCTACGGTCTCCTAGTACCTATTTTAGCGAAGGGGAAGCTC	GenScript synthesised DNA – *cueP S. enterica*	Amplification of the *cueP* insert for insertion into the *specR → 5'upstream* vector
	cueP-specR -F	GGCTACGGTCTCCACTAATGAAAATAGTGAGGAGG		Amplification of the *specR → 5' upstream* vector
	cueP -R	GGCTACGGTCTCAATTATTAGCGAAGGGGAAGCTC		Amplification of the *cueP* for GG assembly of the 4 inserts
copG → specR	*copG-specR* -R	GGCTACGGTCTCAAGTACCTATTCTATTCAATACGCTGGAAG	GenScript synthesised DNA – *copG E. coli*	Amplification of the *copG* insert for insertion into the *specR → 5'upstream* vector
	copG-spec R-F	GGCTACGGTCTCATACTAATGAAAATAGTGAGGAGG		Amplification of the s*pecR → 5' upstream* vector
	copG -R	GGCTACGGTCTCCATTACTATTCAATACGCTGGAAGACC		Amplification of the *copG* for GG assembly of the 4 inserts
pCuAC → specR *cueP → specR* *copG → specR*	M13-F	TGTAAAACGACGGCCAGT	pUC19	Checking GG assembly of full construct into pUC19 and amplification for sequencing
	M13-R	CAGGAAACAGCTATGAC		
Protein overexpression				
pSAT1L:PCuAC	PCu$_A$C O/E-F	CAACAGCAGACGGGAGGTCAAGTTGTACGTGAAGGGTGG	*pCuAC → specR* Golden Gate assembly reaction	Amplification of the *pCuAC* insert for insertion into the pSATL vector
	PCu$_A$C O/E-R	GCGAGAACCAAGGAAAGGTTATTAGCGTGCTTCAACCGGCAAAAC		

***Table 2.3*. Plasmids generated and used in this study**

Plasmid name	Description	Source	Strain stocked
Vectors			
pUC19	Cloning vector	New England Biolabs	*E. coli* DH5α
pUC19::*accA*→*specR*	Cloning vector with template construct	S. Firth-Djoko Lab (Durham)	*E. coli* DH5α
pSATL	His_6-SUMO tagged expression vector	T. Blower Lab (Durham)	*E. coli* DH5α
pTRB479	pUC19 plasmid with *BsaI* cleavage sites	T. Blower Lab (Durham)	*E. coli* DH5α
Overexpression			
pSAT1L:PCu_AC	Plasmid overexpression construct for wild-type PCu_AC. Subcloned between the His_6-SUMO and T7 terminator.	This work	*E. coli* DH5α

2.3 Protein Overexpression and Purification

***Table 2.4*. Buffers used for protein purification** and their recipes

Buffer	Recipe
Resuspension Buffer	50 mM Tris-HCl pH 8.0, 150 mM NaCl, 25 mM imidazole, 15% v/v glycerol
His-Trap A	50 mM Tris-HCl 50 mM Tris-HCl pH 8.0, 150 mM NaCl, 25 mM imidazole
His-Trap B	50 mM Tris-HCl 50 mM Tris-HCl pH 8.0, 150 mM NaCl, 250 mM imidazole
Q-column A 1	50 mM Tris-HCl pH 7.0
Q-column A 2	50 mM Tris-HCl pH 8.0
Q-column B 1	50 mM Tris-HCl pH 7.0, 250 mM NaCl, 15% v/v glycerol
Q-column B 2	50 mM Tris-HCl pH 8.0, 250 mM NaCl, 15% v/v glycerol
SP-column A	50 mM MOPS pH 5.9
SP-column B	50 mM MOPS pH 7.2, 250 mM NaCl, 15% v/v glycerol
SEC-buffer A	20 mM Tris pH 7.9, 150 mM NaCl
SEC-buffer B	50 mM MOPs pH 7.2, 150 mM NaCl

2.3.1 Overexpression and purification of AniA protein

E. coli BL21:AniA, generated by S. Firth (30), was plated on LB agar containing kanamycin and chloramphenicol (*Table* 2.1) and incubated at 37 ˚C overnight. Cells from the plates were resuspended in 10 mL of LB medium, which were then used to inoculate 2 L flasks containing 1 L of LB to an OD_{600} of 0.01 with kanamycin and chloramphenicol then added (*table 2.1*). Cultures were shaken at 200 rpm at 37 ˚C until they reached an OD_{600} of 0.6. The cultures were cooled to 22 ˚C. Protein expression was induced by adding IPTG to a final

concentration of 0.1 mM and more kanamycin (*Table* 2.1) was added to the cultures to maintain the selection pressure or the plasmid. The cultures were then shaken for a further 4 hours. Cells were harvested by centrifugation in an Avanti J26-XP centrifuge with a JLA-16.250 rotor (5000 rpm, 15 min, 4 °C) (Beckman), resuspended in resuspension buffer (*Table* 2.3), lysed by sonication (Amplitde: 40%) using a Q700CA sonicator with 4207 Sonicator probe (Q sonica), and finally clarified by centrifugation (21000 rpm, 4 ˚C, 15 minutes) using an Avanti J26-XP centrifuge with a JA-25:50 rotor (Beckman). Any remaining insoluble debris and aggregates were removed by filtration through 0.45 µm polyethersulfone (PES) filter.

Cell lysates that contained AniA protein were loaded onto a HisTrap™ HP 5 ml column (Cytiva). The column was washed with 20 column volumes (C.V.) of His-Trap A buffer or until the solution absorbance at 280 nm returned to baseline. The bound protein was eluted with 3 C.V. of His-Trap B buffer. Protein-containing fractions were diluted three-fold with Q-column A1 buffer to reach an overall NaCl concentration of <50 mM. The diluted sample was then loaded onto a HiTrap™ Q HP 5 mL column (Cytiva) and washed with 20 C.V. of Q-column A1 buffer to remove any remaining unbound proteins. AniA was then eluted with 3 C.V. of Q-column B1 buffer. Thrombin (10 U or 5 U per 1 mg of protein; Cytiva) was added to the eluted protein and the mixture was incubated overnight (room temperature, 60 rpm) to remove the His_6 tag. The cleaved protein was re-loaded on a HisTrap™ HP 5 ml column. The desired, cleaved AniA protein was found in the flow through. The column was then washed with 20 C.V. of His-Trap A buffer to remove any weakly bound, cleaved AniA. Any uncleaved His_6 tagged AniA was eluted with His-Trap B buffer and stored for future purification. All fractions containing the cleaved AniA were combined and diluted in Q-column A1 buffer to a NaCl concentration <50 mM and finally loaded onto a HiTrap™ Q HP 5 mL column. The column was washed with 20 C.V. of Q-Column A1 buffer then the protein was eluted in 1 mL fractions with Q column B buffer and stored at -80 ˚C.

2.3.2 Overexpression and Purification of PCu_AC

E. coli BL21 codon(+) pSAT1L:PCuAC was grown overnight at 37 ˚C shaking at 200 rpm in LB medium containing both ampicillin and chloramphenicol (*Table* 2.1). The culture medium was then used to inoculate 1 L of LB medium in 2 L flasks to an initial OD_{600} reading of 0.01 with ampicillin and chloramphenicol added (*Table* 2.1). The cultures were then grown at 37 ˚C shaking at 200 rpm until an $OD_{600} > 0.4$ was reached (3-4 hours). The cultures were cooled on ice and protein overexpression was induced by a final concentration of 0.1 mM IPTG. More ampicillin was also added to maintain the selection pressure for the plasmid (*Table* 2.1), and the cultures were shaken at room temperature (22 ˚C) for a further 16 hours. The cultures were centrifuged (6000 rpm, 4 ˚C, 15 minutes) using an Avanti J26-XP centrifuge with a JLA-16.250 rotor. The bacteria were resuspended in the resuspension buffer and lysed by sonication (Amplitude: 40%) using a Q7000CA sonicator with the 4207 Sonicator probe. The lysed cells were clarified via centrifugation (21000 rpm, 4 ˚C, 15 minutes) using an Avanti J26-XP centrifuge with a JA-25:50 rotor. The remaining aggregates and other solid debris were removed through filtration with 0.45 µm PES filter.

Cell lysates containing His_6-SUMO tagged PCu_AC were loaded on to a HisTrap™ HP 5 ml column. The column was then washed with 20 C.V. of His-Trap A buffer or until the absorbance at 280 nm remained constant. The bound His_6-SUMO tagged PCu_AC was then eluted with 3 C.V. of His-trap B buffer. The fractions containing eluted protein were then combined and diluted to a NaCl concentration <50 mM and loaded onto a HiTrap™ Q HP 5 mL column. After washing with 20 C.V. of Q-column A2 buffer, PCu_AC was eluted wit 3 C.V. of Q-column B2 buffer. Fractions containing PCu_AC protein were combined and incubated overnight with His tagged-hSENP2 SUMO protease (Blower Lab, Durham University) at 4 ˚C with shaking at 50 rpm to cleave the His_6-SUMO tag. To remove the tag and protease, the sample was loaded on to a HisTrap™ HP 5 ml column. The PCu_AC protein was found in the flow through which was collected. The column was washed with 20 C.V. of His-trap A buffer to remove weakly bound PCu_AC. Any uncleaved His_6-SUMO tagged PCu_AC was eluted with 3 C.V. of His-trap B buffer and stored for any future purification. The flowthrough and His-trap A buffer wash fractions containing PCu_AC were combined and loaded onto a HiTrap™ Q HP 5 mL column to remove any negatively charged contaminants. PCu_AC was found in the flow through. The pH of the flowthrough was reduced to 5.9 through the addition of solid MOPS free acid. The protein was then loaded onto a HiTrap™ SP HP 5 ml column (Cytiva). The column was washed with 10 C.V. of SP-column A buffer, which resulted in some loss of protein. PCu_AC was eluted in 500 µL fractions with SP-column B buffer.

2.3.3 Confirmation of protein via mass spectrometry

The molecular weights of all purified proteins were confirmed using Time-of-Flight Electrospray ionisation mass spectrometry in the positive ion mode at Durham University's Mass Spectrometry service, Department of Chemistry. Protein sequences were also confirmed by the Proteomics Facility, Department of Biosciences, Durham University.

2.4 Calculating rate of nitrite consumption by *N. gonorrhoeae*

2.4.1 Calculating nitrite consumption

Nitrite consumption by intact *N. gonorrhoeae* cells was measured using Griess reagent (Sigma Aldrich) (59). Frozen pellets from microaerobic cultures were thawed on ice and resuspended in GCBL. The volume of GCBL used depended on the final OD_{600} values. The *ΔaccA/accA*$^+$ strain grew to a high OD_{600} value (> 0.4) and was diluted in 1.5 ml GCBL. Other strains were diluted to achieve approximately the same concentration of cells. Two 250 µl aliquots were taken from the resuspension. The first aliquot was set aside for quantification of protein content (described below). The second aliquot was immediately incubated at 37 ˚C. After 10 minutes, 200 µL of this suspension was added to 3 µL of 100 mM $NaNO_2$, to reach a final nitrite concentration of 1.5 mM and to initiate nitrite consumption. The reaction mixtures were sampled at t = 0, 1, 2, 3, 4, 5, 7, and 10 minutes and 5 µL of each were immediately diluted 20-fold into a 1:1 mixture of deionised water and Griess reagent. When nitrite is added to Griess reagent, the Griess reagent turns pink and absorbs light at 545 nm. Therefore, the concentration of nitrite at each time point was determined by comparing the absorbance of each sample against a standard curve of nitrite (4, 2, 1, 0.5, 0.25, 0.125,

0.0625, and 0 mM) diluted 20-fold in the same 1:1 mixture of deionised water and Griess reagent.

2.4.2 Measurements of protein concentration in cells

Total amounts of protein in *N. gonorrhoeae* pellets were determined using the QuantiPro™ BCA kit (Sigma) following the manufacturer's guidelines. The first 250 µL aliquot from section 2.4.1 was centrifuged at 16,200 × *g* for 1 minute and resuspended in 250 µL of Phosphate-buffered saline (PBS). The suspension was frozen until further use. When needed, the suspension was thawed and serially diluted by 2.5, 5, 10, 20, 40, 80, 160-fold in PBS. Each dilution (20 µL) was then added to the Quantipro™ BCA reagent (180 µL) in a flat-bottomed 96-well microtiter plate, which was wrapped in cling film and incubated at 50 ˚C for 2 hours. The absorbance of each sample was measured at 562 nm and compared to a standard curve of Bovine Serum Albumin (BSA; 400, 300, 200, 100, 50, 25, 12.5, 0 µg/mL).

2.4.3 Calculating percentage rate of nitrite consumption vs WT control

Nitrite concentrations were plotted against time and a linear regression was used to calculate the slope and, therefore, the rate of nitrite consumption in µM / min. This rate was then normalised to the protein concentration in each sample to generate the concentration of nitrite consumed in µmol per min per g of protein.

2.5 Determining metal concentrations of *N. gonorrhoeae* strains

Bacteria were cultured overnight at 37 ˚C on GC agar plates containing $CuSO_4$ (final concentrations of 0 µM and 10 µM for all strains or 0, 1, 5, 10, 20, 40, 100 µM for *N. gonorrhoeae ΔaccA/accA*$^+$). Cells were collected and resuspended in PBS. Half of the suspension was pelleted (4800 RCF, 5 min, 4°C) whilst the other half was stored for protein concentration determination (Chapter 2.4.2). The pellet was washed with 50 mM EDTA, and then digested with nitric acid (45%, 2 hours, 90 °C). The levels of manganese (Mn), iron (Fe), Cu, and zinc (Zn) were determined using Inductively coupled plasma mass spectrometry (ICP-MS) at the Metallomics Facility, Durham Biosciences. Metal levels were normalised to protein concentrations. Cellular metal concentrations were expressed as µmol metal/µg of protein.

2.6 Estimation of metal binding affinity *via* ligand competition

2.6.1 Principles of equilibration competition reactions to estimate K_D

An unknown metal binding affinity of a protein can be accurately determined by equilibrium competition with spectrophotometric probes with known affinities at a particular pH. This process involves measuring the concentration of either the free probe or the metal-bound probe at equilibrium. The binding affinity of the protein can be calculated *via* mass-balance equations.

To determine the dissociation constant (K_D) of a protein, the metal (M) must be able to be transferred from the protein (P) *via* competition with the ligand (L) with a known K_D at a fixed pH. Where all ligands form complexes with the metal in a 2:1 ratio, competition at equilibrium and the exchange constants (K_{ex}) can be described by:

(eq. 1)

$$P + ML_2 \rightleftharpoons PM + 2L \quad K_{ex} = \frac{[ML_2][P]}{[L]^2[MP]} = K_{D(P)}\,\beta_{2(ML2)}$$

Where P = Protein, L = Ligand/Probe, M = Metal, and K_D = dissociation constant and $\beta 2$ = conditional accumulated formation constant for ML_2, for a specific pH. Where:

(eq. 2)

$$\beta_{2(ML2)} = \frac{[ML_2]}{[M_{(aq)}][L]^2}$$

K_{ex} can be measured due to the spectroscopic probes reporting $[ML_2]$ and the other components can be calculated by mass balance. Both the total concentrations and equilibrium concentrations of the probe, protein, and metal can be determined by a competition assay and measuring the absorbance of the solution. DynaFit (BioKin) can then be used to fit the data and if the binding affinity of the probe is known, then the unknown K_D of the studied protein can be calculated (60,61).

2.6.2 Determination of metal and probe concentrations

Concentrations of stock solutions of $CuSO_4$ were estimated using excess bathocuproine disulfonic acid (BCS) as a colorimetric reporter for Cu(I). A master stock was prepared containing excess BCS (1 mM) and sodium ascorbate (2 mM) in 50 mM MOPS buffer pH 7.2. Different serial dilutions of $CuSO_4$ were added to this master mix and left to incubate for ~1 minute. A UV/Vis spectrophotometer (Genesys®) was then used to measure the absorbance at 483 nm of each solution to obtain the concentration of $[Cu^{I}(BCS)_2]^{3-}$ using the Beer-Lambert Law and an extinction coefficient of $\varepsilon_{483} = 13000\ cm^{-1}\ M^{-1}$. This reported the concentration of $CuSO_4$ in the stock.

(eq. 3)

$$2\ BCS + Cu^{I} \rightleftharpoons Cu^{I}(BCS)_2$$

The concentrations of the colorimetric probes BCS, bicinchonic acid (BCA), and ferrozine (Fz) were estimated using the stock of $CuSO_4$ with a known concentration. A master stock solution was prepared of the probe (with a presumed concentration of 120 µM), and sodium ascorbate (2 mM) in 50 mM MOPS buffer pH 7.2. A serial dilution of $CuSO_4$ was prepared in deionised water and 15 µL was added to 135 µL of the master stock solution. The absorbance at 483 nm was then measured and the results were plotted against Cu concentration. DynaFit (BioKin Ltd) was used to fit the curves to an equation describing the equilibrium of Cu binding (eq. 3 as representative for BCS). Each curve showed an abrupt end point

corresponding to the concentration at which the probes became saturated which lay between 2 Cu concentrations. This endpoint was used to determine the stock probe concentrations using the Cu:Probe ratio of 1:2. These generated curves were then used for the control curves in all protein ligand competition assays.

***Table 2.5*. Properties of the colorimetric probes used in this study (60).**

Probe	Complex	Binding constant: β_2 (M^{-2})	*Holo* λ_{max} (nm)	ε (cm^{-1} M^{-1})
BCS	$[Cu^{I}(BCS)_2]^{3-}$	6.3×10^{19}	483	13000
BCA	$[Cu^{I}(BCA)_2]^{3-}$	1.6×10^{17}	562	7900
Fz	$[Cu^{I}(Fz)_2]^{3-}$	1.3×10^{15}	470	4320

2.6.3 Estimation of the Cu(I) binding affinity of PCu_AC

The dissociation constant (K_D) of PCu_AC was determined by competition with the colourimetric probes BCS, BCA, and Fz (*Table* 2.5). A master stock solution containing the probe, PCu_AC (40 µM or 20 µM), and sodium ascorbate (2 mM) in 50 mM MOPS buffer pH 7.2 was prepared. A known concentration of $CuSO_4$ (15 µL) was added to 135 µL of the master stock in a 150 µL UVette® (Eppendorf®). The optical spectrum for each solution was then recorded between 400 nm and 800 nm. The absorbance at λ_{max} for each probe (*Table* 2.5) was plotted against Cu concentrations. The data were fitted to a curve describing the equilibrium between the probe and PCu_AC in DynaFit, which was then used to calculate the K_D value for PCu_AC. The BCS competition assay was performed in triplicate, while the BCA and Fz competition assays in duplicate.

2.7 Measuring copper loading into AniA

To measure the metalation of the T1Cu site of AniA, all Cu loading experiments were performed in 50 mM Tris-HCl (pH 7.4, 150 mM NaCl,15 v/v % glycerol). A known concentration of $CuSO_4$ or Cu(I)-PCu_AC was added to *apo*-AniA (70 µM) in a 2:1 molar ratio. Solution absorbances, either at a fixed wavelength or over the entire visible range were measured over time using the Genesys® UV/vis spectrophotometer or Cary 3500 Compact UV-Vis spectrophotometer (Agilent).

To measure the final stoichiometry of AniA, the protein mixture was loaded onto a 1 mL Q-Column (Cytiva) and washed with Q-column A1. PCu_AC was found in the flow through while AniA was bound to the column and was eluted with Q-column B1. Protein concentrations in the different fractions were determined as above, and the samples were sent for ICP-MS analysis at Durham Biosciences Metallomics facility.

2.8 Estimation of Protein Concentrations

The protein concentration of both PCu_AC and AniA in samples was determined using the solution absorbance at 280 nm. The extinction coefficients (ε) were predicted using ExPASy

ProtParam based on the amino acid sequences. For AniA it was predicted that ε_{280} = 24870 $cm^{-1}M^{-1}$ while for PCu_AC it was ε_{280} = 8480 $cm^{-1}M^{-1}$.

The concentration of PCu_AC was also independently determined by quantifying the concentration of bound Cu(I), assuming a stoichiometry of 1:1 Cu:PCu_AC, as previously demonstrated (12). Excess Cu and excess sodium ascorbate were added to PCu_AC and incubated on ice for 30 minutes. Unbound Cu was removed using a PD-10 desalting column (Cytiva). *Holo*-PCu_AC (50 µL) was denatured in 50 mM MOPS pH 7.2 and 6 M guanidine hydrochloride (50 µL). Exactly 75 µL of the denatured sample was added to 75 µL of 50 mM MOPS pH 7.2 containing excess BCS and 2 mM sodium ascorbate to determine the concentration of Cu. BCS should outcompete the denatured PCu_AC for Cu(I), therefore the total Cu concentration of the sample can be determined using the extinction coefficient for $[Cu^I(BCS)_2]^{3-}$ (*Table* 2.5). Because PCu_AC binds Cu in a 1:1 ratio, the concentration of PCu_AC is the same as that of Cu. This assumes that the metal binding site of PCu_AC is completely saturated with Cu(I).

2.9 Mass photometry

Mass photometry on the Refeyn OneMP instrument (Refeyn) uses light scattering to measure mass of molecules in solution. The instrument was calibrated using commercial protein marker standards and blanked with 1X PBS buffer. Each protein sample was serially diluted to give a final concentration in the 10 nM range. Light scattering was measured for 1 minute and compared to the calibration curve. The calculated mass of the protein was plotted against the number of counts. The experiments were only performed once and therefore the data is preliminary.

Chapter 3: The effect of non-native metallochaperones on *N. gonorrhoeae* and AniA

3.1 The role of non-native metallochaperones in AniA activity *in vivo*

N. gonorrhoeae uses a truncated denitrification pathway to grow under limited-O_2 conditions (Chapter 1.3). These conditions can be generated *in vitro* by growing *N. gonorrhoeae* in static cultures with the addition of nitrite at regular intervals. The bacterial pellets from these growths can then be used to assess nitrite consumption, and therefore activity, of AniA. Under these conditions, it has been shown that the metallochaperone AccA is required metalation of AniA and therefore AniA activity and *N. gonorrhoeae* growth. This requirement disappears when the media is supplemented with Cu, which negates the need for a metallochaperone (30).

There are three possible variables that affect metalation *in vivo*: (1) the ability for the metallochaperone to form favourable interactions with the target protein; (2) a favourable thermodynamic gradient for metal transfer from the metallochaperone to the target; and (3) the ability for the metallochaperone to acquire Cu from the cell (16). The first two of these can be tested *in vitro*. However, due to the very specific, but unknown bioavailability of Cu in the periplasm of *N. gonorrhoeae*, the third possibility can only be tested by comparing the results from both *in vivo* and *in vitro* experiments (discussed later).

For example, previous work by S. Firth showed that, *in vitro*, AccA mutant proteins that displayed reduced binding affinities for Cu(I), such as ΔCu-track-AccA and ΔCu-primary-AccA (*Fig*. 1.7 b), can still metalate the T1Cu site of AniA *in vitro* to a similar extent with the wild-type AccA protein (30). However, a *N. gonorrhoeae* Δ*Cu-primary-accA* mutant strain displayed a complete reduction of growth. This observation suggests that mutant AccA proteins can form the favourable interaction with AniA. However, due to their lower binding affinity to Cu(I), it was hypothesised that these mutant proteins cannot acquire Cu(I) from the buffered periplasmic Cu pool. As a result, Cu(I) cannot then be delivered to AniA.

3.2 Generating *N. gonorrhoeae* metallochaperone mutants

To determine the ability of the non-native metallochaperones, CueP and PCu_AC, to metalate AniA in *N. gonorrhoeae*, the soluble domain the AccA protein in *N. gonorrhoeae* was replaced by the soluble domains of CueP and PCu_AC to generate the Δ*accA/cueP*$^+$ and the Δ*accA/pCu$_A$C*$^+$ mutant strains, respectively. The transcriptional promotor and terminator and the N-terminal leader peptide of *accA* were left intact so that the non-native metallochaperones would be expressed and matured in the same way as AccA. A spectinomycin-resistant cassette was inserted immediately downstream of the protein coding region as a selection marker.

The *accA*$^+$ strain containing the *specR* gene was used as the isogenic parent control in all experiments because it displayed the same growth phenotype as wild-type *N. gonorrhoeae* 1291 (30). Conversely, the Δ*accA* deletion strain containing the *specR* gene was used as the isogenic negative control.

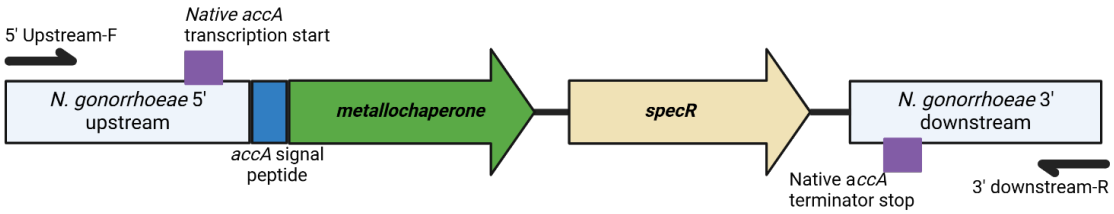

***Figure 3.1*. Visualisation of the constructs for the insertion *cueP* and *pCu$_A$C* genes into *N. gonorrhoeae* 1291**. The *specR* cassette directly follows the *accA* gene. The 5'-upstream and 3'-downstream regions flanking the *metallochaperone→specR* cassette allow for homologous recombination, transcription, and translation of the cassette akin to that of the wild-type *accA* gene. The 5' upstream-forward and 3' downstream-reverse primers were used for amplification from genomic DNA to check correct uptake.

N. gonorrhoeae transformants containing the desired metallochaperone sequence were screened on GC agar plates containing spectinomycin. For the Δ*accA/pCu$_A$C*$^+$ mutants, eight colonies were selected and confirmed by colony PCR using the 5' upstream-forward and 3' downstream-reverse primers (*Fig*. 3.1, 3.2 a) and Sanger Sequencing. For the Δ*accA/cueP*$^+$ mutants, initially no colonies were obtained suggesting no uptake of the *cueP* gene. Supplementation with 10 µM $CuSO_4$ resulted in growth of colonies, suggesting that an increased cellular Cu availability is required for the growth of the Δ*accA/cueP*$^+$ mutants. Uptake of the *cueP→specR* cassette was identified by colony PCR using the 5' upstream-forward and 3' downstream-reverse primers (*Fig*. 3.1, 3.2 b) and Sanger Sequencing. The observation that the Δ*accA/cueP*$^+$ mutants only grew on Cu-supplemented plates suggests that CueP may impact cellular Cu homeostasis, which will be assessed later in this chapter. All future experiments using Δ*accA/cueP*$^+$ were conducted by preparing bacteria initially on GC agar supplemented with 10 µM $CuSO_4$.

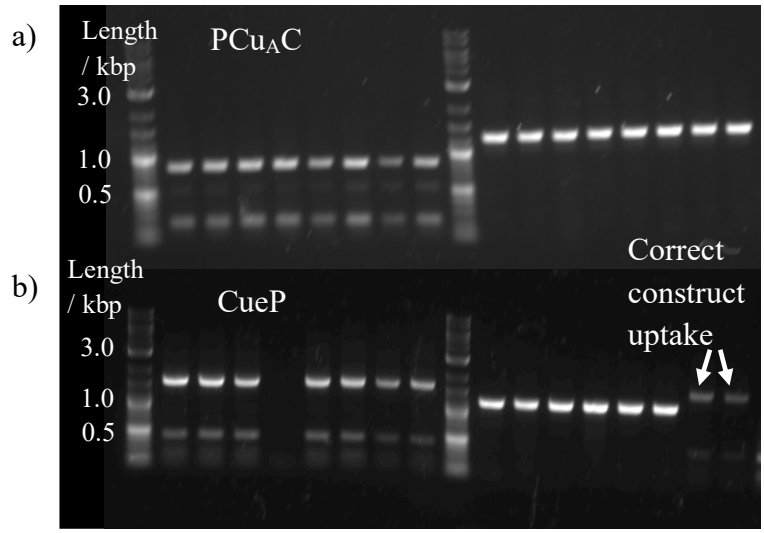

***Figure 3.2*. DNA agarose gel of colony PCR of *N. gonorrhoeae* Δ*accA/pCu$_A$C*$^+$ and Δ*accA/cueP*$^+$ transformants** (**a**) Colony PCR amplification of *pCu$_A$C* to 3'-downstream and 5'-upstream to *pCu$_A$C*, respectively. (**b**) Colony PCR amplification of *cueP* to 3'-downstream and 5'-upstream to *cueP*, respectively.

3.3 PCu_AC cannot functionally replace AccA in *N. gonorrhoeae.*

The ability for PCu_AC to metalate AniA was assessed by measuring growth and NO_2^- consumption under microaerobic conditions of two replicate Δ*accA*/*pCu$_A$C*$^+$ mutant strains. These measurements were compared to both *accA*$^+$ and Δ*accA* control strains, which were grown and assessed in parallel. It was hypothesised that PCu_AC would not metalate AniA. Therefore, there would be no growth under microaerobic conditions due to a lack of AniA activity.

As reported previously, the *accA*$^+$ grew while the Δ*accA* did not (14,30). As expected, the Δ*accA*/*pCu$_A$C*$^+$ strains did not grow, much like Δ*accA* (*Fig*. 3.3a), which is consistent with inactive AniA. Supplementation with Cu(II) salt recovered growth in both Δ*accA*/*pCu$_A$C*$^+$ strains and the Δ*accA* strain, suggesting a restoration of AniA activity.

AniA activity in each strain was then assessed by measuring the rate of nitrite consumption. The control *accA*$^+$ strain consumed nitrite, suggesting active AniA, whereas the Δ*accA* showed no consumption, suggesting inactive AniA (*Fig*. 3.3b). The Δ*accA*/*pCu$_A$C*$^+$ strains did not show any nitrite consumption either, and therefore no AniA activity (*Fig*, 3.3b). Addition of Cu(II) salt restored nitrite consumption. Therefore, PCu_AC cannot functionally replace AccA in the metalation of AniA in *N. gonorrhoeae* since the Δ*accA*/*pCu$_A$C*$^+$ strains exhibited the same phenotype as Δ*accA.* The recovery with supplemented Cu suggests that PCu_AC does not have any other effects on the denitrification pathway and microaerobic growth in *N. gonorrhoeae.*

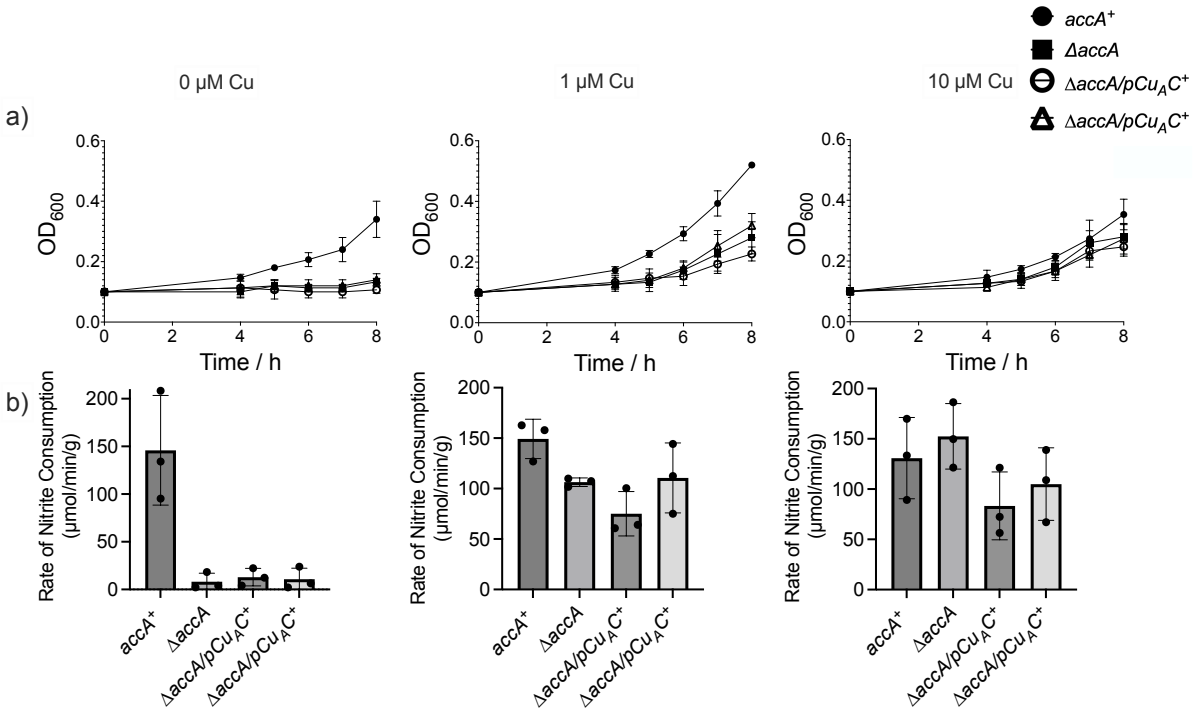

***Figure 3.3*. The *N. gonorrhoeae* Δ*accA/pCu$_A$C*$^+$ mutant phenocopies the *N. gonorrhoeae* Δ*accA* mutant. a)** Growth curves of *accA*$^+$ (filled circles), Δ*accA* (filled squares), and 2 independent Δ*accA/pCu$_A$C*$^+$ (open circles and open triangles) strains of *N. gonorrhoeae* 1291 under microaerobic conditions. Cells were grown in the presence of final concentrations of 0, 1, 10 µM $CuSO_4$. Data points represent n=3, with the error bars being standard deviation. **b)** Rate of nitrite consumption (in µM per minute per µg of *N. gonorrhoeae* protein) in pelleted cells from cultures in panel (a). Individual data points (n=3) are displayed, along with error bars representing standard deviation.

3.4 CueP cannot functionally replace AccA in *N. gonorrhoeae*

As with PCu_AC, the ability for CueP to metalate AniA was assessed by measuring growth and NO_2^- consumption under microaerobic conditions. Due to the structure of CueP being dissimilar to that of AccA, it was hypothesised that CueP would not be able to metalate AniA. However, the previously determined binding affinity of CueP to Cu(I) is more similar to that of AccA (57). For reasons previously stated (section 3.2) all strains in this experiment were grown overnight on plates supplemented with 10 µM $CuSO_4$. The experiments were performed using two replicate Δ*accA/cueP*$^+$ mutant strains with *ΔaccA*/*accA*$^+$ and *ΔaccA* strains as controls.

As observed in Figure 3.3a, the *ΔaccA* strain did not grow while the *ΔaccA*/*accA*$^+$ strain did. As predicted, the *ΔaccA*/*cueP*$^+$ strains exhibited no growth (*Fig*. 3.4a). Upon supplementation with Cu(II), growth of the *ΔaccA*/*cueP*$^+$ and the Δ*accA* strains was recovered. In line with the microaerobic growths, nitrite consumption is restored in both the *ΔaccA*/*cueP*$^+$ and Δ*accA* strains by supplementation with Cu(II) salts. This suggests that CueP cannot metalate AniA in *N. gonorrhoeae.*

There is a minor increase in growth and nitrate consumption of the Δ*accA/cueP*$^{+}$ and Δ*accA* mutant strains in the CueP experiment compared to the Δ*accA/pCu$_A$C* $^{+}$ and Δ*accA* mutant strains in the PCu$_A$C experiments. This is seen more prominently in the growth curves of the *accA*$^{+}$ strains, where the final OD_{600} reading increases from 0.34 in the PCu$_A$C experiment to 0.53 in the CueP experiment (*Fig*. 3.3, *Fig*. 3.4). This increase in growth is seen across all mutant strains, including *accA*$^{+}$ and Δ*accA.* The increases in growth and nitrite consumption are likely due to the higher levels of background Cu present in the cells in the CueP experiment, due to growth on Cu-supplemented plates, as the increase is seen for the Δ*accA* strains, as well as the Δ*accA/cueP*$^{+}$ strains.

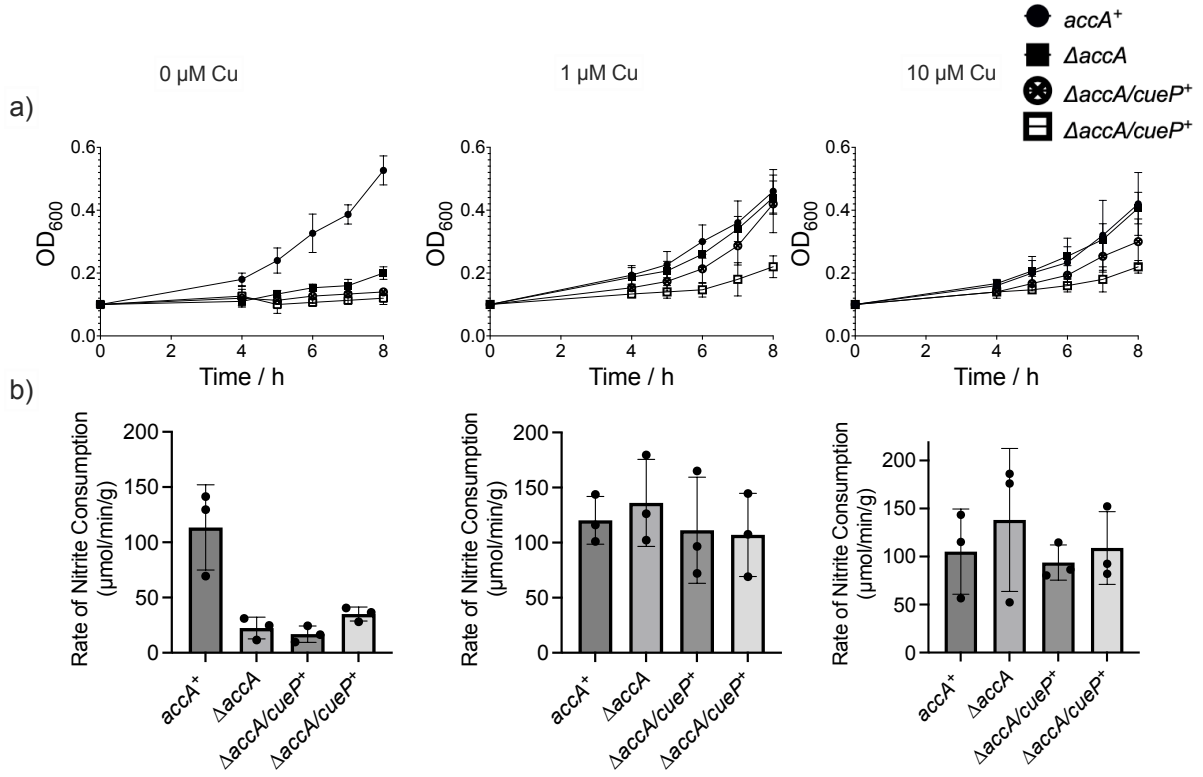

***Figure 3.4*. The *N. gonorrhoeae* Δ*accA/cueP*$^{+}$ mutant phenocopies the *N. gonorrhoeae* Δ*accA* mutant. a)** Growth curves of *accA*$^{+}$ (filled circles), Δ*accA* (filled squares), and 2 independent Δ*accA/cueP*$^{+}$ (crossed circles and open squares) strains of *N. gonorrhoeae* 1291 under microaerobic conditions. Cells were grown in the presence of final concentrations of 0, 1, 10 µM $CuSO_4$. Data points represent n=3, with the error bars being standard deviation. **b)** Rate of nitrite consumption (in µM per minute per µg of *N. gonorrhoeae* protein) in pelleted cells from cultures in panel (a). Individual data points (n=3) are displayed, along with error bars representing standard deviation.

3.5 Replacing AccA with PCu$_A$C or CueP did not affect aerobic growth

The non-native metallochaperones could have an effect outside of the denitrification pathway. In its native *T. thermophilus*, *Tt-PCu$_A$C* metalates the Cu$_A$ centre of cytochrome *c* oxidase (12). The Cytochrome *c* oxidase in *N. gonorrhoeae* does not have a Cu$_A$ centre however it does contain a Cu$_B$ centre (35,62). *Tt*-PCu$_A$C has not been shown to metalate the Cu$_B$ centre which is still present the cytochrome *c* oxidase of *T. thermophilus*. However, a PCu$_A$C

homologue from *Rhodobacter sphaeroides* has been shown to aid in the metalation of the Cu_B centre of its cytochrome *c* oxidase *(52)*. Therefore, PCu_AC could affect the metalation of the Cu_B site of the cytochrome *c* oxidase in N. gonorrhoeae.

The strains were grown under aerobic conditions to confirm whether the metallochaperones had any adverse effects. It was shown that both mutations resulted in no difference in growth phenotype compared to the *accA*$^+$ strains (*Fig*. 3.5). However, the Δ*accA* strain did show a decreased growth phenotype compared to the other strains (*Fig*. 3.5). This has not previously been seen in similar experiments conducted by other group members (30).

The reduced growth of the Δ*accA* strain observed in this study is most likely a result of the growth conditions. The previous studies were conducted with 50 ml media in 250 ml conical flasks, compared to 15 ml in 50 ml Falcon tubes here. The smaller surface area exposed to air in this experiment will likely lead to less oxygen saturation in the media and therefore a greater reliance on the denitrification pathway. Previous work has found that in the experimental set up used in previous experiments, the *accA, aniA* and *norB* genes essential for denitrification are upregulated under these conditions (63). Therefore, under these conditions, *N. gonorrhoeae* likely depends more greatly on the denitrification pathway, as the oxygen saturation is likely less under these conditions compared to those in the previous experimental set up. This observation that *accA*$^+$*/pCu$_A$C*$^+$ and Δ*accA/cueP*$^+$ strains grew as well as the *accA*$^+$ strain suggests that the non-native metallochaperones may partially compensate for the loss of AccA under these partially O_2-limiting culture conditions.

In order to test this hypothesis, the aerobic growths of *accA*$^+$ strain and the Δ*accA* strain, alongside the two metallochaperone mutant strains, should be repeated under the conditions used by S. Firth (30). The upregulation of genes essential for denitrification could also be tested under both experimental set ups to compare the oxygen saturation under both sets of conditions.

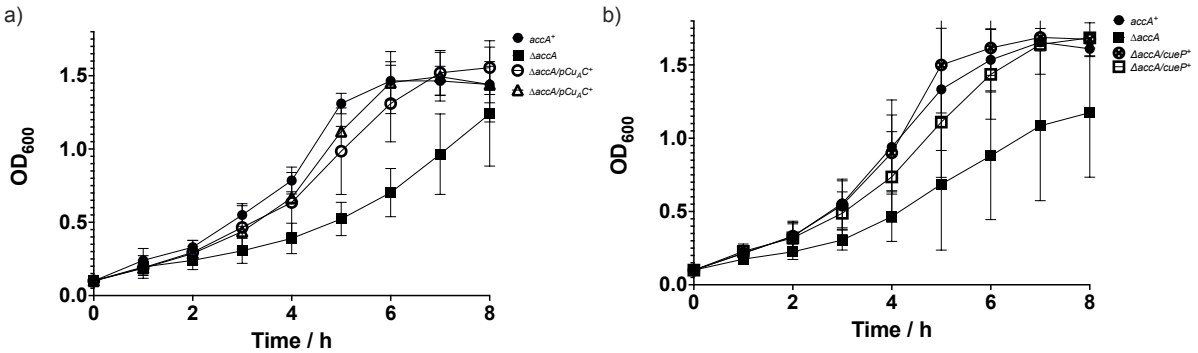

***Figure 3.5*. Replacing AccA with PCu_AC and CueP had no effect on aerobic growth. a**) Growth of *accA*$^+$ (filled circles), Δ*accA* (filled squares), and 2 Δ*accA/pCu$_A$C*$^+$ (open circles and open triangles) strains of *N. gonorrhoeae* 1291. **b**) Growth of *accA*$^+$ (filled circles), Δ*accA* (filled squares), and 2 Δ*accA/cueP*$^+$ (crossed circles and open squares) strains of *N. gonorrhoeae* 1291. Data points represent n=3 with the error bars being standard deviation.

3.6 Supplementation of agar with $CuSO_4$ results in an increase in cellular Cu levels.

N. gonorrhoeae Δ*accA/cueP*$^+$ mutant strain required 10 μM $CuSO_4$ for growth. The final OD_{600} value observed of the *accA*$^+$ and Δ*accA* strains grown on Cu-supplemented plates was greater than those grown without supplementation (*Fig*. 3.3ai, *Fig*. 3.4ai). It was hypothesised that this increase in growth may be due to initial higher levels of cellular Cu, which may lead to some metalation of AniA. ICP-MS was used to measure the cellular Cu levels of the metallochaperone transformants (Δ*accA/pCu$_A$C*$^+$ and Δ*accA/cueP*$^+$), as well as wild-type and Δ*accA* strains of *N. gonorrhoeae* 1291. The background levels of Fe, Mn, and Zn were also measured to evaluate the impact of Cu on other metals essential for *N. gonorrhoeae* growth (64). All metal levels were normalised using protein concentrations within each sample.

The *accA*$^+$ strain showed a ~2-fold increase in cellular Cu when grown on 10 μM Cu-supplemented agar plates compared to none supplemented agar plates. The same result was seen in all other strains of *N. gonorrhoeae* (*Fig*. 3.6a). The Cu concentrations within *N. gonorrhoeae* 1291 Δ*accA/accA*$^+$ were then measured over a series of Cu concentrations supplemented into the agar plates (*Fig*. 3.6b). The increase in total cellular Cu from 0 μM Cu to 10 μM Cu was within the range seen previously and then as the Cu concentration of the agar increased, so did cellular Cu (*Fig*. 3.6b). The levels of all other metals remained constant, suggesting changes in cellular Cu concentration do not affect the levels of other metals within *N. gonorrhoeae.*

Although we do not know the bioavailability of this Cu, it can be presumed that an increase in cellular Cu is responsible for the increase in growth and nitrite consumption. It is likely that much of this Cu is localised to the periplasm of *N. gonorrhoeae* due to homeostatic mechanisms keeping cytoplasmic Cu levels and availability low. A higher level of Cu within the periplasm likely means that Cu is occupying a weaker binding buffer than under normal conditions. This could mean that Cu can be more easily transferred from the buffer into AniA, resulting in the increase in growth and nitrite consumption.

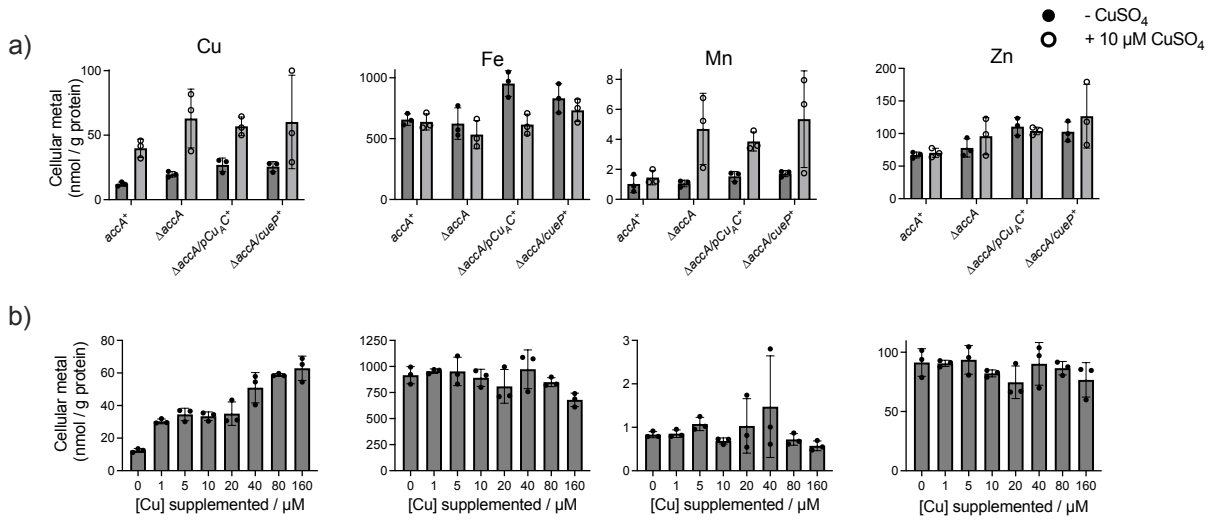

Figure 3.6. **Copper supplementation results in an increase in intracellular copper levels in all strains. a**) Cu, Fe, Zn, and Mn in *accA*$^+$, Δ*accA,* Δ*accA/pCu$_A$C*$^+$ and Δ*accA/cueP*$^+$ strains of *N. gonorrhoeae* 1291. Cells were grown on 0 µM or 10 µM $CuSO_4$ -supplemented agar plates. Individual data points (n=3) are displayed along with error bars representing standard deviation. **b**) Cu, Fe, Zn, and Mn concentrations in the *accA*$^+$ strain of *N. gonorrhoeae* 1291. Cells were grown on 0, 1, 5, 10, 20, 40, 80, 160 µM $CuSO_4$-supplemented agar plates. Individual data points (n=3) are displayed along with error bars representing standard deviation.

3.7 Discussion: neither PCu$_A$C nor CueP support microaerobic growth in the presence of nitrite

Neither the *N. gonorrhoeae* Δ*acca/pCu$_A$C*$^+$ strain nor the *N. gonorrhoeae* Δ*accA/cueP*$^+$ strain showed any growth or AniA activity under microaerobic conditions, in line with the phenotype displayed by *N. gonorrhoeae* Δ*accA*. This suggests that neither PCu$_A$C nor CueP can metalate AniA in *N. gonorrhoeae*. At this stage, there are three potential reasons to why these non-native metallochaperones cannot metalate AniA which are based on the process being both thermodynamically and kinetically favourable. For a favourable thermodynamic reaction to occur, the Cu ion must move from a site of weaker Cu binding affinity (a higher free energy) to a site of stronger binding affinity (a lower free energy) (*Fig*. 3.7 bii) (29). To be kinetically favourable, the transition state formed between the donor and acceptor must have a relatively low free energy (*Fig*. 3.7 biii). This occurs when the metallochaperone, Cu, and the target protein form a transient ternary complex (65).

The first of the three potential reasons why the non-native metallochaperones cannot metalate AniA is that the non-native metallochaperones cannot acquire Cu from the periplasmic Cu buffer (*Fig*. 3.7bi). There is no known or predicted periplasmic Cu sensor in *N. gonorrhoeae*. Therefore, the Cu availability within the periplasm is not known, nor can it be predicted (16). However, it must be that buffered Cu within the periplasm has a similar free energy of metalation to AccA, because AccA can access this Cu pool and transfer it to AniA. Consistent with this proposal, a *N. gonorrhoeae* mutant ΔCu-track AccA variant, which has a K_D value between 7.0 x 10^{-16} M and 8.6 x 10^{-15} M (~30 to 370-fold weaker than AccA), was

able to partially restore AniA activity in *N. gonorrhoeae*. On the other hand, mutants expressing AccA variants with even weaker binding affinity than the ΔCu-track AccA variant failed to grow (30). Therefore, the much lower K_D of PCu_AC stated in the literature (K_D = 2.2 X 10^{-13} M (12)) suggests that PCu_AC will not acquire Cu from the periplasmic buffer. CueP, on the other hand has a binding affinity (K_D = 1 X 10^{-15} M (57)) more similar to that of the ΔCu-track AccA. Therefore, it likely can acquire Cu form the periplasmic buffer, at least partially.

The other two hypotheses relate to the intermolecular interactions between the metallochaperone and AniA. Firstly, the Cu ion must travel down a favourable thermodynamic gradient from a site of higher free energy (weaker binding affinity) to a site of lower free energy (stronger binding affinity) (*Fig*. 3.7 bii). Due to both PCu_AC and CueP having calculated K_D values greater than that of AccA, it is likely that both metallochaperones would set up a favourable thermodynamic gradient for the delivery of Cu Thus, the more likely reason that metalation does not occur is that the metallochaperones cannot form the favourable interactions with AniA in order to form a transient complex. This lack of favourable interactions would mean the free energy of the transient complex would be too high to be viable. PCu_AC and AccA have similar overall structures. However, the specificities of the structures and the individual amino acids likely required for metalation differ, as well as the charged surface and topology of the two proteins (discussed in chapter 5). It has been shown that structurally similar proteins with different charged surfaces cannot form favourable complexes with the other's target protein (66). As for CueP and AccA, there is no similarity in structures or amino acid sequence. Therefore, this complete lack of conservation strengthens the hypothesis that CueP will not interact with AniA.

One caveat to these experiments is that it is unknown whether the nonnative PCu_AC and CueP metallochaperones are correctly exported to and folded in the periplasm, or, whether the metallochaperones are subsequently broken down. Data obtained by qPCR after this study was completed suggested that the metallochaperones are correctly expressed within *N. gonorrhoeae* in line with how AccA would be (K. Djoko). However, no work has been conducted to confirm that the metallochaperones are present and stable in the periplasm, although *Fig.* 3.5 suggests a different phenotype to the Δ*accA* strain. Further work by tagging the metallochaperone and detecting by western blot could be used to determine whether the stable metallochaperones exist within the periplasm of *N. gonorrhoeae* (67).

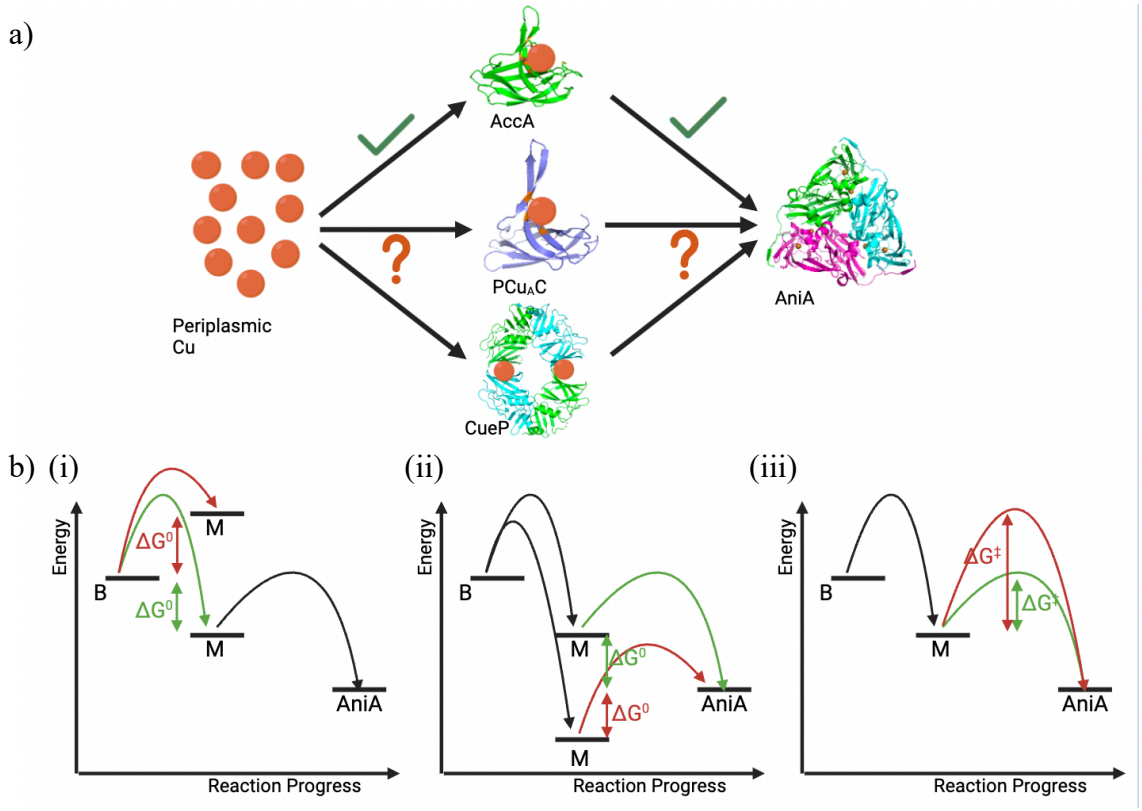

Figure 3.7. **The pathways of metal insertion into AniA a**) AccA can acquire Cu ions from the periplasm and deliver the Cu ions to the Cu sites of AniA. It is not known whether PCu_AC and CueP can acquire Cu from the periplasmic buffer, or if it cannot deliver the Cu ions to the Cu sites within AniA. **b**) **general energy model of insertion of Cu into AniA**. The relative energy of the buffer (B), metallochaperones (M) and AniA. The curved arrows show the direction of Cu transfer and the double headed arrows either represent the change in free energy between sites (ΔG^0) or the activation energy for transfer ($\Delta G^{\ddagger}$). (**i**) A metallochaperone unable to acquire Cu from the periplasmic buffer; (**ii**) a metallochaperone with too strong a binding affinity (too high K_D) to metalate AniA, and (**iii**) a metallochaperone that cannot form favourable interactions with AniA. Green = metalation occurs, Red = metalation will not occur.

Chapter 4: Biochemical analysis of PCu_AC and AniA

Chapter 3 suggests that two different non-native metallochaperones cannot metalate AniA in *N. gonorrhoeae*. From these *in vivo* experiments, it can be predicted that either the non-native metallochaperones cannot form favourable interactions with AniA to transfer Cu, or that they cannot acquire Cu from the buffered Cu pool within the periplasm of *N. gonorrhoeae.* Biochemical analysis of purified metallochaperones can provide an insight into which prediction would be more likely. Since PCu_AC is a homologue of AccA, it was chosen instead of CueP, which has little similarity in sequence or structure to AccA. If purified PCu_AC cannot metalate purified AniA, then it is likely that PCu_AC cannot form favourable interactions with AniA. However, if purified PCu_AC can metalate purified AniA, it is likely that PCu_AC cannot acquire Cu within the periplasm of *N. gonorrhoeae* and therefore cannot deliver Cu to AniA.

4.1 Protein purification

4.1.1 PCu_AC

PCu_AC is a homologue of AccA. However, PCu_AC does not have the Met and His-rich C-terminal tail that was used in the purification of AccA to bind to a His-trap column. Therefore, the purification strategy for PCu_AC followed that employed by S. Firth (30) for the purification of ΔC-terminal tail variant of AccA.

PCu_AC was overexpressed with a His_6-SUMO tag that bound to Nickel in a HisTrap™ column and gave the tagged PCu_AC a theoretical pI of 7.8. Therefore, the protein would stick to a His-trap column followed by the positively charged anionic exchange Q column at pH 8.0 due to the protein being negatively charged at this pH. The His_6-SUMO tag was then cleaved by hSENP2 (Blower lab, Durham University). This produced untagged PCu_AC protein with a theoretical pI of 9.05. This allowed untagged, positively charged PCu_AC to flow through a Q column at pH 8. The pH was then reduced and PCu_AC stuck to a negatively charged cationic exchange SP column, as the protein is positively charged at pH 6.0. This produced the pure PCu_AC protein. The purified PCu_AC protein migrated on an SDS-PAGE gel as three bands, suggesting three distinct proteins (*Fig*. 4.1 a). To separate and identify these proteins, the sample was loaded on to a size exclusion column. Interestingly, the protein eluted from the column as a single, sharp peak (*Fig*. 4.1 bi). Based on the calibration table for this column (Cytiva), the mass of the protein was roughly 13 KDa, which is expected for PCu_AC (exact size = 13295 Da). The protein peak was re-analysed by SDS-PAGE gels and three bands were still present, but, this time, the high molecular weight bands appeared to be concentration-dependent (*Fig*. 4.1 bii). All three bands were confirmed to be PCu_AC by ESI+ Mass Spectrometry and proteomics, suggesting that the higher molecular weight bands are aggregates formed during the denaturing of the protein.

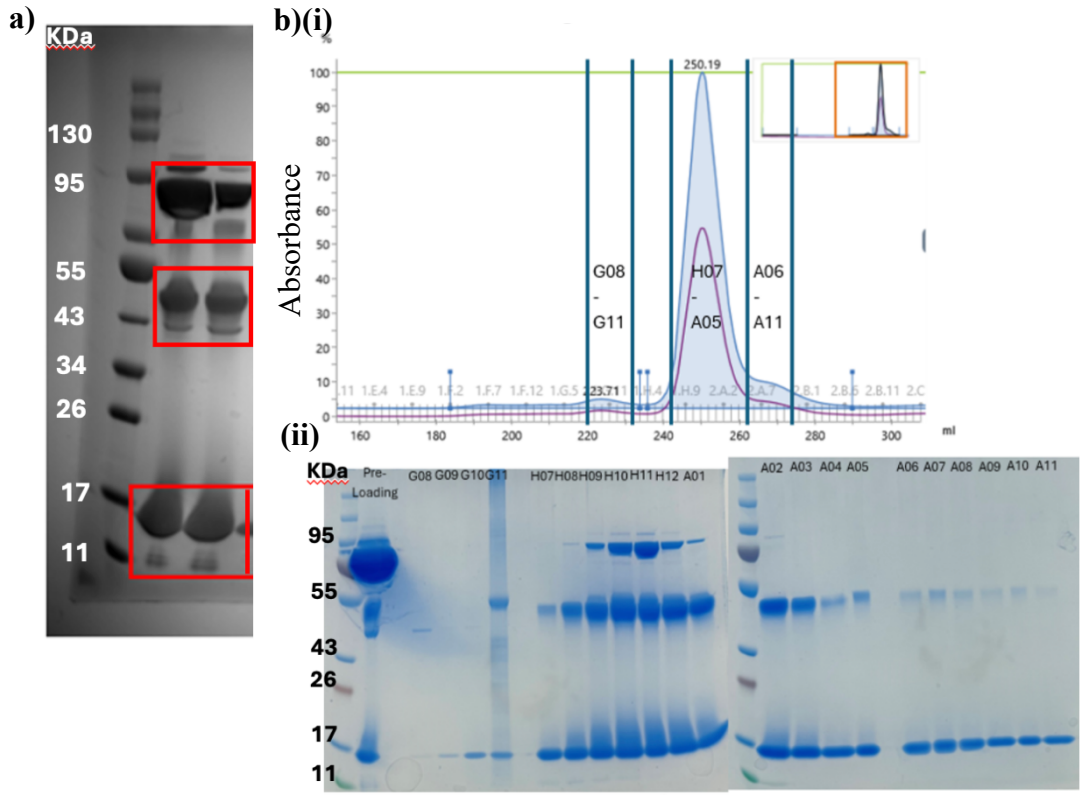

Figure 4.1. **Purification of PCu_AC a**) SDS-PAGE gel of purified PCu_AC after elution off the SP column in the initial purification. **b**) Elution of PCu_AC from SEC showing the chromatogram with A_{280} (blue) and A_{260} (purple) (**i**) and SDS-PAGE gel of PCu_AC pre-load and elution (**ii**). Each gel lane was labelled with their corresponding elution fraction from SEC (**ii**).

4.1.2 AniA

AniA was overexpressed and purified using the method developed by S. Firth (30) and adapted from Boulanger and Murphy (37). A His_6-tag was attached to the C-terminal of the protein. The His_6-tag was cleaved by thrombin and removed. The resulting un-tagged AniA showed the correct expected mass of 35015 Da. However, the mass spectrum also showed a second peak at 33170 Da. This suggests that AniA has been cleaved at a secondary site resulting in a truncated product. The two AniA proteins cannot be separated by size exclusion chromatography due to their similar sizes (*Fig*. 4.2 a). To suppress the undesirable secondary product, cleavage was performed with half the amount of thrombin. This approach resulted in a lower yield of protein, but importantly, only the full length 35015 Da protein was present (*Fig*. 4.2 b).

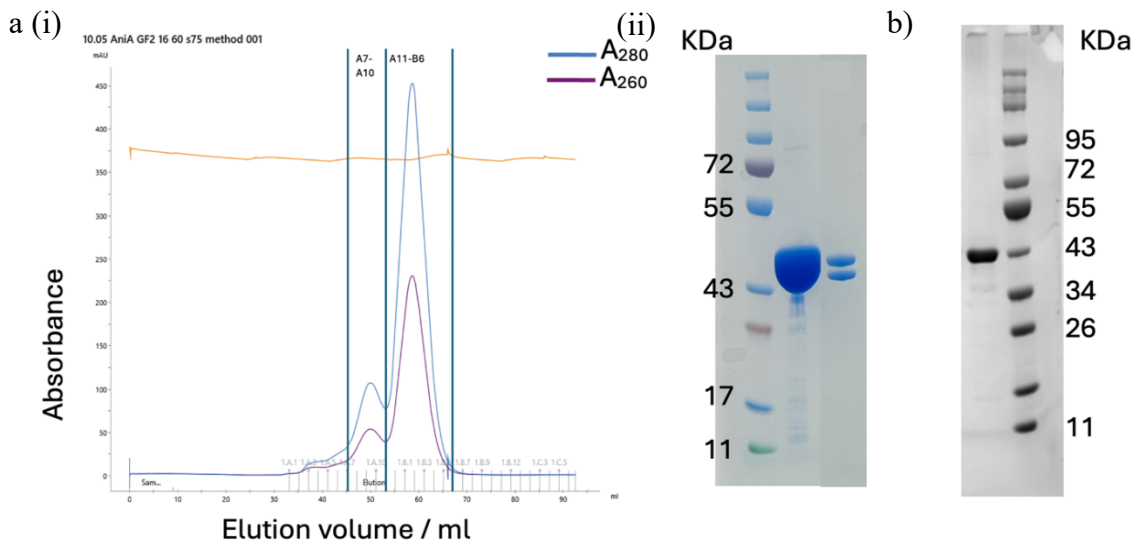

Figure 4.2. **Purification of AniA a**) Size exclusion chromatography purification of AniA: chromatogram of AniA elution (**i**), SDS-PAGE gel of SEC purified AniA showing the sample before loading and the elution in fraction B4 (**ii**). **b**) SDS-PAGE Gel from subsequent purification of AniA using half the recommended amount of thrombin.

4.2 PCu_AC binding affinity to Cu(I).

The binding affinity of PCu_AC to Cu(I) was previously determined to be $K_D = 2.2 \times 10^{-13}$ M (12). This affinity of PCu_AC is 10000-fold weaker than the that of AccA which has been determined to be $K_D = 2.0 \times 10^{-17}$ M (30). Due to this difference, while AccA can acquire Cu(I) from the periplasm of *N. gonorrhoeae*, it is possible that PCu_AC cannot (*Fig*. 3.3 bi). However given the similarities in the structures of the two proteins and the conserved Cu binding site ligands, the reason for this large difference in binding affinities is unclear. Binding affinity depends on the pH and buffer used, as well as the experimental procedure, which could therefore result in different values (60). A closer look at the methods used by Abriata *et al.* (12) revealed that PCu_AC was competed with DTT for binding Cu(I). A K_D value of 6.3×10^{-12} M was used for DTT at pH 7.4. However, more recent studies determined a higher binding affinity, namely $K_D = 2.5 \times 10^{-15}$ for DTT (68). This new affinity is 3 orders of magnitude tighter than previously thought. Therefore, the affinity of Cu(I) for PCu_AC is likely underestimated. To directly compare the binding affinity of PCu_AC and AccA, the K_D of PCu_AC needs to be determined under the same conditions as used for AccA and using the same experimental set up (30).

To re-examine the binding affinity of PCu_AC for Cu(I), three colorimetric probes with known, but varying, binding affinities to Cu(I) were used in ligand exchange competition assays. The three probes all bind Cu(I) with a 2:1 ratio ($[Cu^IL_2]^{3-}$). These probes were ferrozine (Fz), bicinchoninic acid (BCA), and bathocuproine disulfonic acid (BCS) (*Table* 2.5). Adding $CuSO_4$ in the presence of ascorbate as a reductant resulted in a linear increase in absorbance up to the point of saturation, which occurred at ½ of the ligand concentration as expected (*Fig*. 4.3 aii, bii, and cii). This titration gave the control curves for each experiment.

For the initial competition assays with Fz and BCA, Cu was titrated into a mixture containing the probe and 20 μM PCu_AC. Solution absorbances were measured (*Fig*. 4.3 bi, ci). A competition curve was plotted, using the absorbance maxima at each Cu(I) concentration (*Fig*. 4.3 bii, cii). Solution absorbances did not increase until the added Cu concentration surpassed 20 μM, suggesting that PCu_AC outcompeted both probes. At Cu concentrations higher than 20 μM Cu, the Fz and BCA competition curves displayed the same gradients as the control curves, suggesting that there are no extra binding sites for Cu(I) in PCu_AC that could compete with Fz or BCA. The competition curve plateaued at 20 μM higher Cu concentration than the control curves, accounting for the addition of PCu_AC. These data suggest a relatively strong binding affinity of PCu_AC ($K_D < 10^{-15}$ M). The flat line until 20 μM Cu also suggests that PCu_AC binds Cu with a 1:1 stoichiometry as expected.

Titrating Cu into a mixture of 100 μM *apo*-BCS and 40 μM *apo*-PCu_AC resulted in an increase at absorbance at all concentrations of Cu (*Fig*. 4.3 ci). The absorbance at 483 nm for each Cu(I) concentration was plotted and compared to that of the control curve containing no *apo*-PCu_AC (*Fig*. 4.3 cii). The competition curve showed a shift with saturation occurring at 82 μM Cu, as opposed to 50 μM for the control curve, indicating that BCS and PCu_AC directly competed for Cu(I). The competition curve was fitted to an equilibrium model with one PCu_AC Cu(I) binding site using DynaFit®. This yielded a K_D value of 5.7×10^{-17} M ($\pm$ 2.2×10^{-17} M), similar to that of the primary Cu(I) binding site of AccA ($K_D = 2.0 \times 10^{-17}$ M (30)). Curves with binding affinities 10× stronger and 10× weaker were simulated (*Fig*. 4.3 cii). The curve generated from the data clearly sits between the two simulated curves, increasing confidence in our estimate.

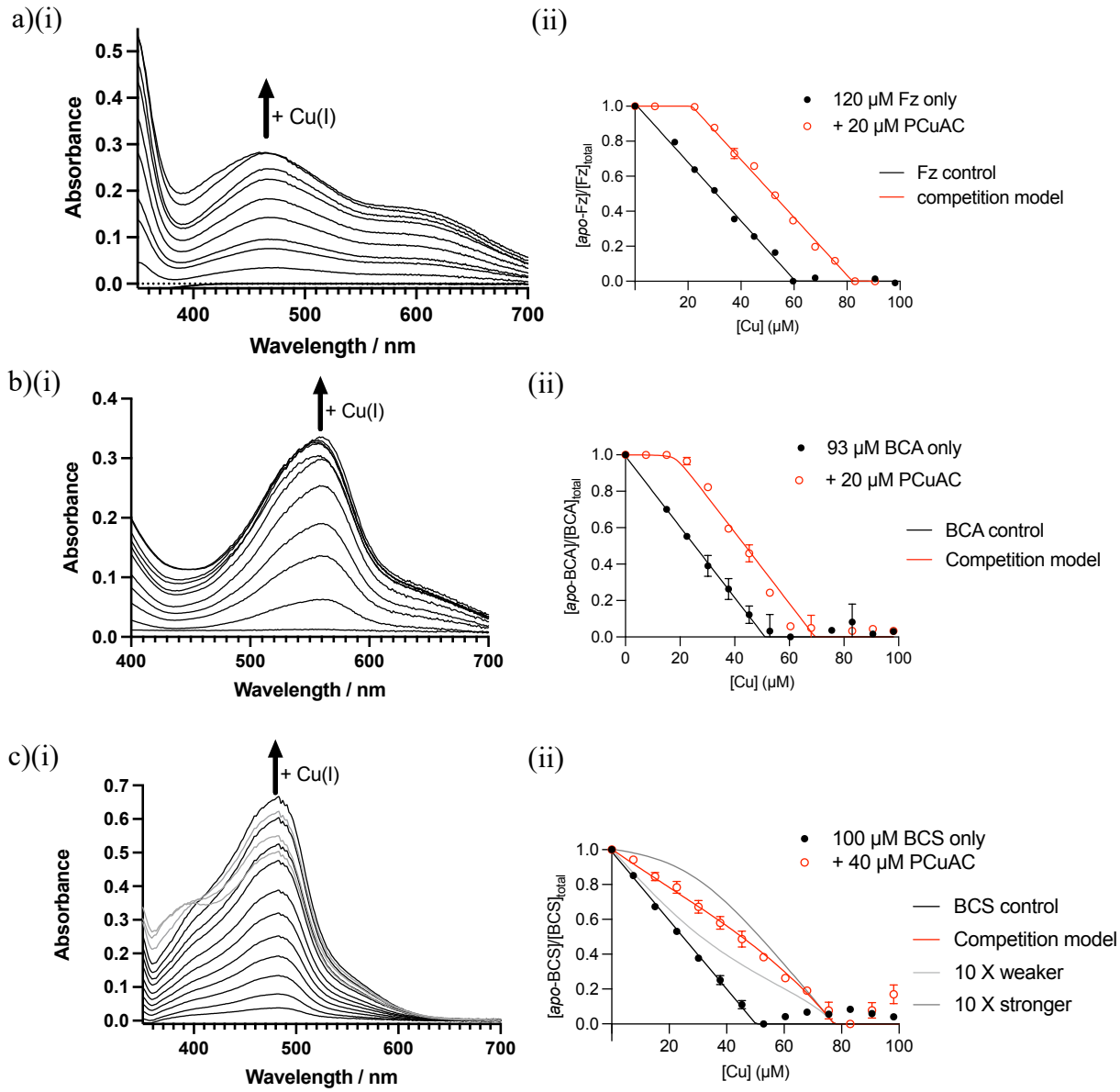

***Figure 4.3*. PCu$_A$C competes with BCS for Cu(I). i**) Absorption spectra of a Cu(I) titration into PCu$_A$C (for Fz and BCA: [PCu$_A$C] = 20 μM, and for BCS: [PCu$_A$C] = 40 μM) and spectroscopic probe (**a**) Fz: 120 μM, **b**) BCA: 93 μM, and **c**) BCS: 94 μM,). **ii**) Ligand competition titration of the spectroscopic probe (**a**) Fz, (**b**) BCA, and (**c**) BCS, PCu$_A$C and Cu(I), measured by the ratio of *apo*-probe to total probe calculated using the know extinction coefficients at the absorbance maxima (Fz: 470 nm, BCA: 562 nm, and BCS: 483 nm. All experiments were conducted in 50 mM MOPS pH 7.2.

4.3 Copper transfer from PCu$_A$C to AniA

Based on the binding affinity of PCu$_A$C, which is similar to that of AccA, it can be speculated that PCu$_A$C can acquire Cu(I) from the periplasmic Cu(I) buffer of *N. gonorrhoeae*. Therefore, the likely hypothesis for the growth defect observed in the Δ*accA/pCu$_A$C*$^+$ mutant is that PCuAC cannot transfer its bound Cu to AniA. This is likely due to a lack of favourable protein-protein interactions. To test this hypothesis, Cu transfer was assessed between purified AniA and PCu$_A$C proteins *in vitro*. The T1Cu centre of AniA is spectroscopically

active, absorbing light in the UV/vis region with peaks at 460 nm and 600 nm (37). The T2Cu site is spectroscopically silent and does not interfere with measurements conducted. Adding 2 molar equivalents of $CuSO_4$ to 70 μM of purified AniA increased the absorbances at both 460 nm and 600 nm. The increase was initially rapid and then plateaued over time (*Fig*. 4.4 ai and c). The final scan of the protein after 3 hours showed the major peak at 600 nm and a smaller peak at 460 nm, characteristic of AniA

To determine if PCu_AC can metalate AniA, 2 molar equivalents of Cu(I)-PCu_AC were added to *apo*-AniA solution, as AniA has 2 Cu binding sites whereas PCu_AC only has one. The results showed a minimal increase in absorbance. The rate of absorbance increase by PCu_AC was 28× slower than that of $CuSO_4$ (*Fig*. 4.4 aii and c). This suggests that PCu_AC cannot metalate AniA *in vitro*, likely because it does not form favourable interactions with AniA. When compared to Cu(I)Cu(II)-AccA, the rate of metalation by PCu_AC was approximately 15× slower.

No method was used to assess the rate of metalation into the T2Cu site of AniA, which is spectroscopically silent. The PCu_AC loading experiments were performed with Cu(I) whereas the $CuSO_4$ loading experiments were conducted with Cu(II). The T1Cu centre is only spectroscopically active if Cu(II) is bound and not Cu(I). We assumed that any Cu(I) transferred to AniA would be oxidised to Cu(II) since the experiment was exposed to air. However, we could not be sure that this was the case. Therefore, to determine whether any Cu (either Cu(I) or Cu(II)) was in fact transferred to AniA, the Cu content of each protein must be measured. The two proteins were first separated using HiTrap Q column, which binds negatively charged species. PCu_AC (theoretical pI: 9.05), was found in the flow through, while AniA (theoretical pI: 5.33) was eluted using salt. The concentration of Cu in each protein fraction was then measured by ICP-MS. After three hours, an average of 0.64 equivalents of Cu remained per PCu_AC and an average of 0.14 equivalents of Cu in AniA (*Fig*. 4.4 c). This small increase in Cu equivalents in the AniA sample supports the proposal that only a small amount of Cu is transferred from PCu_AC to AniA, in line with the small increase in absorbance shown in figures 4.3 b and c. However, this only accounts for 1.42 equivalents of the original Cu added, which should be 2.0. This suggests that either some Cu has been lost in the separation process, which could occur during the washing of AniA before elution. The more likely outcome is that either the protein or Cu concentration was incorrect. Cu(I) interferes with A_{280} in PCu_AC. Therefore, the concentration of PCu_AC could have been overestimated. Alternatively the high levels of NaCl could interfere with the ICP-MS readings for Cu (69). In future experiments, the protein concentrations should be calculated using BCA assays to avoid interference in the A_{280} values. To check if Cu is lost, the exact volumes of each sample containing protein should be measured to account for the exact amount of Cu both before and after.

These experimental results confirm that purified Cu(I)-PCu_AC did not metalate the T1Cu site in purified AniA. AccA can metalate AniA *in vitro* (30), therefore it must form favourable interactions and provide a favourable thermodynamic gradient for the transfer of Cu from its primary Cu site to the Cu sites in AniA. Based on the comparable binding affinities of AccA and PCu_AC, it is likely that the thermodynamic gradient the Cu centre in PCu_AC to the Cu

sites in AniA is favourable. Therefore, this supports the hypothesis that PCu_AC and AniA cannot form the favourable interactions and therefore form the transient complex required to allow for Cu to be transferred.

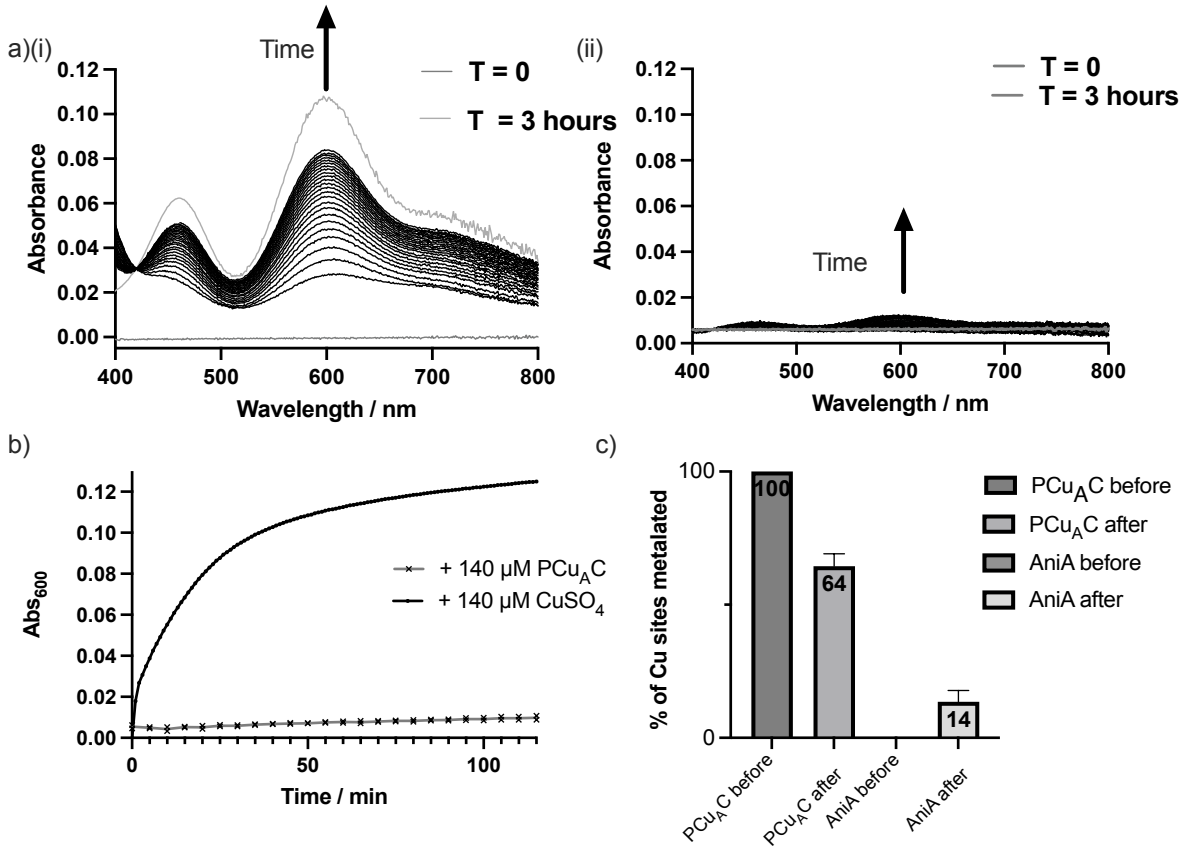

Figure 4.4. **PCu_AC cannot transfer Cu to AniA *in vitro.*** **a**) UV-Vis spectra of the T1Cu centre of 70 µM AniA over time upon addition of 2 equivalents of $CuSO_4$ (**i**), and 2 equivalents of Cu(I)-PCu_AC (**ii**). Grey lines represent T = 0 and the experiment end point. The time points represent T = 1 minute for (**ai**) and T= 5 minutes for (**bii**). (**aii**) is representative spectrum of two independent repeats. **b**) The absorbance of the T1Cu centre of AniA, at 600 nm in the presence of 2 molar equivalents $CuSO_4$ (black) and 2 molar equivalents Cu(I)-PCu_AC (grey) over 120 minutes from the spectra of (a). Experiments were performed in duplicate. **c**) Percentage metalation of metal binding sites of PCu_AC and AniA before and after the reaction time course. Experiments were performed in duplicate. All kinetic experiments were performed in 50 mM Tris buffer pH 7.4, 150 mM NaCl, and 20% glycerol.

4.4 Copper induces the trimerization of AniA over time

Purified *holo*-AniA protein exists as a homotrimer containing six Cu ions, with the T2Cu centres sitting at the monomer-monomer interfaces with ligands from both. As it is thought that *apo*-AniA exists as a monomer (30), it was speculated that Cu insertion at monomer-monomer T2Cu sites may be essential for trimer formation. To verify these previous observations, both *apo*- and *holo*-AniA were analysed by mass photometry. For *holo*-AniA, a mass of 103 kDa was measured (*Fig*. 4.5a), which is consistent with the presence of a

homotrimer of a mass of 105 kDa. For *apo*-AniA, the buffer signal obscured the protein signal at 30 kDa, meaning that the mass of *apo*-AniA could not be determined. However, the lack of the peak at 105 kDa suggests an absence of trimer, consistent with the previous work.

After confirming that *holo*-AniA exists as a trimer and *apo*-AniA does not, we tested whether trimerization could be measured over time. A rough experiment was conducted where the mass of AniA solution was measured upon the addition of 3 molar equivalents of $CuSO_4$. The presence of a peak at 103 KDa was measured before, immediately after, and an hour after the addition of Cu. This showed that the amount of trimer increased over time, but only a small amount was detected (*Fig*. 4.5b). There was no standard peak to compare the size of the trimer peak to, nor could the area under the peak be calculated. Therefore, the exact amount of trimer could not be quantified. Refinement of this experiment would have to be conducted to obtain data to determine the rate of trimerization of AniA. This would include using a buffer which does not cause interference at lower molecular weights, so that the monomer could be visualised. Also, using a protein standard of known concentration, could be used to normalise the size of each AniA peak for each reading. The experiment would also have to be conducted at regular time intervals.

What we can tell from this preliminary data is that the addition of Cu(II) ions induces trimerization of AniA. The roles of the T1Cu and T2Cu centres in trimerization are not known. However, both ΔT1Cu and ΔT2Cu AniA show some trimerization in the *holo* form, however this is not complete, suggesting a less stable complex (30). This suggests that the Cu-protein bonds of the T2Cu centre are not essential for trimerization of AniA but may aid in its formation and stability once formed. It was hypothesised that binding of Cu ions to T1Cu site results in a conformational change elsewhere in the monomer, which subsequently allow for favourable intermolecular interactions between the monomers to form a trimer(70). Therefore, it may be that metalation of both sites individually aid in trimerization, but metalation of both sites in wild-type AniA allow for a fully stable trimer to occur.

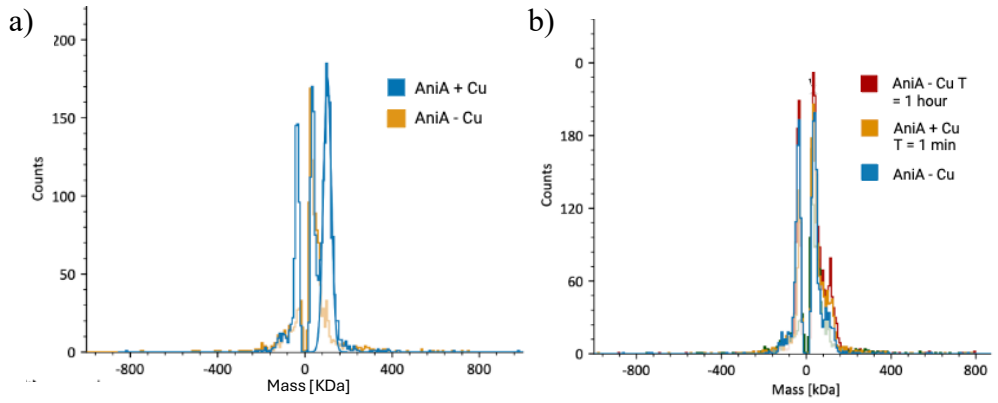

***Figure 4.5*. *Holo*-AccA but not *apo*-AniA exists as a trimer**. Refeyn mass photometry data of (**a**) *apo*- and *holo*- AniA (**b)** time course experiment of the addition of excess $CuSO_4$. Measurements were conducted in 1X PBS with AniA in the 10^{-8} M range.

4.5 Discussion

4.5.1 Tt-PCu$_A$C has a similar binding affinity to AccA

The newly calculated K_D of *Tt*-PCu$_A$C (K_D = 5.7 × 10^{-17} M) suggests that its binding affinity to Cu(I) is comparable to AccA (K_D = 2.0 × 10^{-17} M), as well as other PCu$_A$C homologues from *Streptomyces lividans* (K_D: 2 × 10^{-16} M (71)) and *Bradyrhizobium japonicum* (K_D: ≤ 1× 10^{-16} M (72)). This finding was expected, based on the shared $HX_nMX_{21/22}HXM$ binding motif and overall structural homogeneity between the PCu$_A$C-family metallochaperones. Unlike AccA, PCu$_A$C does not contain a Cu track, which is suggested to increase the binding affinity of the primary site to Cu(I) (30). Therefore, the K_D of PCu$_A$C to Cu(I) was predicted to be more similar to that of the ΔCu-track AccA mutant, which was calculated with BCS and BCA to give 7.0 x 10^{-16} M and 8.6 x 10^{-15} M, respectively. However, the value for BCS, which was used to calculate the K_D for PCu$_A$C, is within the range seen for other PCu$_A$C proteins. Therefore, the Cu track may play a less important role in Cu binding than previously thought.

This newly determined $K_{D(CuI)}$ value for PCu$_A$C is in the same range as that of AccA, which suggests that PCu$_A$C should be able to acquire Cu in the periplasm of *N. gonorrhoeae,* whilst also allowing for a favourable thermodynamic gradient for the transfer of Cu to AniA. Therefore, as two of the three criteria for Cu loading *in vivo* are met, this suggests that AniA and PCu$_A$C cannot form transient complexes to allow for the delivery of Cu to AniA.

4.5.2 AccA-AniA is a specific metallochaperone-target protein pair

Despite the similar structures of AccA and *Tt*-PCu$_A$C (discussed in chapter 5), PCu$_A$C was unable to metalate either Cu site in AniA *in vitro.* Therefore, it is likely that no other structurally distinct metallochaperone, like CueP, will be able to metalate AniA.

One major difference between Tt-PCu$_A$C and AccA is that *Tt*-PCu$_A$C does not have a C-terminal tail. Therefore, it only binds one molar equivalent of Cu as Cu(I). The AccA mutant most similar to that of PCu$_A$C is the ΔC-terminal tail AccA mutant that lacks the C-terminal tail domain and only binds one equivalent of Cu. Cu(II)-ΔC-terminal AccA metalated AniA at a slower rate than the wt-AccA and other AccA variants tested (30), but still at a higher rate than that of Cu(I)-PCu$_A$C to AniA. Cu(I) was used for the PCu$_A$C loading experiments, and although the Cu(I)-ΔC-terminal AccA experiments are yet to be performed, Cu(I)-ΔC-terminal AccA will likely still metalate AniA at a higher rate.

Performing metalation studies with both of the proteins loaded with Cu(I) instead of Cu(II) would provide greater context for the role of the overall structure in the metalation of AniA. Future work could also be conducted using another protein from the PCu$_A$C family which contains a C-terminal tail such as PCuC from *Bradyrhizobium japonicum*(72).

Chapter 5: Conclusions and future work

5.1 AccA is a specific metallochaperone for AniA

The key finding from this work is that PCu_AC cannot functionally replace AccA in the metalation of AniA. Therefore, it is likely that AccA is a specific metallochaperone for AniA. This is likely due to the requirement for specific interactions between amino acids of AccA and AniA that cannot occur between PCu_AC and AniA. Despite the overall structures of the two proteins being very similar, their amino acid sequences only share a 34% similarity. This difference may account for their different protein targets, which are AniA for AccA and cytochrome *c* oxidase for PCu_AC. Structural alignment of the backbones of AccA and PCu_AC (*Fig*. 5.1 a) shows that both proteins share the highly conserved cupredoxin-like fold, which is responsible for Cu binding (73). The spatial orientation of the conserved Cu(I) binding site is near identical (*Fig* 5.1. b).

It has been established that Cu must be delivered *via* a transient complex involving ligands from both the metallochaperone and target protein (74). Therefore, the regions either side of the primary Cu binding site of both AccA and PCu_AC are likely involved in interactions with their target proteins. Comparing AccA and PCu_AC, these regions share little identity, leading to distinct surface topology and surface charge distribution (*Fig* 5.1). AccA must form the correct interactions with AniA for complex formation. Therefore, AccA likely has key amino acids that pair with key amino acids in AniA to allow for docking to occur. AccA has a large positive region below the primary Cu binding site surrounding Arg30, as well as distinct charges on the end of the cupredoxin-like fold comprising of Glu34 and Lys114. The same end of the cupredoxin-like fold is also much bulkier than that of PCu_AC. The loop on AccA consists of 9 amino acids, with the four protruding being Val, Glu, Gly, and Met. In comparison, the same loop in PCu_AC consists of 7 amino acids, with the four most prominent being Pro, Gly, and Pro. Therefore, it is unlikely that this region of PCu_AC would be able to dock with AniA. PCu_AC also has a much longer finger domain with distinct positively and negatively charged regions seen in front on view (*Fig*. 5.2 b) which are in an opposite orientation in AccA (*Fig*. 5.2 a). Therefore, steric and electrostatic hindrance likely occurs between AniA and PCu_AC. In comparison, the charges on AccA likely allow for specific salt bridges to form with AniA and the overall topology of AccA will likely allow for complementary docking. In PCu_AC, the lack of/difference in charge at a set location would likely prevent the correct electrostatic interactions from occurring. The difference in overall topology between PCu_AC and AccA may prevent complementary docking or cause steric hindrance between PCu_AC and AniA, causing repulsion between the two proteins. Previous work has shown no metal transfer occurs between metallochaperones with identical folding, but distinct charged faces due to unfavourable electrostatic interactions (66)(Chapter 1.2.3).

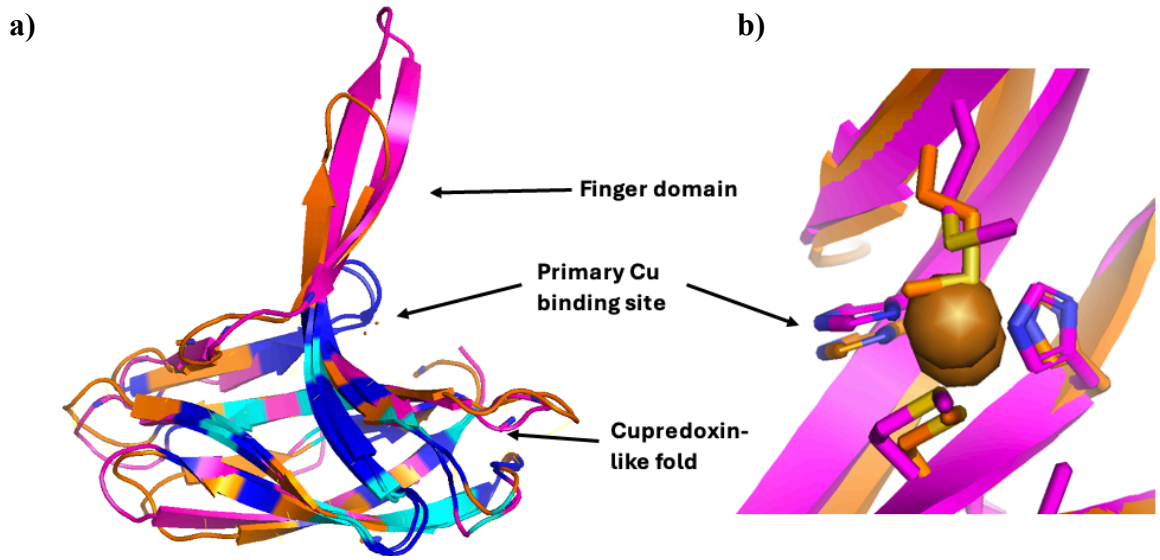

Figure 5.1: **Structural alignment of AccA and PCu$_A$C. a**) structural alignment of AccA (orange) and PCu$_A$C (magenta) with conserved (blue) and similar (Cyan) amino acids within 2 Å. **b)** Primary Cu binding sites showing the side chains of the Cu binding ligands. AccA: Draft Structure(48), PCu$_A$C PDB ID: 2K70 (12).

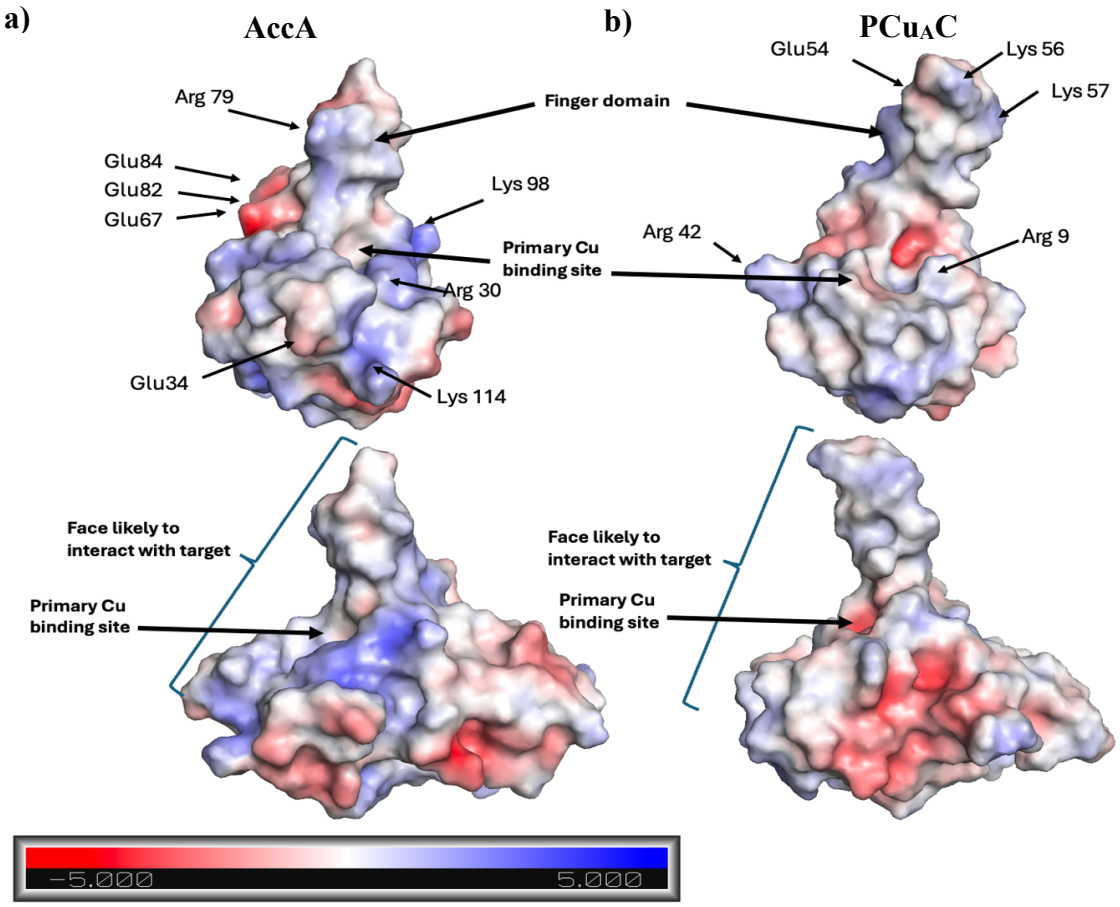

Figure 5.2. **Surface charge distribution of AccA and PCu$_A$C**, showing the front on and side view of AccA (**a**) and PCu$_A$C (**b**), highlighting the region surrounding the primary Cu binding site with negative (red) and positive (blue) charges. AccA: Draft Structure (48), PCu$_A$C PDB ID: 2K70

The exact interactions that occur between AccA and AniA during metal transfer are currently not known. On top of this, the mechanism of ligand exchange is also unknown. AccA coordinates Cu(I) with 4 ligands and has a full coordination sphere. In contrast, more classical, cytoplasmic Cu-binding metallochaperones have at least one empty coordination site, allowing for associative ligand exchange to occur with the target (*Fig*. 1.4 a) (28). Another periplasmic Cu metallochaperone, CusF from *E. coli*, which transfers Cu(I) to the Cu(I)-effluxing CusABC transporter, also coordinates Cu(I) with a full coordination sphere. Molecular dynamics simulations have shown that during the interactions between CusCBA and CusF, the cation-π bond between Trp and Cu(I) is broken *via* a conformational change, which then allows for associative ligand exchange to occur (75). Similarly, CopC from *Pseudomonas syringae* has been crystallised with bound Cu(I) and Cu(II) with either complete or incomplete coordination of the Cu ions depending on the pH. This suggests that the a ligand may dissociate to allow for associative ligand exchange to occur when CopC is in contact with its target protein (76).

To explain how AccA delivers Cu(I) to AniA with a full coordination sphere, we proposed the following model (*Fig.* 5.3). AccA has a low K_D value for Cu, therefore it can acquire Cu from the buffer even under Cu starvation. The finger-domain of AccA is potentially flexible. This allows the interaction with AniA to trigger a conformational change, "pushing" the finger domain away from the Cu binding site. This would overcome the energy barrier for dissociation of either one or both of the Cu-S_{met} bonds. The lack of a full coordination sphere would then allow for associative ligand exchange to occur as seen in *Fig.* 1.4 (a). The Cu binding site consisting of only three (or less) ligands will have a weaker binding affinity than the Cu binding site consisting of the complete set of four ligands and would allow for Cu to be transferred down a thermodynamic gradient to AniA. Therefore, this could mean AccA could have a stronger affinity to Cu(I) than AniA, and thus explain why AniA cannot acquire copper without the aid of AccA under conditions of Cu starvation (*Fig.* 5.3. b). Once AccA transfers this Cu to AniA, Cu is likely trapped due to a lack of solvent exposure of the T1Cu site (*Fig*. 5.3). If it is true that PCu_AC cannot form favourable interactions with AniA, the finger domain of PCu_AC likely cannot be "pushed" back to break the Cu-ligand bonds. Therefore, the lower binding affinity state of the metallochaperone will not be achieved and Cu cannot be transferred down a favourable thermodynamic gradient.

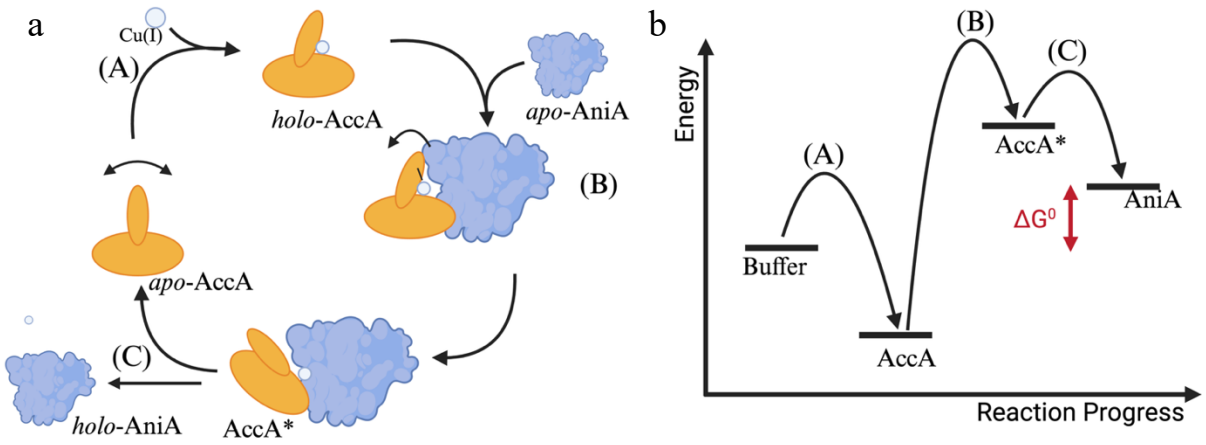

Figure. 5.3. **Proposed scheme for Cu acquisition and transfer by the primary Cu site of AccA to the T1Cu site of AniA**. **a)** schematic of the proposed Cu transfer mechanism from AccA to AniA. **b)** the proposed energy diagram for Cu transfer from the Cu buffer to AccA to AniA under Cu starvation conditions. Red = unfavourable reaction. **The steps in this process are labelled on both diagrams: (A)** The finger domain of *apo*-AniA is flexible to allow for the acquisition of Cu, upon Cu binding the finger domain is set in the position seen in the *holo*-AccA crystal structure with a full coordination sphere (48). This gives the strong binding affinity calculated (30). **(B)** *Holo*-AccA interacts with *apo*-AniA which pushes the finger extension, breaking the Cu-ligand bonds. **(C)** *Holo*-AccA* now binds Cu with 2 or 3 ligands, allowing for associative ligand exchange and Cu transfer to occur, resulting in the release of *holo*-AniA and *apo*-AccA (a). The process would repeat or occur simultaneously until all 6 Cu sites are filled.

There was not enough time in this project to experimentally deduce the interactions between AccA and AniA *via* NMR or co-crystallisation. Instead, we predicted them *in silico* using AlphaFold 3. AlphaFold 3 predicted that AccA can bind to AniA but not PCu_AC. However, these predictions have relatively low confidence at the protein-protein interface. The predicted interactions between AccA and the AniA monomer and the AniA trimer both situate the correct Cu-containing face of AccA near the T1Cu site of AniA (*Fig*. 5.5a). On the other hand, PCu_AC, is predicted to interact with AniA *via* the non-Cu- containing face (*Fig*. 5.5b). These predictions support the idea that the interactions between the correct face of PCu_AC and the Cu-binding region of AniA are weak and/or unfavourable.

Looking at the AlphaFold 3 predictions of AccA-AniA complexes in more detail (*Fig*. 5.5a), the predictions with the trimer are much more consistent with little or no variation between predictions. For the monomer, each prediction shows some variation in the position around the T1Cu, suggesting weaker interactions between the two proteins. This is interesting because our current hypothesis is that *apo*-AniA receives Cu as a monomer, not a trimer. In addition, there is evidence that the monomer conformation is different to that of the trimer. This is due to evidence that the T1Cu undergoes a change in orientation from a more square planar conformation to a more tetrahedral conformation, based on a change in the ratio of the peaks at 460 nm and 600 nm (70). This change would likely require a conformational change across the whole protein to overcome both steric and energetic constraints. This can be supported by the T1Cu site of AniA not being solvent accessible in the trimeric structure (*Fig*.5.4). This site must be more solvent accessible in the *apo*-structure to receive Cu. AlphaFold bases the structural predictions on the rigid crystal structure of *holo*-AniA. Therefore, it does not take into account that this hypothesised conformational change may occur. Therefore, to better predict the interactions, a structure of *apo*-AniA is needed.

We presume that AccA metalates both the T1Cu and T2Cu sites of AniA. However, AlphaFold 3 does not predict any interaction between AccA and AniA near the T2Cu site. We have varied the stoichiometry of AccA, AniA, and Cu (all simulations not shown), but these variations do not change the predictions. Therefore, AlphaFold 3 offers no insight into how the T2Cu site of AniA acquires Cu from AccA.

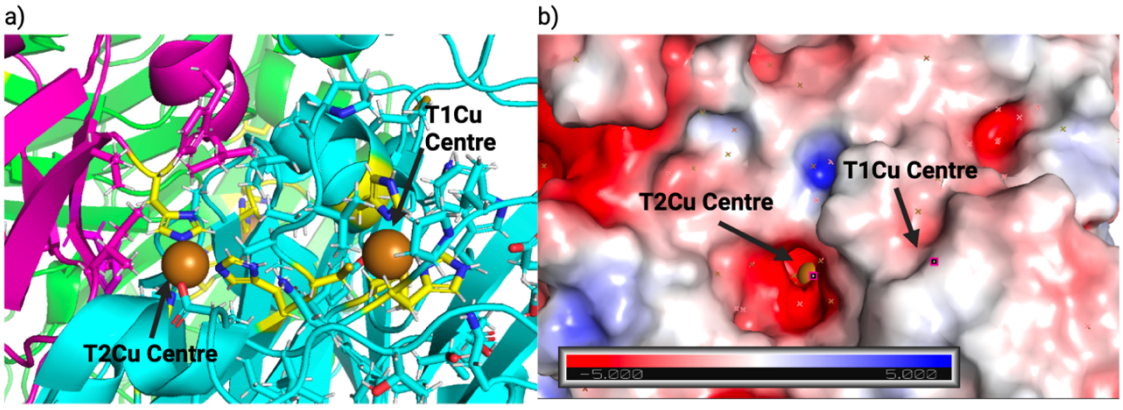

Figure 5.4. **The T1Cu centre is not solvent exposed.** Amino acids (**a**) and electrostatic potential surface (**b**) surrounding the T1Cu and T2Cu centres in AniA

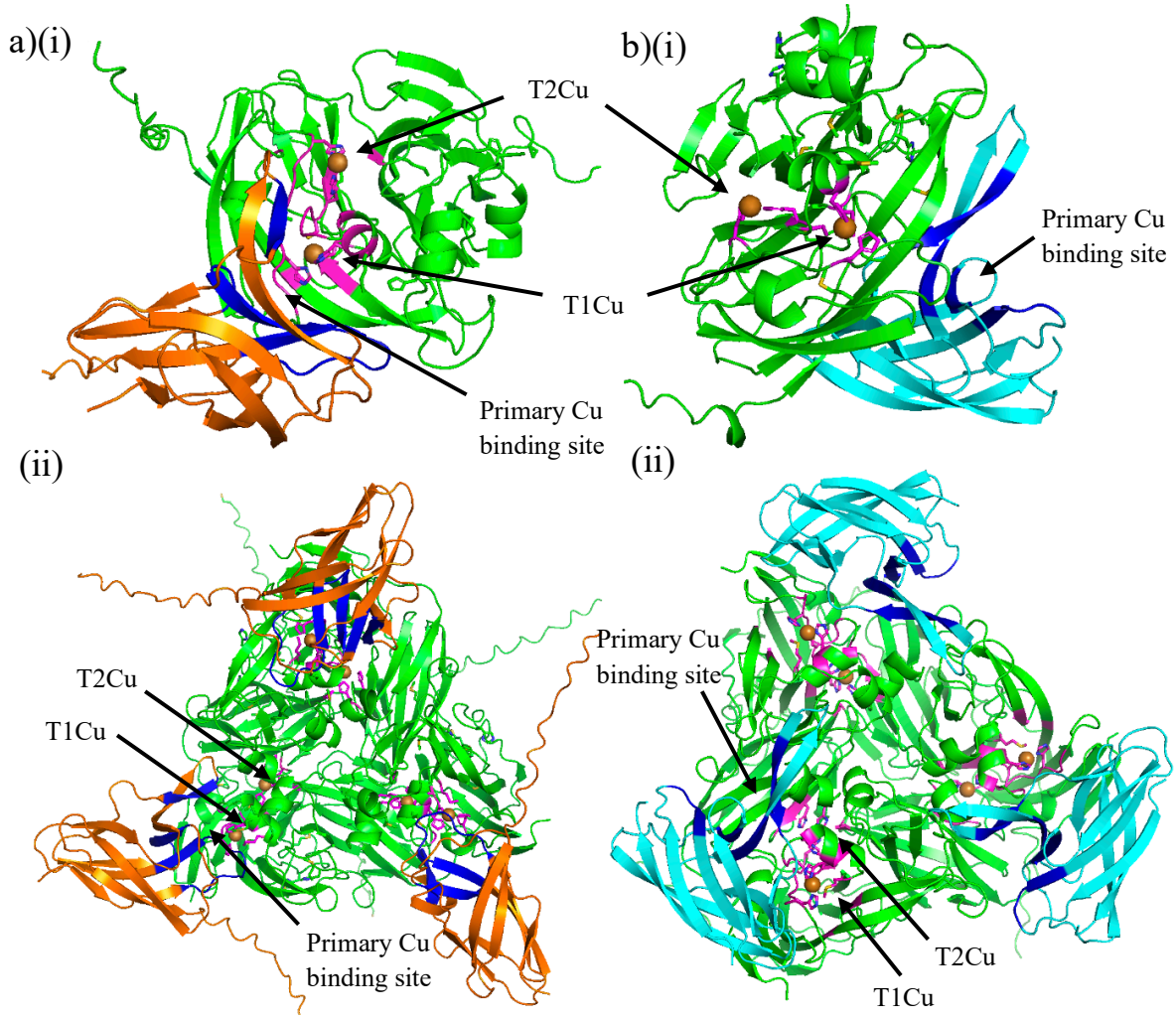

Figure 5.5. **Representative structures from AlphaFold 3 generated structures** of **a**) 1AccA:1AniA:2Cu (**i**) and 3AccA:3AniA:6Cu (**ii**) and **b**) 1PCu$_A$C:1AniA:2Cu (**i**) and 3PCu$_A$C:3AniA:6Cu (**ii**). Regions surrounding the primary Cu sites of the metallochaperones are highlighted in blue and the Cu centres in AniA are highlighted in magenta.

5.2 Comparing AccA with other PCu_AC homologues

Table 5.1. **The publicly available structurally characterised PCu_AC-family proteins**, including their Cu binding ligands and target for Cu transfer.

Protein	Organism	PDB ID of Cu-bound protein	Metal binding motifs	Target Protein	Target Cu site structure
AccA	*Neisseria gonorrhoeae*	N/A	$HX_{10}MX_{22}HXM$	NirK	T1Cu, T2Cu
Tt-PCu_AC	*Thermus thermophilus*	2K70, 2K67	$H(M)X_{10}MX_{21}HXM$	Cytochrome *c* oxidase	Cu_A
ECuC	*Streptomyces lividans*	3ZJA	$HX_6MX_{21}HXM$	Sco	CxxxC
PmoF1	*Methylocystis sp.*	6P16, 6P1E	$HX_{10}H$	pMMO complex	unknown
PmoF2	*Methylosinus trichosporium*	6P1G	$HX_3HX_{23}HXE$ or $HX_{10}H$	pMMO complex	unknown
DR1885	*Deinococcus radiodurans*	1X9L	$MX_{10}MX_{21}HXM$	Cytochrome *c* oxidase	Cu_A

Table 5.2. **Comparison of the identity of the PCu_AC-family proteins with AccA**. Finger domain sequence is defined as the first binding residue of the extension to the end of the beta fold where present.

Protein	Sequence identity with AccA	C-terminal tail	Finger domain length	Finger domain sequence
AccA	100%	Yes	13	HTHINDNGVMRMR
Tt-PCu_AC	34% (50% positive)	No	17	HETFMREVEGKKVMGMR
ECuC	33% (44% positive)	No	9	HETIDGTMK
PmoF1	29% (40% positive)	Yes	9	HGDAKNLAL
PmoF2	27% (40% positive)	Yes	7	HIAPHLV
DR1885	29% (50% positive)	No	14	MTTTHSGGMAGMKM

There are 5 structurally characterised PCu_AC-family proteins in the PDB database. These are AccA and *Tt*-PCu_AC, which were studied in this work, as well as ECuC from *Streptomyces lividans* (50), PmoF1 and PmoF2 from Methanotrophs (51), and DR1885 from *Deinococcus radiodurans* (77). Each of these proteins consist of the recognisable cupredoxin-like fold with an elongated finger domain (*Fig*. 5.6). All but PmoF1 have a metal binding site in the opening between the finger domain and the cupredoxin-like fold, although the identities of

the Cu(I)-binding ligands vary. Backbone structural alignment of all the proteins shows the cupredoxin-like Cu-binding domain all align with high similarity. However, the finger domain varies in length between 7 and 17 amino acids. In addition, only *Tt*-PCu_AC and AccA share any amino acid sequence in this domain with both containing a VMXMR motif at the C-terminal end of the finger (*Table* 5.2).

The amino acid backbones and overall structural folds across the PCu_AC family of proteins is well conserved, but the sequence identities of the proteins is relatively low (*Table* 5.2). AccA, *Tt*-PCu_AC, and ECuC appear to have the highest level of structural alignment. These metallochaperones also share the His-X_{10}-Met-$X_{21,22}$-His-X-Met Cu binding motif. This has given the three metallochaperones similar affinities for Cu in the subfemtomolar range (This work; (30,50)). Therefore, the conservation seen within the proteins is predominantly in the binding motif and overall structural fold, which likely maintains the high binding affinity for Cu(I). The low sequence identity between the proteins likely results in the difference in electrostatic surfaces of the proteins and therefore the differing protein targets. Despite AccA, *Tt*-PCu_AC, and ECuC sharing the highest identity, and PCu_AC and ECuC the same target, the charged surfaces, and the amino acids that are likely involved in protein-protein interactions, differ greatly. This is likely due to a lack of conservation in charged surfaces in their target enzymes, where the topology and charges of the target enzymes will play key roles in their position and functions within the cell. The role of metallochaperones is to interact with and transfer Cu to their target proteins. Therefore, the metallochaperones must be the protein that evolves to fill the required role, whilst the target enzyme must be conserved for its overall function.

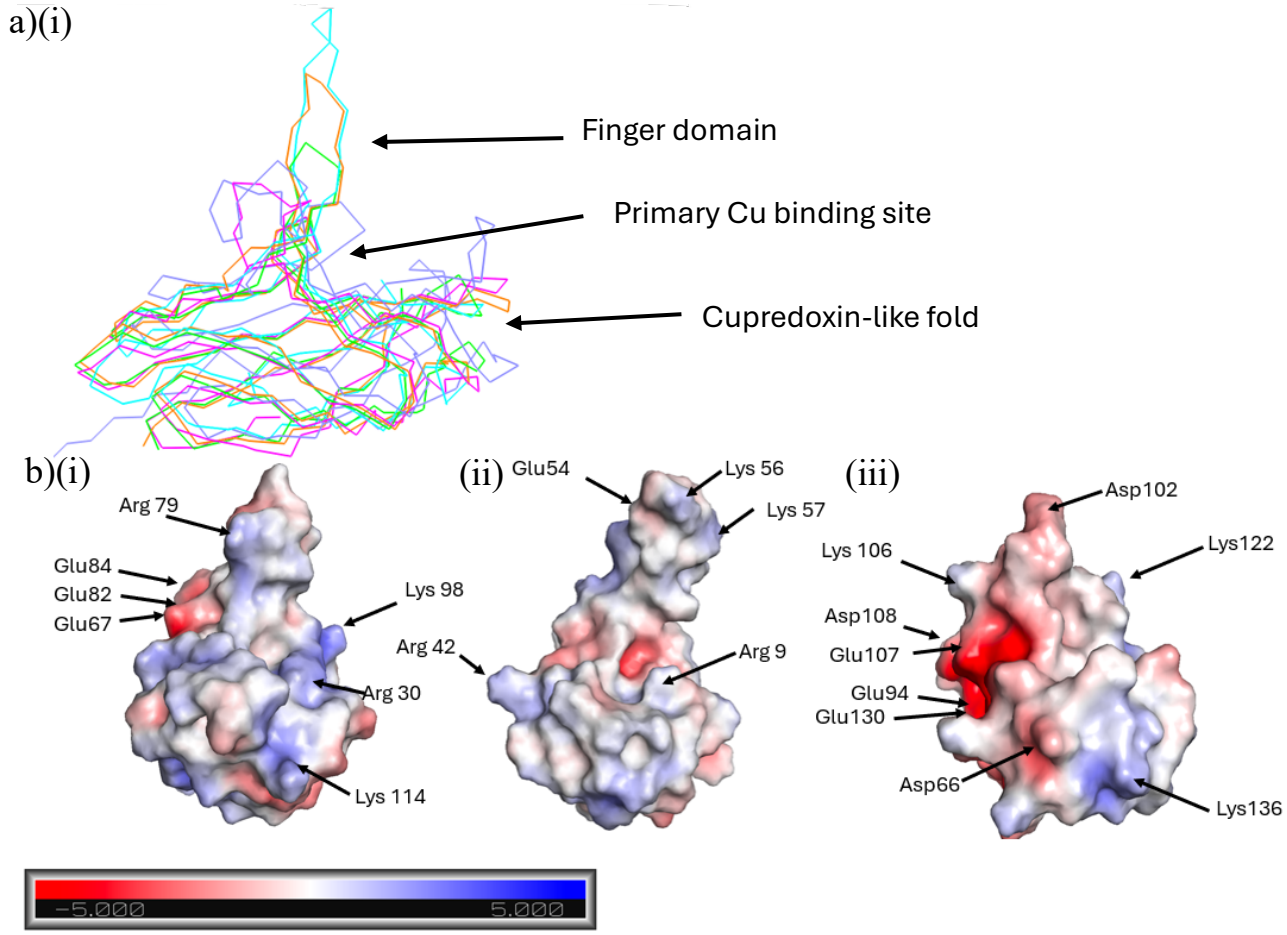

***Figure 5.6*. Structural comparison of the structurally characterised PCu$_A$C family proteins. a**) Structural alignment of PCu$_A$C family proteins: AccA (orange), *Tt*-PCu$_A$C (PDB: 2K70) (cyan), *Sl*-ECuC (PDB: 3ZJA)(green), *Msp*-PCu$_A$C (PDB:6P16) (pink), DR1885 (PDB:1X9L)(purple). **b**) Surfaces of AccA (**i**), PCu$_A$C (**ii**), and ECuC (**iii**), showing charge and topology around the primary Cu binding site of each metallochaperone.

The diversity of PCu$_A$C-family proteins is seen not only across bacterial species, but also within species, and more specifically, within the same operon. The genome of *Methylosinus trichosporium* and other methanotrophs encodes 3 PCu$_A$C homologues all within the *pMMO* operon. pMMO is a Cu-dependent enzyme that oxidises methane to methanol and is the main metabolic enzyme for methanotrophic bacteria. The three PCu$_A$C homologues present are PmoF1, PmoF2, and PmoF3. The exact target of each metallochaperone is unknown, but each may play a different role in the metalation of the pMMO complex. Therefore, despite likely originating as one enzyme, the 3 PCu$_A$C variants have evolved vastly different structures to perform a specific function within the cell. PmoF3 contains the Cu-binding motif His-X$_{10}$-Met-X$_{21,22}$-His-X-Met, seen in AccA and PCu$_A$C. However, PmoF1 and PmoF2, bind only Cu(II) *via* an N-terminal, HX$_{10}$H, histidine brace. PmoF2 can also bind zinc, in the primary PCu$_A$C binding site, coordinated by His-111, His-83, and Glu-113, and may also be able to bind Cu (51) (Fisher et al., 2019). PmoF1 and PmoF2 share a sequence identity of 54%, with 67% positive matches (NCBI Blastp) and also share almost identical structural folds and similar electrostatic surfaces (*Fig*. 5.7). Again, differences in electrostatic surfaces can be seen

particularly around the Cu-binding sites (*Fig*. 5.7b). These regions may be responsible for the metallochaperone interacting with the target protein and consequently result in different cellular functions of the metallochaperones.

The finding that AccA exists in some genomes when AniA does not could be explained by the high conservation of the overall fold of the protein but lack of conservation in key regions of the proteins (like in PmoF1 and PmoF2). It may be the case the metallochaperones have evolved with new target proteins, whilst conserving the regions of the protein responsible for Cu-binding.

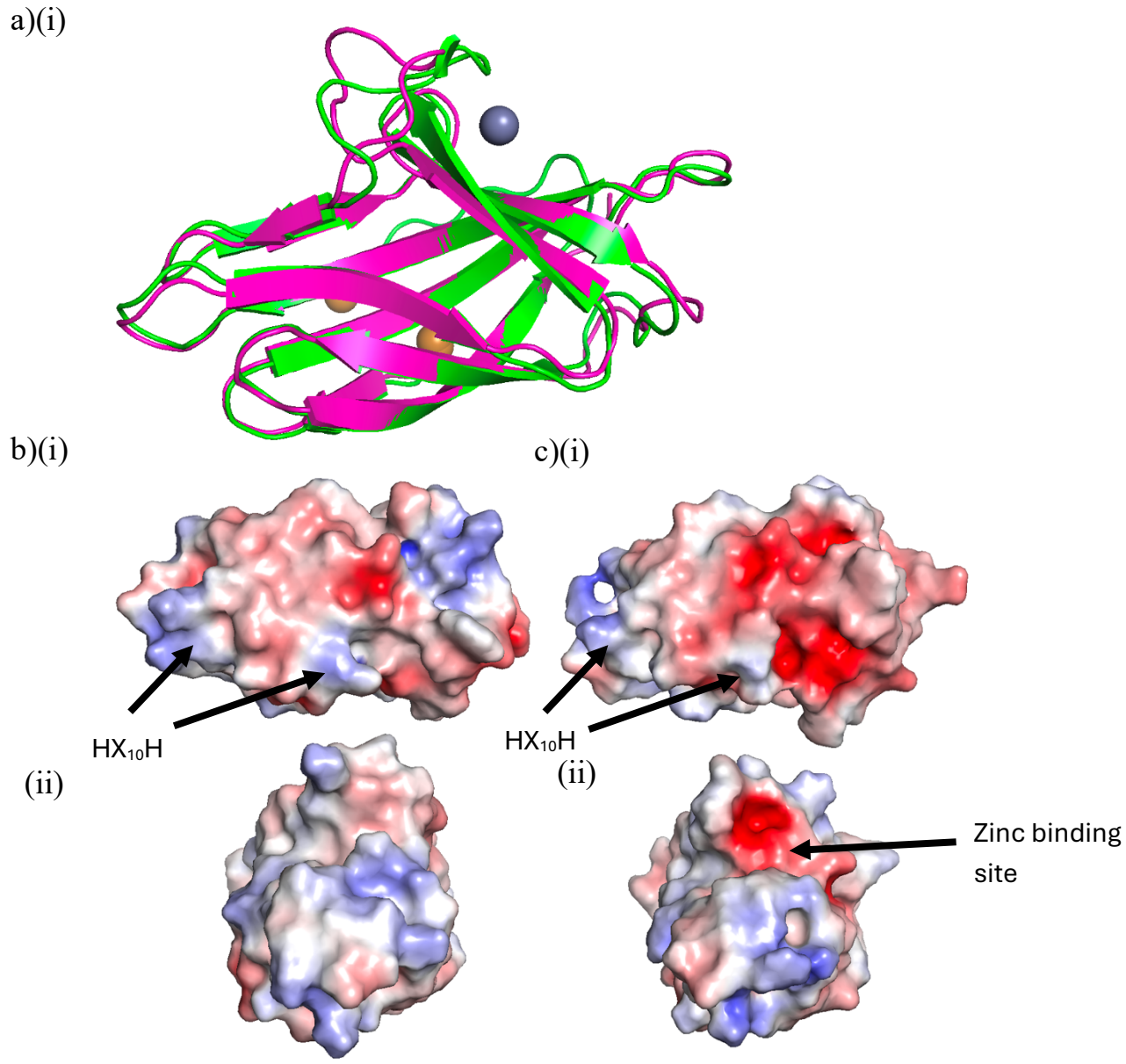

***Figure 5.7*. Structural comparison of PmoF1 and PmoF2. f**) Structural alignment of *holo*-PmoF1 (pink) and *holo*-PmoF2 (green). Electrostatic surfaces of PmoF1 (**b**) and PmoF2 (**c**) showing the histidine brace binding site (**i**) and the site of the classic PCu_AC-family Cu binding site where PmoF2 binds Zn (**ii**)

5.3 The PCu_AC-family of metallochaperones deliver nutrient copper

Many Cu metallochaperones in the literature are reported to be transcriptionally activated in response to increased Cu availability within cells (15). These include CopZ and CusF, which function to buffer high Cu and protect cells from Cu toxicity (78,79). CueP is another example - it both appears to sequester Cu and metalate enzymes associated with Cu toxicity (80). Therefore, Cu metallochaperones were thought to exist to prevent the well-known deleterious cellular effects of Cu (15).

Despite having multiple different targets, the PCu_AC-family proteins all aid in Cu insertion into key metabolic enzymes essential for growth (81) (*Table* 5.1). These PCu_AC-family proteins also tend to have relatively low *K*D values in the subfemtomolar range (this work; (30,50,72)). In comparison, other periplasmic Cu metallochaperones that respond to Cu toxicity, such as CueP and CusF, have higher K_D values of ~10^{-15} M and >10^{-12} M, respectively (79,82). The conservation of the PCu_AC family's high binding affinities to Cu(I) is certainly consistent with a role for AccA in metalating AniA under conditions of Cu limitation in *N. gonorrhoeae* (30), PCu_AC from *R. spharaeroides* being essential only under Cu limited conditions (52), and PCuC from *B. japonicium* being induced in response to Cu starvation (72). However, under these conditions of low Cu, Cu is unlikely to have deleterious effects. Therefore, all PCu_AC metallochaperones likely follow the model for Cu transfer described in chapter 5.1 (*Fig.* 5.3) rather than following the previous metallochaperone model and energy diagram described in *Fig.* 1.4 (a and biii), with the PCu_AC having a lower K_D value than both the buffer and the target protein. This would result in the metallochaperones having an essential role in bacterial metabolism.

Often, the supplementation of Cu into Δ*pCu_AC* bacterial strains rescues the growth phenotype, suggesting that Cu can be transferred directly from the buffer to the target protein (30,49,52). In the presence of higher cellular, it may be that Cu can be transferred directly from the buffer via mass action, as seen in the addition of 1 μM $CuSO_4$ in *Fig.* 3.3 and 3.4. However, copper insertion is still slow due to the kinetic barrier to direct metalation and the similar free energies leading to transfer of Cu or the equilibrium favouring the higher number of metal binding sites in the buffer. Therefore, the presence of a metallochaperone with a higher affinity than the buffer and the target protein will likely speed up metalation, but it would not be the sole mechanism of Cu insertion into the target protein.

This mechanism of Cu insertion may be a key indication as to why AniA appears in some genomes where AccA does not (30). It may be the case that AccA is not present in some genomes where AniA exists, because AniA not the key enzyme in metabolism. More likely, if the bacteria species occupies conditions where Cu starvation is rare, there may be no need for a high binding affinity metallochaperone to acquire Cu. Notably, supplementation of Cu into *N. gonorrhoeae* cultures resulted in no requirement of AccA for the metalation of AniA to occur.

5.4 Future work

The purpose of this work was to determine whether AccA and AniA form a specific metallochaperone-metalloenzyme pair, which would enhance the understanding of the

mechanism of Cu delivery from AccA to AniA. One further experiment to explore the specificity of AccA for AniA would be to conduct point mutations of PCu_AC, as conducted by Cobine *et al.* (32). These could include mutating E54 to K and K56 to E: switching the charges of the finger domain to mimic the charged surface of AccA. To mimic the topology of the AccA, the loop on the left-hand side of the cupredoxin-like fold in PCu_AC could be extended and a glutamate added in, to mimic the loop in AccA (*Fig*. 5.2). Conducting an experiment where the charged surfaces of the proteins are the same, but the length of the finger domain still differs, could provide an understanding of the flexibility of *apo*-AniA. Opposite experiments could also be conducted to mutate amino acids in AccA that potentially play a role in complex formation. These could be mutations of charged amino acids to give opposite or neutral charges, or mutations of small or bulky amino acids to change the overall topology. Mutating one, or a few, at a time, could provide an insight into which amino acids have an essential role in Cu insertion.

To gain a greater understanding of the interactions between AccA and AniA, structural analysis could be conducted. Most metallochaperone-metalloenzyme complexes are transient, meaning that they form and dissociate instantaneously upon the transfer of the metal and consequently do not exist without the metal being present (31). However, there is evidence from mass photometry that *apo*-AniA and *apo*-AccA form a complex (30). The formation of the complex between AccA and AniA can be confirmed by performing analytical SEC as the complex should be eluted from column as one singular peak. Using a technique such as SEC-MALS could be used to determine the mass of the complex if eluted. If it is confirmed that AniA and AccA form a complex, this could be isolated and crystalised for the structure to be resolved *via* X-ray diffraction. If the complex cannot be formed or is relatively unstable, AccA could be labelled for NMR to determine the protein regions in close contact upon complex formation. In addition, the complex could potentially be trapped *via* cross-inking, or by using a metal that cannot be transferred. Conversely, an approach using computational techniques could be used. Cross-linking mass spectrometry could be coupled with AlphaLink to provide a more confident prediction for the interactions between AccA and AniA. This method focuses sampling of potential binding sights by identifying interfaces; providing a more confident prediction for the overall structure of the complex formed (83).

References

1. Waldron KJ, Rutherford JC, Ford D, Robinson NJ. Metalloproteins and metal sensing. Nature. 2009 Aug;460(7257):823–30.

2. Fernandes HS, Teixeira CSS, Sousa SF, Cerqueira NMFSA. Formation of Unstable and very Reactive Chemical Species Catalyzed by Metalloenzymes: A Mechanistic Overview. Molecules. 2019 Jan;24(13):2462.

3. Waldron KJ, Robinson NJ. How do bacterial cells ensure that metalloproteins get the correct metal? Nat Rev Microbiol. 2009 Jan;7(1):25–35.

4. Pitcher RS, Watmough NJ. The bacterial cytochrome *cbb*3 oxidases. Biochim Biophys Acta BBA - Bioenerg. 2004 Apr 12;1655:388–99.

5. Foster AW, Young TR, Chivers PT, Robinson NJ. Protein metalation in biology. Curr Opin Chem Biol. 2022 Feb 1;66:102095.

6. Permyakov EA. Metal Binding Proteins. Encyclopedia. 2021 Mar;1(1):261–92.

7. Irving H, Williams RJP. Order of Stability of Metal Complexes. Nature. 1948 Nov;162(4123):746–7.

8. Osman D, Robinson NJ. Protein metalation in a nutshell. Febs Lett. 2023 Jan;597(1):141–50.

9. Chandrangsu P, Rensing C, Helmann JD. Metal Homeostasis and Resistance in Bacteria. Nat Rev Microbiol. 2017 Jun;15(6):338–50.

10. Macomber L, Imlay JA. The iron-sulfur clusters of dehydratases are primary intracellular targets of copper toxicity. Proc Natl Acad Sci U S A. 2009 May 19;106(20):8344–9.

11. Decker H, Terwilliger N. Cops and Robbers: Putative Evolution of Copper Oxygen-Binding Proteins. J Exp Biol. 2000 Jun 15;203(12):1777–82.

12. Abriata LA, Banci L, Bertini I, Ciofi-Baffoni S, Gkazonis P, Spyroulias GA, et al. Mechanism of CuA assembly. Nat Chem Biol. 2008 Oct;4(10):599–601.

13. Osman D, Patterson CJ, Bailey K, Fisher K, Robinson NJ, Rigby SEJ, et al. The copper supply pathway to a Salmonella Cu,Zn-superoxide dismutase (SodCII) involves P1B-type ATPase copper efflux and periplasmic CueP. Mol Microbiol. 2013;87(3):466–77.

14. Jen FEC, Djoko KY, Bent SJ, Day CJ, McEwan AG, Jennings MP. A genetic screen reveals a periplasmic copper chaperone required for nitrite reductase activity in pathogenic Neisseria. FASEB J. 2015;29(9):3828–38.

15. Robinson NJ, Winge DR. Copper Metallochaperones. Annu Rev Biochem. 2010 Jun 7;79(1):537–62.

16. Stewart LJ, Thaqi D, Kobe B, McEwan AG, Waldron KJ, Djoko KY. Handling of nutrient copper in the bacterial envelope. Metallomics. 2019 Jan 23;11(1):50–63.

17. Osman D, Martini MA, Foster AW, Chen J, Scott AJP, Morton RJ, et al. Bacterial sensors define intracellular free energies for correct enzyme metalation. Nat Chem Biol. 2019 Mar;15(3):241–9.

18. Sameach H, Narunsky A, Azoulay-Ginsburg S, Gevorkyan-Aiapetov L, Zehavi Y, Moskovitz Y, et al. Structural and Dynamics Characterization of the MerR Family Metalloregulator CueR in its Repression and Activation States. Structure. 2017 Jul 5;25(7):988-996.e3.

19. Hausrath AC, Ramirez NA, Ly AT, McEvoy MM. The bacterial copper resistance protein CopG contains a cysteine-bridged tetranuclear copper cluster. J Biol Chem. 2020 Aug 7;295(32):11364–76.

20. Osman D, Waldron KJ, Denton H, Taylor CM, Grant AJ, Mastroeni P, et al. Copper Homeostasis in Salmonella Is Atypical and Copper-CueP Is a Major Periplasmic Metal Complex*. J Biol Chem. 2010 Aug 13;285(33):25259–68.

21. Tottey S, Waldron KJ, Firbank SJ, Reale B, Bessant C, Sato K, et al. Protein-folding location can regulate manganese-binding versus copper- or zinc-binding. Nature. 2008 Oct;455(7216):1138–42.

22. Roat-Malone RM. Bioinorganic chemistry: a short course. Hoboken, New Jersey: Wiley-Interscience; 2002. 348 p.

23. Thermodynamic equilibrium between blue and green copper sites and the role of the protein in controlling function [Internet]. [cited 2024 Nov 19]. Available from: https://www.pnas.org/doi/epdf/10.1073/pnas.0900995106

24. Eady RR, Samar Hasnain S. New horizons in structure-function studies of copper nitrite reductase. Coord Chem Rev. 2022 Jun 1;460:214463.

25. MacPherson IS, Murphy MEP. Type-2 copper-containing enzymes. Cell Mol Life Sci CMLS. 2007 Nov;64(22):2887–99.

26. Koebke KJ, Alfaro VS, Pinter TBJ, Deb A, Lehnert N, Tard C, et al. Traversing the Red-Green-Blue Color Spectrum in Rationally Designed Cupredoxins. J Am Chem Soc. 2020 Aug 24;142(36):15282.

27. Ryde U, Olsson MHM, Pierloot K, Roos BO. The Cupric Geometry of Blue Copper Proteins is not Strained. J Mol Biol. 1996 Aug 30;261(4):586–96.

28. Banci L, Bertini I, Cantini F, Felli IC, Gonnelli L, Hadjiliadis N, et al. The Atx1-Ccc2 complex is a metal-mediated protein-protein interaction. Nat Chem Biol. 2006 Jul;2(7):367–8.

29. Banci L, Bertini I, Ciofi-Baffoni S, Kozyreva T, Zovo K, Palumaa P. Affinity gradients drive copper to cellular destinations. Nature. 2010 Jun;465(7298):645–8.

30. Firth SJ. The role of the periplasmic Cu metallochaperone AccA in metalating the Cu-dependent nitrite reductase AniA in Neisseria gonorrhoeae.

31. Niemiec MS, Weise CF, Wittung-Stafshede P. In Vitro Thermodynamic Dissection of Human Copper Transfer from Chaperone to Target Protein. PLoS ONE. 2012 May 4;7(5):e36102.

32. Cobine PA, George GN, Jones CE, Wickramasinghe WA, Solioz M, Dameron CT. Copper Transfer from the Cu(I) Chaperone, CopZ, to the Repressor, Zn(II)CopY: Metal Coordination Environments and Protein Interactions. Biochemistry. 2002 May 1;41(18):5822–9.

33. Banci L, Bertini I, Calderone V, Della-Malva N, Felli IC, Neri S, et al. Copper(I)-mediated protein–protein interactions result from suboptimal interaction surfaces. Biochem J. 2009 Aug 15;422(1):37–42.

34. Branch AH, Stoudenmire JL, Seib KL, Cornelissen CN. Acclimation to Nutritional Immunity and Metal Intoxication Requires Zinc, Manganese, and Copper Homeostasis in the Pathogenic Neisseriae. Front Cell Infect Microbiol. 2022 Jun 30;12:909888.

35. Deeudom M, Koomey M, Moir JWB. Roles of c-type cytochromes in respiration in Neisseria meningitidis. Microbiology. 2008;154(9):2857–64.

36. Djoko KY, Franiek JA, Edwards JL, Falsetta ML, Kidd SP, Potter AJ, et al. Phenotypic Characterization of a copA Mutant of Neisseria gonorrhoeae Identifies a Link between Copper and Nitrosative Stress. Infect Immun. 2012 Mar;80(3):1065–71.

37. Boulanger MJ, Murphy MEP. Crystal structure of the soluble domain of the major anaerobically induced outer membrane protein (AniA) from pathogenic *Neisseria*: a new class of copper-containing nitrite reductases1. J Mol Biol. 2002 Feb 1;315(5):1111–27.

38. Whitehead RN, Overton TW, Snyder LA, McGowan SJ, Smith H, Cole JA, et al. The small FNR regulon of Neisseria gonorrhoeae: comparison with the larger Escherichia coli FNR regulon and interaction with the NarQ-NarP regulon. BMC Genomics. 2007 Jan 29;8:35.

39. Phillips NJ, Steichen CT, Schilling B, Post DMB, Niles RK, Bair TB, et al. Proteomic Analysis of Neisseria gonorrhoeae Biofilms Shows Shift to Anaerobic Respiration and Changes in Nutrient Transport and Outermembrane Proteins. PLOS ONE. 2012 Jun 6;7(6):e38303.

40. Clark VL, Knapp JS, Thompson S, Klimpel KW. Presence of antibodies to the major anaerobically induced gonococcal outer membrane protein in sera from patients with gonococcal infections. Microb Pathog. 1988 Nov 1;5(5):381–90.

41. Sikora AE, Mills RH, Weber JV, Hamza A, Passow BW, Romaine A, et al. Peptide Inhibitors Targeting the Neisseria gonorrhoeae Pivotal Anaerobic Respiration Factor AniA. Antimicrob Agents Chemother. 2017 Jul 25;61(8):10.1128/aac.00186-17.

42. Jerse AE, Bash MC, Russell MW. Vaccines against Gonorrhea: Current status and Future Challenges. Vaccine. 2013 Sep 6;32(14):1579.

43. Horrell S, Kekilli D, Strange RW, Hough MA. Recent structural insights into the function of copper nitrite reductases. Metallomics. 2017 Nov 1;9(11):1470–82.

44. Li HT, Chang T, Liu MY, Le Gall J, An XM, Gui LL, et al. Preliminary crystallographic studies of two C-terminally truncated copper-containing nitrite reductases from *Achromobacter cycloclastes*: changed crystallizing behaviors caused by residue deletion. Biochem Biophys Res Commun. 2002 Nov 29;299(2):173–6.

45. Li HT, Wang C, Chang T, Chang WC, Liu MY, Gall JL, et al. pH-profile crystal structure studies of C-terminal despentapeptide nitrite reductase from *Achromobacter cycloclastes*. Biochem Biophys Res Commun. 2004 Mar 26;316(1):107–13.

46. Li HT, Chang T, Chang WC, Chen CJ, Liu MY, Gui LL, et al. Crystal structure of C-terminal desundecapeptide nitrite reductase from *Achromobacter cycloclastes*. Biochem Biophys Res Commun. 2005 Dec 30;338(4):1935–42.

47. Chang WC, Chen JY, Chang T, Liu MY, Payne WJ, LeGall J, et al. The C-Terminal Segment Is Essential for Maintaining the Quaternary Structure and Enzyme Activity of the Nitric Oxide Forming Nitrite Reductase from*Achromobacter cycloclastes*. Biochem Biophys Res Commun. 1998 Sep 29;250(3):782–5.

48. Thaqi D. Structural and biochemical characterisation of the periplasmic copper chaperone AccA in Neisseria gonorrhoeae [Internet] [PhD Thesis]. The University of Queensland; 2021 [cited 2025 Jun 10]. Available from: https://espace.library.uq.edu.au/view/UQ:e960520

49. Canonica F, Klose D, Ledermann R, Sauer MM, Abicht HK, Quade N, et al. Structural basis and mechanism for metallochaperone-assisted assembly of the CuA center in cytochrome oxidase. Sci Adv. 2019 Jul 31;5(7):eaaw8478.

50. Blundell KLIM, Hough MA, Vijgenboom E, Worrall JAR. Structural and mechanistic insights into an extracytoplasmic copper trafficking pathway in *Streptomyces lividans*. Biochem J. 2014 May 1;459(3):525–38.

51. Fisher OS, Sendzik MR, Ross MO, Lawton TJ, Hoffman BM, Rosenzweig AC. PCuAC domains from methane-oxidizing bacteria use a histidine brace to bind copper. J Biol Chem. 2019 Nov 1;294(44):16351–63.

52. Thompson AK, Gray J, Liu A, Hosler JP. The roles of Rhodobacter sphaeroides copper chaperones PCuAC and Sco (PrrC) in the assembly of the copper centers of the aa3-type and the cbb3-type cytochrome c oxidases. Biochim Biophys Acta. 2012 Jun;1817(6):955–64.

53. Hausrath AC, McEvoy MM. Structural Analyses of the Multicopper Site of CopG Support a Role as a Redox Enzyme. In: Atassi MZ, editor. Protein Reviews [Internet]. Cham: Springer International Publishing; 2023 [cited 2023 Oct 31]. p. 97–121. (Advances in Experimental Medicine and Biology; vol. 1414). Available from: https://link.springer.com/10.1007/5584_2022_753

54. Ramírez CS, Tolmie C, Opperman DJ, González PJ, Rivas MG, Brondino CD, et al. Copper nitrite reductase from Sinorhizobium meliloti 2011: Crystal structure and interaction with the physiological versus a nonmetabolically related cupredoxin-like mediator. Protein Sci Publ Protein Soc. 2021 Nov;30(11):2310–23.

55. Yoon BY, Kim YH, Kim N, Yun BY, Kim JS, Lee JH, et al. Structure of the periplasmic copper-binding protein CueP from Salmonella enterica serovar Typhimurium. Acta Crystallogr D Biol Crystallogr. 2013 Oct;69(Pt 10):1867–75.

56. Abriata LA, Pontel LB, Vila AJ, Dal Peraro M, Soncini FC. A dimerization interface mediated by functionally critical residues creates interfacial disulfide bonds and copper sites in CueP. J Inorg Biochem. 2014 Nov;140:199–201.

57. Subedi P, Paxman JJ, Wang G, Ukuwela AA, Xiao Z, Heras B. The Scs disulfide reductase system cooperates with the metallochaperone CueP in Salmonella copper resistance. J Biol Chem. 2019 Nov 1;294(44):15876–88.

58. Dillard JP. Genetic Manipulation of Neisseria gonorrhoeae. Curr Protoc Microbiol. 2011 Nov;0 4:Unit4A.2.

59. Fox JB. Kinetics and mechanisms of the Griess reaction. Anal Chem. 1979 Aug 1;51(9):1493–502.

60. Young TR, Xiao Z. Principles and practice of determining metal–protein affinities. Biochem J. 2021 Mar 12;478(5):1085–116.

61. Kuzmič P. Program DYNAFIT for the Analysis of Enzyme Kinetic Data: Application to HIV Proteinase. Anal Biochem. 1996 Jun 1;237(2):260–73.

62. Buschmann S, Warkentin E, Xie H, Langer JD, Ermler U, Michel H. The Structure of cbb3 Cytochrome Oxidase Provides Insights into Proton Pumping. Science. 2010 Jul 16;329(5989):327–30.

63. Bolton JRF. The nitrous oxide reductase of Neisseria gonorrhoeae is a transcriptionally active yet translationally silent potogene.

64. Quillin SJ, Seifert HS. Neisseria gonorrhoeae host adaptation and pathogenesis. Nat Rev Microbiol. 2018 Apr;16(4):226–40.

65. Banci L, Bertini I, Cantini F, Felli IC, Gonnelli L, Hadjiliadis N, et al. The Atx1-Ccc2 complex is a metal-mediated protein-protein interaction. Nat Chem Biol. 2006 Jul;2(7):367–8.

66. Cobine PA, George GN, Jones CE, Wickramasinghe WA, Solioz M, Dameron CT. Copper Transfer from the Cu(I) Chaperone, CopZ, to the Repressor, Zn(II)CopY: Metal Coordination Environments and Protein Interactions. Biochemistry. 2002 May 1;41(18):5822–9.

67. Mahmood T, Yang PC. Western Blot: Technique, Theory, and Trouble Shooting. North Am J Med Sci. 2012 Sep;4(9):429–34.

68. Xiao Z, Brose J, Schimo S, Ackland SM, La Fontaine S, Wedd AG. Unification of the Copper(I) Binding Affinities of the Metallo-chaperones Atx1, Atox1, and Related Proteins. J Biol Chem. 2011 Apr 1;286(13):11047–55.

69. Loula M, Kaňa A, Mestek O. Non-spectral interferences in single-particle ICP-MS analysis: An underestimated phenomenon. Talanta. 2019 Sep 1;202:565–71.

70. Richards J. Cu insertion into Cu-dependent nitrite reductase AniA from Neisseria gonorrhoeae.

71. Chaplin AK, Wilson MT, Hough MA, Svistunenko DA, Hemsworth GR, Walton PH, et al. Heterogeneity in the Histidine-brace Copper Coordination Sphere in Auxiliary Activity Family 10 (AA10) Lytic Polysaccharide Monooxygenases*. J Biol Chem. 2016 Jun 10;291(24):12838–50.

72. Serventi F, Youard ZA, Murset V, Huwiler S, Bühler D, Richter M, et al. Copper Starvation-inducible Protein for Cytochrome Oxidase Biogenesis in Bradyrhizobium japonicum. J Biol Chem. 2012 Nov 9;287(46):38812–23.

73. Guo J, Fisher OS. Orchestrating copper binding: structure and variations on the cupredoxin fold. JBIC J Biol Inorg Chem. 2022 Sep 1;27(6):529–40.

74. Banci L, Bertini I, Calderone V, Della-Malva N, Felli IC, Neri S, et al. Copper(I)-mediated protein-protein interactions result from suboptimal interaction surfaces. Biochem J. 2009 Jul;422(1):37–42.

75. Chakravorty DK, Li P, Tran TT, Bayse CA, Merz KMJr. Metal Ion Capture Mechanism of a Copper Metallochaperone. Biochemistry. 2016 Jan 26;55(3):501–9.

76. Zhang L, Koay M, Maher MJ, Xiao Z, Wedd AG. Intermolecular Transfer of Copper Ions from the CopC Protein of Pseudomonas syringae. Crystal Structures of Fully Loaded CuICuII Forms. J Am Chem Soc. 2006 May 1;128(17):5834–50.

77. Banci L, Bertini I, Ciofi-Baffoni S, Katsari E, Katsaros N, Kubicek K, et al. A copper(I) protein possibly involved in the assembly of CuA center of bacterial cytochrome c oxidase. Proc Natl Acad Sci. 2005 Mar 15;102(11):3994–9.

78. Odermatt A, Solioz M. Two trans-Acting Metalloregulatory Proteins Controlling Expression of the Copper-ATPases of Enterococcus hirae*. J Biol Chem. 1995 Mar 3;270(9):4349–54.

79. Loftin IR, McEvoy MM, Blackburn NJ. Tryptophan Cu(I)–π interaction fine-tunes the metal binding properties of the bacterial metallochaperone CusF. J Biol Inorg Chem JBIC Publ Soc Biol Inorg Chem. 2009 Aug;14(6):905–12.

80. Osman D, Patterson CJ, Bailey K, Fisher K, Robinson NJ, Rigby SEJ, et al. The copper supply pathway to a Salmonella Cu,Zn-superoxide dismutase (SodCII) involves P1B-type ATPase copper efflux and periplasmic CueP. Mol Microbiol. 2013;87(3):466–77.

81. Price MN, Arkin AP. PaperBLAST: Text Mining Papers for Information about Homologs. mSystems. 2017 Aug 15;2(4):e00039-17.

82. Subedi P, Paxman JJ, Wang G, Ukuwela AA, Xiao Z, Heras B. The Scs disulfide reductase system cooperates with the metallochaperone CueP in Salmonella copper resistance. J Biol Chem. 2019 Nov;294(44):15876–88.

83. Stahl K, Warneke R, Demann L, Bremenkamp R, Hormes B, Brock O, et al. Modelling protein complexes with crosslinking mass spectrometry and deep learning. Nat Commun. 2024 Sep 9;15(1):7866.